The Michigan State University Six Gap β-Ray Spectrometer and its Application to the β- and γ-Ray Spectroscopic Studies of ^{83}Sr and ^{131m}Te*

Thesis for the Degree of Ph. D.

MICHIGAN STATE UNIVERSITY

LOUIS M. BEYER

1967

*Research Supported by the National Science Foundation

ABSTRACT

THE MICHIGAN STATE UNIVERSITY SIX GAP β-RAY SPECTROMETER AND ITS APPLICATION TO THE β- AND γ-RAY SPECTROSCOPIC STUDIES OF ^{83}Sr AND ^{131m}Te

by Louis M. Beyer

A six gap, iron core β-ray spectrometer has been constructed. The instrument, often called the "orange" spectrometer because of its geometric similarity to an orange, is similar to the one described by Bisgard. The spectrometer and its associated components are discussed in detail. A semi-quantitative theory of the focusing properties of a 1/r field is included and the defocusing components of the field that are characteristic of this type of instrument are discussed.

The orange spectrometer and the MSU iron free $\pi\sqrt{2}$ spectrometer have been used to investigate the internal conversion electron and positron spectra emitted in the decay of ^{83}Sr. Information on the multipolarities of the strongest transitions has been obtained. The M2 multipolarity assignment of the 42.3 keV transition, in conjunction with existing coincidence and lifetime measurements, show that the low energy features ($\leq$ 804.6 keV) of the decay scheme are uniquely determined. These data, when combined with log ft values obtained from a Fermi analysis of the positron spectra, lead to spin-parity assignments (in parentheses) to the

ground state of $^{83}Sr(7/2^+)$ and to the 5.0 keV$(3/2^-)$, 42.3 keV$(9/2^+)$, 99.2 keV$(1/2^-)$, 389.2 keV$(3/2^-)$, 423.5 keV $(5/2^+)$ and 804.6 keV$(7/2^+)$ states of ^{83}Rb.

The $7/2^+$ assignment to the ground state of ^{83}Sr does not agree with the shell model calculations of Talmi and Unna, although their calculations do predict a low-lying $7/2^+$ state at 320 keV. The level scheme of ^{83}Rb is also discussed with respect to expectations based on shell model systematics.

The gamma-ray spectrum of ^{131m}Te has been thoroughly investigated with the high resolution Ge(Li) detectors, accurately determining the energies and relative intensities of 45 transitions in the spectrum. The use of the NaI(Tl)-Ge(Li) coincidence technique has resulted in the placement of all but six very weak transitions into a consistent decay scheme. The orange and $\pi\sqrt{2}$ spectrometers have been used to investigate the internal conversion electron spectrum. Conversion coefficients were obtained for the 80.9, 102.3, 149.7, 200.7, 240.6, 334.5, 452.7 and 773.7 keV transitions. Further information on spin-parity assignments has been provided by the calculated log ft values which were obtained using gamma-ray intensities. The combined data provide a level scheme for ^{131}I with the following energies (in keV) and spin-parity assignments: $0(7/2^+)$, $149.7(5/2^+)$, $493(3/2^+)$, $603(3/2^+, 5/2^+)$, $773.7(9/2^+, 11/2^+)$, $852.1(9/2^+, 11/2^+)$, $1059.7(7/2^+)$, $1315(7/2^+)$, $1556.4(7/2^+, 9/2^+)$, $1596.5(7/2^+, 9/2^+)$, $1646(9/2, 11/2)$, $1797(9/2^-, 11/2^-)$, 1888, $1899(9/2^-,$

$11/2^-$), 1980($9/2^-$, $11/2^-$), 2001, 2168 and 2270.

Recent theoretical calculations for the states of ^{131}I have been performed by Kisslinger and Sorensen and by O'Dwyer and Choudhury. Although there are insufficient data available for a quantitative analysis, a qualitative comparison of the data has been made for both sets of calculations.

Finally, a survey has been made of the energy level systematics of the low energy states of all the odd mass iodine isotopes. Of special interest is the observed quadratic behavior of the energies of separation of the $1/2^+$, $3/2^+$ and $5/2^+$ states with respect to the $7/2^+$ state, as a function of the neutron number.

THE MICHIGAN STATE UNIVERSITY SIX GAP β-RAY SPECTROMETER AND ITS APPLICATION TO THE β- AND γ-RAY SPECTROSCOPIC STUDIES OF ^{83}Sr AND ^{131m}Te

By

Louis M. Beyer

A THESIS

Submitted to
Michigan State University
in partial fulfillment of the requirements
for the degree of

DOCTOR OF PHILOSOPHY

Department of Physics

1967

ACKNOWLEDGEMENTS

I wish to thank Dr. W. H. Kelly for the suggestion of this thesis project and for his guidance and continued encouragement throughout the construction phases of the spectrometer as well as the period of data acquisition and analysis.

I am indebted to the members of the shops for their assistance and advice in the construction of the spectrometer, especially Mr. N. Mercer, Mr. R. Geyer and Mr. N. Bird of the cyclotron machine shop, Mr. R. Hoskins and Mr. N. Rutter of the physics machine shop and Mr. E. Brandt of the physics electronics shop.

Mr. G. Berzins, Dr. R. Auble, Mr. R. Etherton and Mr. W. Johnston have aided in the acquisition and analysis of the data. Discussions with Dr. S. K. Haynes concerning the data recorded with the $\pi\sqrt{2}$ spectrometer and his interest in this investigation have also been very helpful. In addition, discussions with Dr. D. J. Horen of the U. S. Naval Radiological Defense Laboratory have been informative.

I wish to express my appreciation to Drs. W. P. Johnson and H. G. Blosser for their assistance with the cyclotron operation during the early irradiations.

I am grateful to Mr. R. Dickenson and Mr. A. Kaye for efficiently handling many of the acquisition problems associated with the spectrometer construction and radioactive source delivery, and to Miss Wilma Sanders for typing the thesis.

I wish to acknowledge the financial assistance of the National Science Foundation which provided partial support for

the experimental program and the spectrometer construction. During much of the time this program was in progress, I was supported by an NDEA Title IV Fellowship.

Finally, I express my gratitude to my wife, Faye, for helping to make this an enjoyable as well as profitable experience.

TABLE OF CONTENTS

LIST OF TABLES

LIST OF FIGURES

Figure Page

INTRODUCTION

A. General Objectives

A large fraction of our knowledge concerning nuclear structure and nuclear forces comes from the study of radioactive decay and nuclear reactions. The low energy structure of nuclei is often more precisely determined by the former. However, nuclear reactions have the advantage of access to the higher excitation energies, as well as being able to populate new lower states which are forbidden in radioactive decay, due to the operation of selection rules. The phenomena which are accessible for study through radioactive decay are still of basic importance for the understanding of nuclear structure in general. The studies presented in this thesis are intended as an extension of such attainable knowledge using the techniques of beta- and gamma-ray spectroscopy.

Information on nuclear level structure is obtained from beta- and gamma-ray spectroscopy via the construction of decay schemes. The decay scheme gives information on the energy level structure of the nucleus of interest, as well as transitions between the levels, and the energy level spins and parities. The experimental results thus obtained can then often be compared with existing theoretical calculations, which serve as a test of the proposed models, as well as providing more complete and accurate information for future calculations.

B. Specific Objectives of this Study

One of the most interesting series of nuclei to be studied, both experimentally and theoretically, are those having odd A and spherical equilibrium shapes[1,2]. In particular, systematic trends of isotopes having closed shell plus one or closed shell plus three nucleons are presumably amenable to calculation by known techniques. The single particle states are expected as the lowest energy states, while the higher energy states should arise from coupling of the single particle states to collective excitations of the core. To test this hypothesis, a large fraction of the experimental studies presented in this thesis is devoted to a study of the systematic trends of the energy levels in the odd mass iodine isotopes, which have three protons outside a major shell closure of fifty. The observed results, although limited in character, are then compared with existing calculations by Kisslinger and Sorensen[3] and by O'Dwyer and Choudhury[4].

A second set of experiments has been performed to study the level structure of ^{83}Rb populated by the decay of ^{83}Sr. Although no calculations have been performed for the levels of the odd mass rubidium isotopes, the ground state spin and parity of ^{83}Sr can be inferred from such a study. Talmi and Unna[5] have performed shell model calculations for ^{83}Sr, predicting the ground state to have spin and parity $9/2^+$. Thus the experimental results serve as an initial test of these calculations. The level scheme of ^{83}Rb, hitherto un-

known, serves to extend the energy level systematics in this little known region of the periodic table. In addition, it is of interest to see if a simple relationship exists between an even-even nucleus and an adjacent odd nucleus in this region of the periodic table. The ^{83}Rb nucleus differs by a single proton from the ^{82}Kr nucleus, whose states are well known[6]. The energy level diagram has, in this case, proven to be so complex as to mask the effects sought after. Nevertheless, considerable information has been obtained for the low lying single particle states.

C. Methods of Constructing the Decay Schemes

The data analysis approach that is described herein has been to first construct the proper energy level diagrams for the nuclei of interest, and then perform experiments to determine the spins and parities of the levels. The former is accomplished by accurate measurement of the gamma-ray energies and relative intensities, and by coincidence counting techniques. The methods employed are not new, but the equipment now available is a vast improvement over that which was in use only a few years ago. In the studies presented here, advantage has been taken of the high resolution Ge(Li) radiation detectors, both in singles and coincidence counting experiments. Multichannel pulse height analyzers with split memories and multiple coincidence circuits aided in the faster accumulation of the data.

The assignment of spins and parities to the various observed energy levels is not quite so straightforward. A commonly used method of spin parity assignment is via gamma-gamma angular correlation experiments[7]. The anisotropy of the coincidence counting rate, as a function of the angle of emission between two cascading transitions, gives an indication of the spin sequence of the levels involved. Conversion electron-gamma angular correlation functions contain an additional term in the matrix element which depends on the parities of the levels of interest[7]. However, the two decay schemes studied by the author were found to be too complex to allow the obtaining of reliable angular correlation results with present methods. Thus the spin and parity assignments have been based on measurements of internal conversion coefficients and log ft values.

In beta-decay, the quantity f is defined as[8]

$$f = \int_0^{p_m} dp\ p^2 q^2 F_o(p,Z) S_n$$

where p = the electron momentum, q = the neutrino momentum, $F_o(p,Z)$ the Coulomb correction factor. The shape factor, S_n, is introduced to extend the validity of the calculation to forbidden transitions[8]. For allowed transition, $S_1 = 1$. The quantity f times the half life of the transition is proportional to ξ^{-1}, where ξ is the square of the beta decay matrix element. Since ξ is a quantity independent of the lepton energies, the "comparative" or "reduced" half-life, ft, should

not be very different for transitions with the same degree of forbiddenness. The ft value is also independent of the decay energy and nuclear charge.

Empirical results have shown that log ft values, within specified limits, are indeed characteristic of certain spin-parity changes[9]. The partial half-life t can be easily obtained by experiment, while f is tabulated[8]. Thus beta decay transition probabilities immediately give us an indication of spin limits.

The ratio of the number of conversion electrons to the number of gamma-rays emitted in a nuclear de-excitation is the internal conversion coefficient[10] α,

$$\alpha = \frac{Ne}{N\gamma} .$$

The internal conversion coefficients are sensitive functions of multipolarity, especially for low energy transitions[10]. A measurement of α often can be used to determine the multipolarity, L, of the transition between the initial and final states, i and f. The spin change between the two states is then limited by

$$|J_i - J_f| \leq L \leq J_i + J_f .$$

The parity selection rule is

$\Delta\Pi = (-1)^L$ if the transition is electric (EL)

$\Delta\Pi = (-1)^{L+1}$ if the transition is magnetic (ML).

Most of the spin-parity assignments in the decay schemes in this study have been made by use of measured α's and log ft values.

In order to measure the beta and conversion electron spectra, a magnetic spectrometer has been constructed. The instrument is similar to the six gap, iron core, toroidal spectrometer described by Bisgord[11]. The instrument has proven to be a valuable addition to the already impressive array of techniques now at our disposal.

Chapter 1 contains a brief summary of some of the most popular nuclear models in use today. The discussion is mostly qualitative in description, designed to give a cursory understanding of the types of calculations being performed. Chapter 2 describes the orange spectrometer, the construction of which accounts for a large fraction of this thesis project. The applications of the spectrometer, in conjunction with a gamma-ray counting system, to the decay schemes of ^{131m}Te and ^{83}Sr are described in Chapters 3 and 4. A short summary of the results are presented in Chapter 5.

CHAPTER 1

NUCLEAR MODELS

As in many other areas of scientific endeavor, the theoretical development of nuclear physics proceeds in two separate phases. In the one case, people develop models which correlate experimental results and provide simple descriptions of the phenomena involved. Attempts are then constantly made to broaden the range of applicability of each model, remove conflicts between the different ones and ultimately fuse the various models into a single unified picture. On the other hand, theories are developed which attempt to explain the properties from the fundamental laws of nature. Nuclear theory has not been able to develop as completely as some other fields due to incomplete knowledge of nuclear forces.

Since a major objective of experimental study is for comparison with theoretical predictions, a brief survey of a few of the more successful nuclear models will be presented.

1.A. The Shell Model: Spherical Nuclei

1.A.1. The Auxiliary Potential

It has been known for many years that nuclei of neutron or proton numbers of 2, 8, 20, 28, 50 or 82 and neutron numbers of 126 exhibit exceptional properties of stability, analogous to shell closures of atomic electrons[12]. The

above have often been referred to as the "magic numbers" of atomic nuclei. Magic number nuclei have been found to have higher than average binding energy, an abundance of isotopes (magic Z) or isotones (magic N), very small quadrupole moments (spherical), and the very small thermal neutron absorption cross section $\sigma(n,\gamma)$ for N = 50, 82 or 126. The "Shell Model" or "Single Particle Model", proposed independently by Mayer[13] and by Haxel, Jensen and Suess[14], has enjoyed great success in explaining the magic numbers and predicting other properties of low lying levels in many nuclei.

It had long been known that the assumption of individual nucleons moving in an auxiliary central potential V(r) would produce the magic numbers 2, 8 and 20 [15]. The requirements of V(r) were that it be fairly constant inside the nuclear radius and have a short range, i.e., it does not extend far beyond the nuclear radius. It was then found that the introduction of an additional term in the auxiliary potential gave a unique explanation of the shell closures at all observed magic numbers. It was postulated that there exists a strong coupling between the spin and orbital angular momentum of each individual nucleon. The sign of the term is opposite to that found for atomic electrons, and its magnitude is approximately 30 times that predicted by relativistic Thomas coupling[13,14]. In such a theory, which neglects tensor forces between nucleons, conservation of the orbital angular momentum ℓ is still implied.

With inverted spin-orbit coupling, every level of given ℓ splits into two levels with angular momentum $j = \ell - 1/2$ and $j = \ell + 1/2$, the latter lying lower. The energy difference between these two levels is proportional to $2\ell + 1$, which means that splitting increases with increasing ℓ. Calculations based on the model predict energy gaps after proton or neutron numbers which correspond to the magic numbers, as the shells are filled.

The shell model, as described above, also makes unique predictions about the properties of nuclei which have only one neutron or proton outside of, or missing from, a closed shell. The angular momentum, parity and magnetic moment are that of the extra nucleon or hole. For this reason, the model is sometimes called the "extreme single particle model". For such nuclei, shell model predictions are in substantial agreement with experimental results. The same holds true in many cases for single particles outside closed subshells. The more general case, of course, is that of several particles outside closed shells. Mayer and Jensen[16] have augmented the shell model by the inclusion of j-j coupling together with some very simple coupling rules. With such a scheme, the ground state spin and orbital angular momentum can be predicted, as well as more model sensitive properties like electric quadrupole and magnetic dipole moments, and transition matrix elements. The model has enjoyed considerable success, especially for ground states and low excited states of some odd A spherical nuclei.

1.A.2. Residual Interactions

a) Nucleon-Nucleon Coupling

Except for low energy excitations in odd A nuclei, the model of Mayer and Jensen[16] is not expected to give good results. The "extended" or "intermediate coupling" single particle model has been introduced in an attempt to extend the useful range of predictions[17]. The fact that coupling rules were necessary in the original model demonstrated that the effect of nuclear interactions cannot be completely replaced by a potential well plus spin-orbit coupling. One expects a residual interaction potential arising from nucleon-nucleon forces. Such a residual interaction is important in determining properties of excited states.

Initial calculations based on the intermediate coupling scheme consisted of solving

$$\mathcal{H}\psi = [H_o + A\sum_i \vec{\ell}_i \cdot \vec{s}_i + \sum_{i>K} V_{iK}]\psi = E\psi$$

where H_o is the Hamiltonian for independent particles in a harmonic oscillator well[17]. The additional terms are the single nucleon spin-orbit potential plus a residual two body interaction. The procedure is to obtain the closely spaced single particle levels determined by the first two terms in $\mathcal{H}$. Nucleons are distributed in these levels in all possible ways consistent with the Pauli principle. The single nucleon angular momenta and isotopic spins are then coupled to obtain

all possible resultant angular momenta and isotopic spins. The resultant wave functions, which are many particle wave functions, are then used to diagonalize the total Hamiltonian. The calculation is feasible only if the number of nucleons in unfilled levels is small. Results of this type of calculation are exemplified by the calculation of Elliot and Flowers[18] for ^{19}F. The agreement between experimental and calculated quantities is very good except for the electric quadrupole (E2) transition rates. This discrepancy is typical for intermediate coupling calculations. One solution to this problem has been to use a potential which will enhance E2 transition rates, i.e., a potential well with a quadrupole deformation instead of a spherical shape.

A somewhat different approach to shell model calculations with nucleon-nucleon interactions is that of Talmi and Unna[5] who determine an effective nuclear interaction rather than use a phenomenological potential. The method, applicable to regions near closed subshells, determines the unknown diagonal matrix elements of two-body effective interactions between nucleons by comparisons with experimental data, and then assumes the interaction to be the same for all nuclei in which the same subshells are being filled. The non-diagonal elements, arising from configuration interaction, are determined along with the diagonal elements by comparison with experimental data. These terms are also assumed to have the same values in all nuclei in which the same subshell is being filled. The success of the approach depends on the considera-

tion of as many data points as possible. Predictions made by the model in the ^{90}Zr region do indeed seem to be realistic.

b) Pairing Plus Quadrupole Forces

The recent model proposed by Kisslinger and Sorensen[3]* has at least partially removed objectionable features of the intermediate coupling shell model. These authors have utilized the pairing force introduced from the superconductivity theory by Belyaev[19], plus a quadrupole force term. The inclusion of such a pairing force tends to abstract the features of interaction calculations into a more simplified form, which can thus be applied over a wide range of more complicated nuclei. The quadrupole term has the effect of introducing coherent behavior amoung nucleons which is needed for enhancement of E2 transition rates. The main assumption in the calculations of K S is that the low lying states of spherical nuclei can be treated in terms of two basic excitations, quasi-particles and phonons. The pairing force gives rise to the former and the quadrupole term accounts for the latter type of excitation. For the most part, K S treat these as separate modes of motion. The quasi-particle excitations, E_j, are calculated in terms of the single particle energies ε_j, the average Fermi energy λ, and a quantity called Δ, which is approximately one-half the gap in the even proton or neutron spectrum. The expression for E_j is:

$$E_j = \{(\varepsilon_j - \lambda)^2 + \Delta^2\}^{1/2}$$

*Hereafter referred to as K S.

In order to treat a large group of nuclei, K S have chosen ϵ_j for the various single particle levels and allowed them to vary as a smooth function of A in order to agree with experimental results. Different level spacings were used for neutrons and protons. In the region of their calculations, neutrons and protons are filling different shells, and since the pairing force is most effective for shell model pairs coupled to J = 0, two pairing force strength parameters were used, G_p and G_n. The quadrupole force is effective for all types of pairs, and thus has three strength parameters, X_p, X_n and X_{np}.

Having chosen the parameter, K S approximately diagonalize the pairing Hamiltonian by use of the quasi-particle transformation[19] for neutrons and protons separately. The quadrupole force is then described as an interaction between the proton and neutron quasi-particles, which gives rise to the phonon excitations.

The treatment of the quadrupole force is via the "quasi-particle random phase approximation". The reason for using this approximation instead of ordinary perturbation theory is that only 2^+ states among the many two quasi-particle states are affected. This gives rise to a spectrum of energy levels characteristic of energy levels in even-even nuclei[1], i.e., a 2^+ first excited state followed by a 0^+, 2^+, 4^+ triplet at twice the energy $\hbar\omega$ of the first 2^+ state. Thus, for even-even nuclei, the essence of the QRPA is to neglect terms in the quadrupole operator whose effects are spread over many

pair states of various angular momenta.

The model has been successfully applied[3] to nuclei from Ni to Pb, excluding the strongly deformed region ($150 \lesssim A \lesssim 190$). Agreement with energy level systematics throughout the region is qualitative, and E2 transition probabilities for the even-even nuclei are within a factor of two of the experimental values for the $2^+ \rightarrow 0^+$ gamma transitions.

More recently, Sorensen has performed calculations on E2 transition rates in odd mass spherical nuclei[20]. His results agree with experimental values to within a factor of two, while the actual values range over a factor of 1000. Thus, even though the calculations based on pairing plus quadrupole forces are, relatively speaking, very simple, the success is undeniable. The underlying reason is because this particular combination of forces leads naturally to the two most important residual effects, i.e., pairing effects and quadrupole deformation[21].

Although the K S calculations have given good results for spherical nuclei, they are not intended to be accurate for deformed regions for the simple reason that K S have considered the quadrupole term weak in comparison with the pairing effect. Investigations have now been undertaken to extend this type of calculation into the deformed regions by considering the former to be slightly stronger[22]. Initial calculations on the samarium isotopes indicate the model to be very promising[23].

1.B. The Shell Model: Deformed Nuclei

1.B.1. The Nilsson Single Particle Levels

For nuclei sufficiently far away from closed shell configurations, nucleon coupling gives rise to non-spherical nuclei. That such a phenomenon should exist can be pictorially explained in a progressive manner. If there is a single nucleon outside a closed shell moving in a shell model orbital, the nucleon density distribution is already non-spherical and concentrated in an equatorial plane. The addition of a second nucleon will best correlate with the average field of the first by moving as close to the plane of the first as possible. As can be seen, this is a compounding process. Thus, far from closed shells, nuclei are expected to be ellipsoidal. The amount of deformation is limited, of course, by the pairing correlation which tends to couple pairs to total angular momentum $I = 0$ spherical distributions.

Two different models have been used for calculations in the deformed region. The first, the collective model, separates the nucleus into a core and extra-core nucleons. This model is considered in the next section. The second, labeled as the Nilsson model[24], is in reality an extended single particle model. The auxiliary potential is considered nonspherical, the energies of the single particle states are calculated as a function of a deformation parameter δ, and the distortion which gives the minimum energy is taken as the actual distortion. δ is, in general, different for each single par-

ticle state. The actual potential used by Nilsson is

$$V_i = V_o\{(1 + 2\delta/3)(x_i^2 + y_i^2) + (1 - 4\delta/3)z_i^2 + C\ell_i \cdot s_i + D\ell_i^2$$

The above is, of course, an axially symmetric potential with $\delta_x = \delta_y = \delta/3$, $\delta_z = -2\delta/3$. The term in ℓ^2 serves to depress higher angular momentum states, leading to better agreement with the observed order. The constants C and D are chosen to yield the shell model states for $\delta = 0$. Nilsson has presented[24] his results in now famous diagrams, depicting the level spacing as a function of δ.

1.B.2. Additional Levels Built on the Deformed Single Particle Levels

Collective motions of the core nucleons are also known to give rise to rotational levels, i.e., levels with spacing

$$\Delta E = \frac{\hbar^2}{2\mathcal{I}} i(i + 1), \qquad i = K, K + 1, K + 2, \ldots,$$

where K is the projection of j on the nuclear symmetry axis. Thus, for odd A nuclei in the weak coupling limit, the spectrum of energy levels should be a few intrinsic states with a superposition of bands of rotational levels built on each.

More recent calculations including additional force terms due to pairing and Coulomb effects have been performed[25] to obtain an expression for δ. Such calculations are two-fold. First, they give a general contour of deformation over a much

broader range of nuclei than have been experimentally observed. Second, nuclear regions are searched where deformations might be expected but have not yet been experimentally observed, serving as a guide to future experiments to test the model.

The Nilsson model has enjoyed tremendous success in explaining the properties of odd-particle states in deformed nuclei[26]. It has also been successfully applied to nuclei which were not previously thought to be deformed. A case in point is the discovery by Paul[27] that the spectrum of ^{19}F can be described by the Nilsson model and that, in addition, the quadrupole transition rates are in better agreement with experiment than those derived from complicated shell model calculations[18].

1.C. The Collective Model: Even-Even Nuclei

1.C.1. The Various Collective Excitations

As introduced in the previous section, the collective model treats the nuclear core macroscopically as a deformable liquid drop with perhaps a few extra nucleons in an unfilled shell. For nuclear considerations, the core is considered as an incompressible, irrotational fluid, and the system then quantized[12]. Excited states of the nucleus can then arise from collective motions of the core, either through rotation of the body-fixed axes about the space-fixed axis, or by vibrations of the nuclear surface with respect to the body-fixed

axes. The system has been treated in detail by A. Bohr[28] and extended by Bohr and Mottelson[29].

1.C.2. Quadrupole Vibrations of Spherical Nuclei

Let us consider the vibrational effect first. The surface of the figure of general shape can be expressed as

$$R(\theta,\phi) = R_o[1 + \sum_{\lambda=o}^{\infty} \sum_{\mu=-\lambda}^{\lambda} \alpha_{\lambda\mu} Y_\lambda^\mu(\theta,\phi)]$$

where the $Y_\lambda^\mu(\theta,\phi)$ are the spherical harmonics. Surface motions are expressed by allowing $\alpha_{\lambda\mu}$ to vary in time. In the quadratic approximation, the kinetic and potential energies are of the form

$$T = 1/2 \sum_{\lambda,\mu} B_\lambda |\dot{\alpha}_{\lambda\mu}|^2$$

$$V = 1/2 \sum_{\lambda,\mu} C_\lambda |\alpha_{\lambda\mu}|^2.$$

C_λ and B_λ are related to the equilibrium radius, R_o, and to the surface tension, S. Such estimates are useful for nuclei provided appropriate values of R_o and S are used.

The frequency associated with the variable $\alpha_{\lambda\mu}$ is

$$\omega_\lambda = (C_\lambda/B_\lambda)^{1/2}$$

so

$$E_\lambda = n_\lambda \hbar \omega_\lambda.$$

The $\lambda = 0$ term describes density oscillations of a spherical nucleus which, if they occur, would be at much higher energies than incompressible vibrations. The $\lambda = 1$ terms simply describe translations of the center of mass and are not internal degrees of freedom. Thus, the first excited vibrational state corresponds to the $\lambda = 2$ quadrupole excitation and is therefore a 2^+ state (the ground state of all even-even nuclei have $J = 0^+$ andmost nuclei have a 2^+ first excited state). Because of λ dependence of ω_λ, $\omega_3 \cong 2\omega_2$ and $\omega_4 \cong 3\omega_2$. Hence, no additional terms are needed to describe low energy excitations.

Nuclei which can oscillate collectively about a spherical shape should thus show characteristic spacing of energy levels. The first excited state should have a 2^+ state corresponding to $\lambda = 2$. A $\lambda = 3$ phonon excitation has about the same energy as two $\lambda = 2$ phonons, so the second excited state should be a 3^- state or a 0^+, 2^+, 4^+ triplet. The latter is usually separated by perturbations arising from the coupling of two $\lambda = 2$ phonons to the 0^+ ground state. The center of gravity of the two phonon triplets should be about twice the energy of the one phonon state. The hydrodynamic model predicts $\hbar\omega_2$ should be about 2 MeV for A near 100 and fall to 1 MeV for A near 200. In reality, $E_{2'}/E_2$ does in fact cluster around a value near 2, but $\hbar\omega_2$ is approximately half that predicted. This simply means that the hydrodynamic calculations for C_λ and B_λ are not accurate enough. The crucial test of the theory is the comparison of the E2 transition rates with experiment. They are in substantial agreement, indicating that the low

lying states of even-even nuclei are probably one and two phonon quadrupole vibrations. The regions of deviation are those where nuclei are known to have permanent deformations.

I.C.3. Excitations of Permanently Deformed Spheroidal Nuclei

Nuclei with permanent, non-spherical shapes can also be considered in the framework of this model, but a different set of coordinates is more convenient. Considering only spheroidal ($\lambda = 2$) deformations, the orientation of the principal axes of the nucleus with respect to the space fixed axes is specified by the Euler angles. By well known transformation equations, the five variables $\alpha_{2\mu}$ are replaced by the three Euler angles, and β and γ. β is a measure of the total deformation of the nucleus and γ indicates its shape. The equations defining β and γ show that if β changes in time, producing β vibrations, while γ remains fixed, the nucleus preserves its symmetry axis but alters the eccentricity of its elliptical cross-section. The axial symmetry of the nucleus is lost in γ vibrations.

In the new coordinate system,

$$\mathcal{H}_c = 1/2B(\dot{\beta}^2 + \beta^2\dot{\gamma}^2) + 1/2\sum_{K=1}^{3} \mathcal{I}_K \omega_K^2$$

where the ω_K are the angular velocities of the principle axes with respect to the space fixed axes and $\mathcal{I}_K$ corresponds to the moments of inertia. Thus, terms corresponding to rotational motion are automatically incorporated into the theory.

For axial symmetry, such a term predicts low lying states

$$E_J = \frac{\hbar^2}{2\mathcal{I}} J(J+1), \qquad J = 0,2,4, \text{----}.$$

Experimentally observed level spacings agree quite well with this prediction. Small deviations may be ascribed to weak coupling of the rotational modes of motion to other modes, either vibrational or particle. The remarkable accuracy with which experimentally observed energy levels in distorted nuclei fit the rotational formula[1,12] leaves little doubt about the collective nature of the excitations.

β and γ vibrational levels are expected to be much higher in energy than the rotational bands. Thus, distorted nuclei will, in general, be expected to exhibit rotational bands built on the vibrational levels. Due to weak coupling, the rotational spectra of succeedingly higher bands are expected to show more deviation from the predicted level spacing. Of course, the possibility of particle excitations is also present, but is not expected below 1 MeV for even-even nuclei.

1.C.4. Ellipsoidal Nuclei

Davydov and coworkers have considered the rotational levels of permanently deformed non-symmetric nuclei in a series of articles, beginning in 1958 [30]. The model predicts slight deviations from the J(J + 1) energy level separation of the rotational states, but such an effect could be masked by coupling to β or γ vibrations. A very sensitive test of the model

lies in the fact that it predicts a 3^+ state, whose energy is the sum of the first two 2^+ states. This prediction has been confirmed in about a dozen cases. The model has also been tested in the spherical region[6,31] and, for reasonable values of the parameters, predicted E2 transition rates are in agreement.

1.D. The Collective Model: Odd Mass Nuclei

Odd mass nuclei exist with both spherical and deformed shapes, just as in the case of even-even nuclei. Those with permanent deformations fall in the same regions of the periodic table. The odd nucleon is expected to give rise to low energy states and the ground state should be characterized by a shell model configuration. For spherical nuclei, the single particle model predicts the ground state, while the Nilsson model is applicable in the (axially symmetric) deformed regions. In addition, there should be states arising from the coupling of states of the odd particle with collective excitations of the core in both regions.

Let us first consider the near spherical nuclei, where the Hamiltonian can be written as

$$\mathcal{H} = H_c + H_{sp} + H_{int}.$$

H_{int} is a weak surface coupling term. It is only appreciable in the tail where the nuclear density is changing, and can be treated by perturbation methods. De Shalit has discussed pos-

sible experimental evidence for such a model[32]. The expectations based on such a model are as follows: The lowest lying states will be the single particle states. At higher energies the core can give rise to quadrupole vibrations and, when coupled to the single particle state j, can produce a multiplet of states with spin $J = j \pm 2$, $j \pm 1$, or j. The "center of gravity" of the multiplet should be $\hbar\omega$, the first phonon energy of the core. The splitting of the multiplet arises from, and perhaps gives a measure of, the perturbing effects of the interaction term.

A more complex problem arises when two $\lambda = 2$ phonons or a $\lambda = 3$ phonon excitation of the core is considered. In such cases both particle and collective states are expected to be modified and considerable mixing of the states may occur. Under these circumstances one can no longer expect to describe a state as particle or collective, but as an admixture of both. The situation is then described as "intermediate coupling". Calculations based on such a scheme have been performed for specific nuclei by Choudhury[33], Glendenning[34], Bannerjee and Gupta[35], and O'Dwyer and Choudhury[4]. The calculations of O'Dwyer and Choudhury are of particular interest here since they have been performed for the odd mass iodine isotopes. They have considered the last odd proton of these 53 proton nuclei to have the $2d_{5/2}$, $1g_{7/2}$ and $2d_{3/2}$ single particle states available. The proton state is then coupled to the collective surface vibrations of the even-even core. The resulting Hamiltonian of the coupled system, including one and

two phonon states associated with quadrupole vibrations, is then diagonalized. The inclusion of the $d_{3/2}$ state was found to favorably influence the results, depressing the $g_{7/2}$ state sufficiently to make it the ground state for the higher mass isotopes, in agreement with experimental results. The model predictions are discussed further in Chapter 3. It should also be pointed out that this type of calculation is expected to improve as better experimental data for fitting of the parameters become available.

Excited states of deformed nuclei have been discussed by Kerman[36] and, from a different approach, by Pashkevich and Sardaryan[31]. Kerman has obtained an expression for the energy level spectrum for axially symmetric nuclei by considering strong coupling of the Nilsson levels to rotational states of the deformed core. The energies of the excited states $E_{J,K}$ are given by

$$E_{J,K} = \varepsilon_K + \frac{h^2}{2\mathcal{J}}[J(J+1) - 2K^2 + \delta_{K,1/2}a(-1)^{J+1/2}(J+1/2)]$$

where ε_K = Nilsson single particle energy, J = total angular momentum, K = projection of J on the nuclear symmetry axis, $\mathcal{J}$ = the moment of inertia, and a = the decoupling parameter. The fact that only one moment of inertia, $\mathcal{J}$, enters into the equation stems from the axial symmetry of the motion of the nucleons. There is no quasi-rigid rotation about the symmetry axis, but collective oscillations of nucleons giving rise to surface waves. Thus $\mathcal{J}_3 = 0$ and $\mathcal{J} = \mathcal{J}_1 = \mathcal{J}_2$. The de-

coupling parameter expresses the strength of the particle-rotational motion coupling. The energy level spectrum is then a rotational band built on each single particle level. All values $J \geq K$ are permitted, and when $K \neq 1/2$, the spectrum order is $J = K, K + 1, K + 2, \ldots$. If $K = 1/2$, the ordering is determined by the value of a; viz. $a = -2.5$, the order is 3/2, 1/2, 7/2, 5/2, 11/2, 9/2, ... Additional correction terms arise from weak coupling of rotational-vibrational coupling. Kerman's calculations have been successfully applied to describe the levels of odd A deformed nuclei[36].

The calculations of Pashkevich and Sardaryan[31] involve asymmetric deformations. They are quite successful for nuclei in the deformed regions. The authors have also performed calculations for the "spherical" ^{119}Sb nucleus. Comparison of the predictions with the most recent experimental data shows some agreement with the low energy states, but cannot explain the observed negative parity state nor the low spin states occurring above 1 MeV[37]. However, the overall agreement is probably as good as that of Kisslinger and Sorensen's calculations[3].

1.E. Summary

To summarize, the model calculations of particular interest to the experimental results reported here are those of Kisslinger and Sorensen[3] and of O'Dwyer and Choudhury[4] for the iodine isotopes, and those of Talmi and Unna[5] and Mayer and Jensen[16] for the strontium and rubidium level schemes.

The results are presented in more detail in Chapters 3 and 4 in connection with the decay scheme discussions.

CHAPTER 2

THE TOROIDAL FIELD ELECTRON SPECTROMETER

One of the most valuable instruments in nuclear spectroscopy for the study of internal conversion electrons still is the magnetic spectrograph, in spite of the recent advances in high resolution semiconductor detectors. Conversion electron spectra afford accurate determinations of nuclear transition energies as well as allowing the separation of many peaks not resolved in the NaI(Tl) gamma scintillation detectors. Until recently, typical resolutions for gamma-ray detectors were in the vicinity of 8% while electron spectrometers operate in the range from 4% down to 0.01%, depending on the type of instrument. The lithium-drifted germanium detectors [Ge(Li)] have now removed the resolution problem to a great extent for gamma rays. However, the electron spectrometer remains important because of the additional information which it makes available.

The relative intensities of the internal conversion electron lines and photons from transitions between nuclear energy levels can give accurate information on the multipolarities of the transitions. In particular, the internal conversion coefficient α, defined as[10]

$$\alpha = \frac{Ne}{N\gamma},$$

is a very sensitive function of multipolarity for a particular

energy. Thus, measurements of the electron line intensities of a single nuclear transition, denoted by K, L_I, L_{II}, L_{III} ..., with respect to the number of gamma rays of that transition, determine the α_K, α_{L_I}, $\alpha_{L_{II}}$, $\alpha_{L_{III}}$, ... When these numbers are compared with the accurate theoretical values[10] for the α's, the multipolarities are determined. The conversion coefficients become quite large for low energy, high multipolarity transitions. Thus, if such a transition exists, conversion electron measurements become essential for a complete decay scheme analysis since such transitions are often almost totally converted.

Aside from conversion electron spectra, magnetic spectrometers are well suited for detailed study of continuous beta spectra, which also yields additional information to the experimenter.

The first beta-ray spectrometer that utilized the focusing properties of a magnetic field was constructed by J. Danysz[38] in 1912 while an assistant in the laboratory of Marie Curie. Following the success of this first simple instrument, empirical and theoretical studies on magnetic focusing have advanced tremendously[39]. Spectrometer design and construction have taken on many facets. However, the spectrometers can be categorized into two general types: a) the transverse field or "plane focusing" and b) the longitudinal field or "space focusing" spectrometer. In the transverse field spectrometer, the electron orbits are circular, lying in a plane, while a longitudinal field produces helical particle paths. The lat-

ter is generally referred to as a "lens" spectrometer. The type of spectrometer constructed is governed by the experimental situation, e.g., the famous transverse field $\pi\sqrt{2}$ instrument gives the highest resolution yet attained while the lens type has a higher transmission.

Prior to 1950, spectrometers had the inherent (and undesirable) feature that $T/R \leq 2$, where T is the transmission of the instrument and $R = \Delta p/p$ is the resolving power. Thus a $\pi\sqrt{2}$ spectrometer operating at 0.10% resolution would have a comparable transmission, while a lens spectrometer operating at 2.0% resolution may have a transmission as high as 4% for the double lens system. At this point Nielsen and Kofoed-Hansen[40] turned their attention to investigating a totally different design whereby, with modest resolution of the order of 1%, transmissions as high as 10% could be attained. The result of this work is the "orange" spectrometer, so named because the magnet wedges and air gaps are a geometric facsimile of orange segments. The original machine and the majority of those which followed are constructed of six wedge shaped magnets, separated by six wedge shaped gaps through which the electrons travel. Thus, it is actually six spectrometers, symmetrically arranged around a circle. The symmetry of the machine has led to additional advantages other than the originally intended one of higher T/R ratio.

The orange spectrometer, as originally constructed by Nielsen and Kofoed-Hansen[41] and later enlarged by Bisgård[11], is a completely symmetric instrument. The source and detector

are placed on the symmetry axis equidistant above and below the median symmetry plane of the spectrometer. The gaps and magnet wedges are placed around the symmetry axis. In theory, the entrance and exit profiles of the pole tips are identical. Thus, the field is essentially a toroid, with the central portion of the machine free of magnetic fields. This facilitates the placement of an alpha, beta or gamma detector directly above the source for experiments involving coincidences of these radiations with the focused electrons.

The geometry is also amenable to the introduction of an accelerator beam, using the target as a source[42]. The high transmission of the instrument should thus make electron studies of very short-lived isotopes or states ($\lesssim$ 1 sec) feasible. The group at Chalk River has recently performed such experiments with a 7 gap orange spectrometer and a Tandem Van de Graaff[42]. It is also possible to use a separate detector for each gap and with such an arrangement, directly accumulate information on the angular distributions of the conversion electron spectrum in coincidence with direct reaction particle groups. The MSU instrument was originally conceived for such on-line cyclotron experiments, independent of the above reference[42]. However, the incomplete beam transport system has thus far limited our studies to conventional radioactivity investigations.

2.A. Theory of Toroidal Spectrometers

The theory of the focusing of a $\frac{1}{r}$ type magnetic field, and its application to orange type spectrometers, has been studied in detail by Jaffey and co-workers[43]. For a complete description, the reader is referred to their work. However, the semi-quantitative features of the theory can be presented with little difficulty if a few simplifying assumptions are made.

It is convenient to apply cylindrical coordinates to this situation where the z axis passes through the source and focus. The magnet wedges and gaps are placed in a circle about the z axis. The distance of the electron orbit from the z axis is r and $\phi(o \leq \phi \leq 2\pi)$ is the angle of rotation about the axis. The electron orbits thus lie in the z-r plane. The current in the z-r plane closely approximates a closed curve, so the field component in the r direction is zero. The magnetic field is assumed to follow a closed curve, describing the toroidal boundaries of the pole faces. Thus, neglecting fringing effects, the space outside the closed ring has zero magnetic field while inside the ring

$$B_r = B_z = 0,$$

$$\text{and} \qquad B_\phi \sim 1/r. \tag{1}$$

B_ϕ can be calculated by applying Ampere's circuital law. In Gaussian units

$$\frac{4\pi NI}{c} = \oint \vec{H} \cdot d\vec{\ell} \qquad (2)$$

where N is the total number of turns in the ring of coils and c is the speed of light. Applying (2) to the different regions of the field

$$\frac{4\pi NI}{c} = \underset{\text{gap regions}}{\int \vec{H}_o \cdot d\vec{l}_o} + \underset{\text{iron regions}}{\int \vec{H}_i \cdot d\vec{l}_i} \qquad (3)$$

Since $\vec{B}$ and $\vec{H}$ are exactly parallel in a vacuum and very nearly parallel in the iron, assume

$$\vec{B} = \mu \vec{H}$$

where $\mu = \mu_o$ for vacuum and μ_i for iron.

$$\frac{4\pi NI}{c} = \frac{1}{\mu_o} \underset{\text{gaps}}{\int \vec{B}_o \cdot d\vec{l}_o} + \frac{1}{\mu_i} \underset{\text{iron}}{\int \vec{B}_i \cdot d\vec{l}_i} \qquad (4)$$

Since $(B)_N$, the normal component of B, is continuous across the boundaries between the regions of different permeabilities,

$$(B_o)_N = (B_i)_N = B_\phi \qquad (5)$$

Upon integration, equation (4) becomes

$$\frac{4\pi NI}{c} = \frac{B_\phi \alpha}{\mu_o}\left[1 + \frac{\beta}{\alpha}\frac{\mu o}{\mu_i}\right]$$

where α is the total gap width and β is the total iron width. For the present instrument, $\beta/\alpha = 2$ while the ratio of permeabilities of vacuum to iron is $\approx 10^{-4}$. Thus, neglecting the last term,

$$\frac{4\pi NI}{c} = \frac{B_\phi \alpha}{\mu_o}$$

With $\alpha = 6r\phi$ (six gaps each of angle ϕ) the ϕ component of B can be written

$$B_\phi = \frac{2\pi \mu_o NI}{3\phi c}\frac{1}{r} \qquad (6)$$

In order to arrive at an expression for electron orbits in a 1/r field, consider the general formula for the radius of curvature, ρ, of a curve $y = f(x)$ at any point $P(x,y)$.

$$\rho = [1 + (dy/dx)^2]^{3/2}/(d^2y/dx^2)$$

$$= [1 + (f'(x))^2]^{3/2}/f''(x) \qquad (7)$$

The radius of curvature of electron orbits, ρ, is given by the famous expression

$$\rho = cp/eB \qquad (8)$$

where p = the electron momentum and e = the electron charge.

Let

$$\rho = br.$$

Then, from (6)

$$b = \frac{3pc^2\phi}{2eNI\mu_o} \tag{9}$$

The present instrument has a value b = 0.6. For an inhomogeneous field, eq. (8) is still true, except that B and ρ are no longer constants.

Applying (7) to (8) and using the identities

$$f(x) \equiv r(z),\ f'(x) \equiv r'(z),\ f''(x) \equiv r''(z) \equiv \frac{dr'(z)}{dz},$$

equation (7) becomes, upon integration,

$$z = \int \frac{\log(y/z)\ dy}{\{b^2-[\log(y/a)]^2\}^{1/2}} + z_o \tag{10}$$

where a and z_o are two constants of integration.

Equation (10) gives rise to trajectories of the type shown in fig. 1. These curves are more conveniently described in terms of the parameter θ which is defined as the angle between the z axis and the tangent to the curve. In the parametric representation,

$$\begin{aligned} r &= a\cdot e^{-b\cos(\theta)} \\ z &= a\cdot b\cdot U(b,\theta) + z_o \\ \text{and}\quad U(b,\theta) &= \int_{\pi}^{\theta} \cos(x)\cdot e^{-b\cdot\cos(x)}\,dx \end{aligned} \tag{11}$$

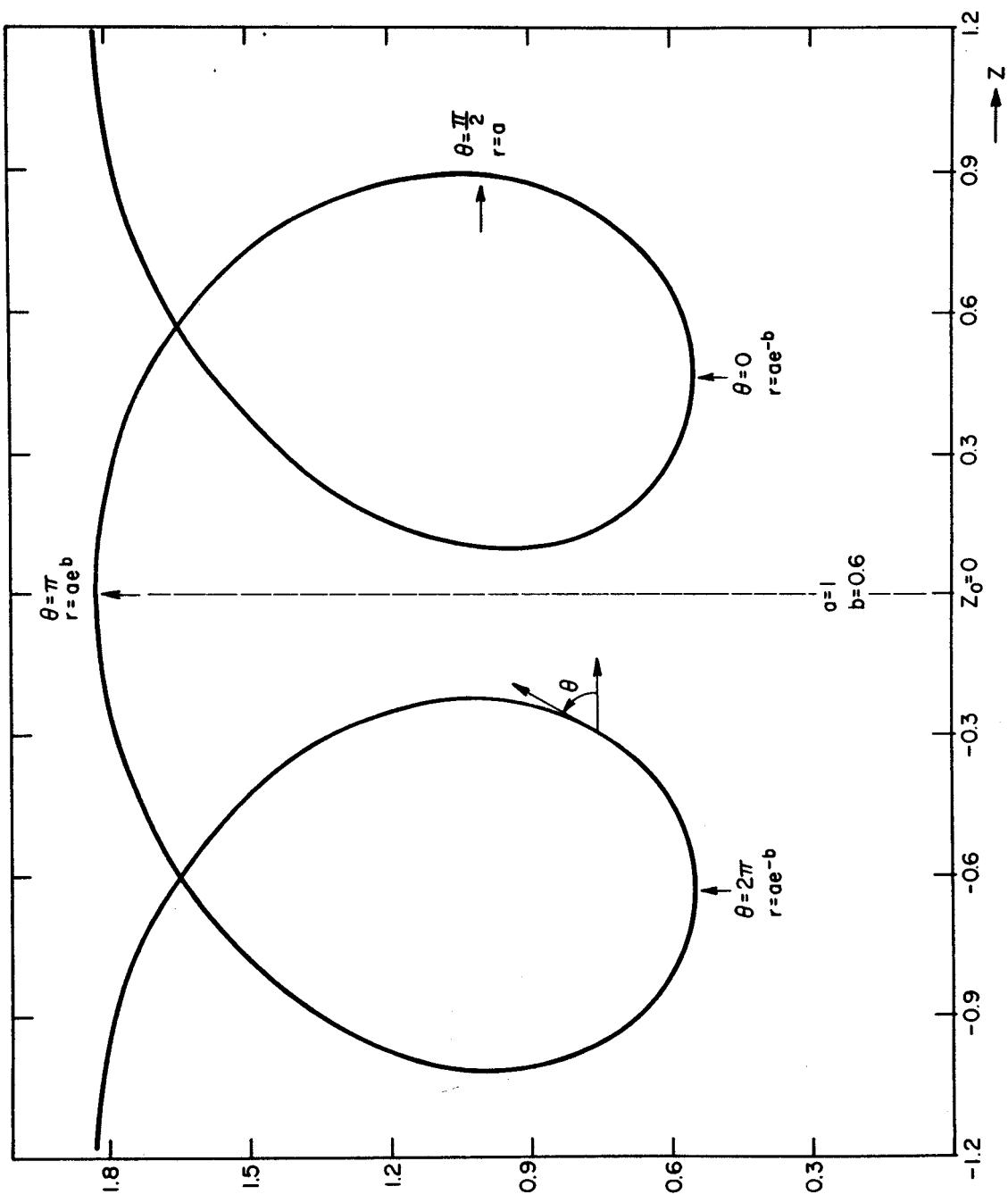

Figure 1. A typical electron trajectory in a 1/r field, which has infinite extent in the Z direction. The curve was calculated by a numerical integration of equations (11), with the parameters a = 1.0 and b = 0.6. The units of length for Z and r are arbitrary.

Then $z = z_o$ for $\theta = \pi$ and a corresponds to the value of r for $\theta = \pi/2$. Also,

$$r_{min} = ae^{-b}, \quad r_{max} = ae^{b}.$$

Thus,
$$\frac{r_{min}}{r_{max}} = e^{-2b} = \text{constant} \tag{12}$$

independent of a, the integration constant. a is simply a scale factor describing the family of curves which are similar with respect to $z - z_o$ on the z axis.

Figure 2 shows how portions of a 1/r field can be used as a focusing spectrometer. Theoretically, the boundaries of the pole faces can be determined from a numerical integration of eqs. (11) if no corrections are assumed necessary for fringing field. As in fig. 2, a value of b is chosen as well as the position of the source on the z axis. A family of trajectories is then drawn by varying the parameter a. From eqs. (11), $r' = \tan\theta$ from which it follows that a tangent can be drawn from the source position $(z_s, 0)$ to any trajectory. Then the points (r_j, z_j) should trace out the transition point from a $B = 0$ to the $B = \frac{Bi}{r}\hat{\phi}$ field, i.e. the profile of the pole face. The theoretical boundaries shown in fig. 2 have actually been calculated from closed expressions. In practice, there are fringing fields which distort the orbits near the entrance and exit slits. These aberrations are empirically corrected by shaping the pole profile.

Finally, it should be clear that if z_o is picked as the point for the location of a symmetry plane, then the entrance and exit profiles are identical. Then $z_f = 2z_o - z_s$. How-

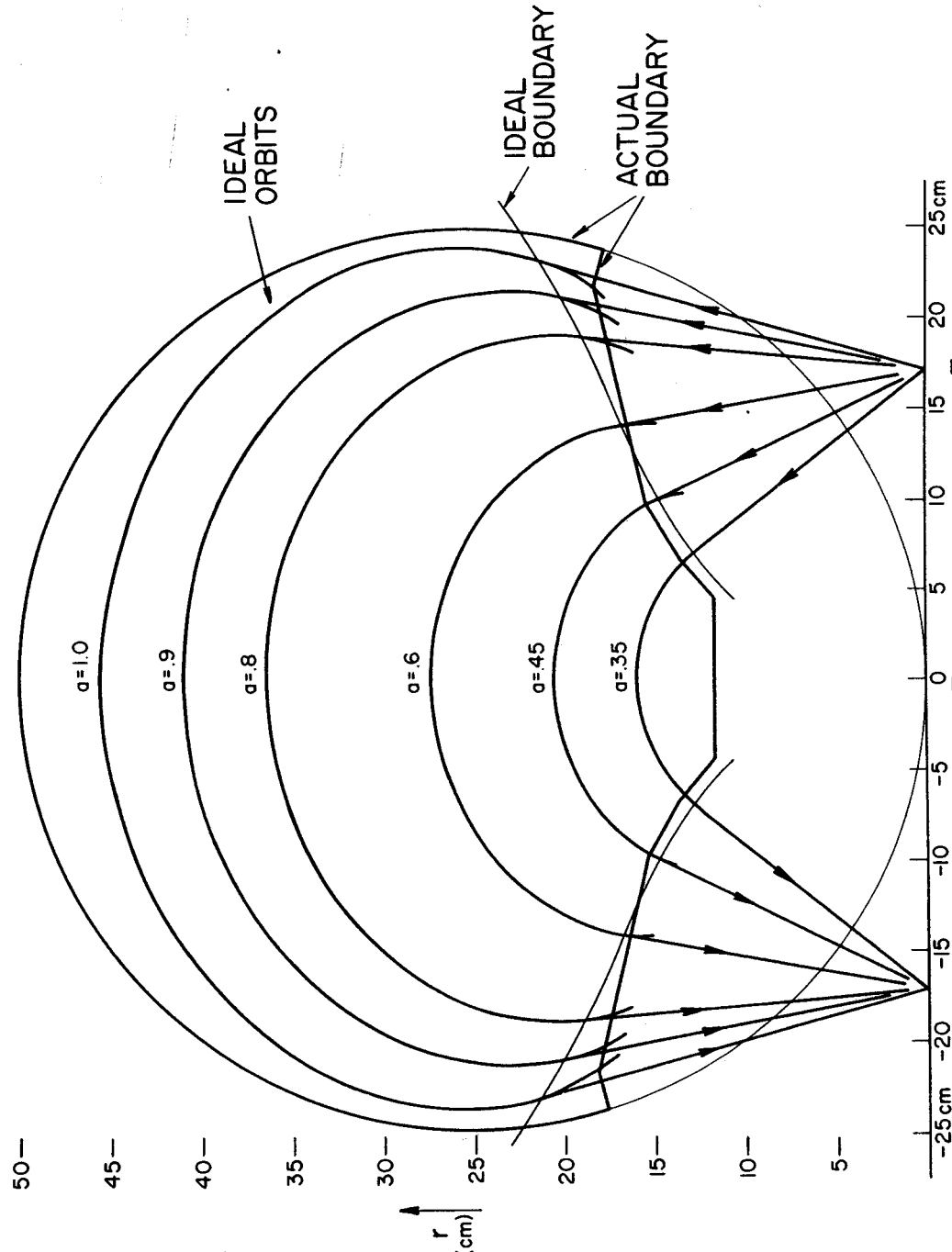

Figure 2. Typical electron trajectories in a 1/r field as a function of the parameter a for b = 0.6. This figure thus shows how portions of the field can be used for focusing. The orbits are drawn to scale for the present spectrometer, and the actual pole boundaries are shown. The theoretical boundary for focusing neglecting fringing fields, is also shown.

ever, as Nielsen et al. point out in their original article[40], an asymmetric machine would also produce focusing if the geometrical situation (i.e. $z_f \neq 2z_o - z_s$) warrants the additional experimental difficulties of shaping both entrance and exit profiles separately.

In a spectrometer with symmetrical entrance and exit curves, there should be a first order focusing with a magnification of unity. This should also hold true for particles emitted from points lying at small distances from the z-plane, as discussed by Nielsen et al.[40].

The instrumental dispersion, defined as $D = \frac{\Delta x}{\Delta p} p$, has been evaluated both theoretically and empirically. In this expression, Δx is the distance between foci of particles with momentum between p and $p + \Delta p$. In both instances the dispersion has been shown to be a strong function of ψ, the angle of electron emission measured with respect to the symmetry axis. The dispersion varies from about 400 mm in the inner parts of the gap to 900 mm in the outer portions for instruments of the size of the MSU spectrometer. For normal gap openings the average dispersion is about 600 mm.

The major fraction of the resolution problems with this type of spectrograph are those associated with the fringing fields. In the proper shaping of the pole profiles to give the best resolution, the following effects were considered: Axial defocusing, the lens effect, an effect due to a non-uniform field, source size, and mechanical alignment. These are discussed in this order.

Axial Defocusing. The fringing field will have a component in the direction of the interior toroidal field. Thus, there will be an additional deflection due to the effective boundaries being outside the real boundaries. Furthermore, the fringing field has different effects for different ψ values. Thus, the theoretical profiles shown in fig. 2 will no longer be quite correct. One would expect to correct this effect by reducing the region enclosed by the profile, and changing the profile somewhat. This is the procedure followed to some extent by Bisgord[11]. Unfortunately, B_ϕ in the fringing region also changes with ϕ, as can be seen from fig. 3. Thus, a correction for the axial defocusing in the median plane does not work for all ϕ values. This is one of the reasons that the part of the gaps close to the pole plates are not usually employed in the spectrometer.

The Lens Effect. The fringing field at a given point near the entrance can be decomposed into B_ϕ and B_{rz}, as shown in fig. 3. B_{rz} can be further decomposed into B_t and B_i, where B_t is along the trajectory and B_i is perpendicular to it. The net result of B_i is to extend point sources into line images. The axial defocusing problem discussed above actually causes the line image to have considerable curvature.

Non-Uniform Field Effect. An indirect effect of the fringing field is to cause a variation of B_ϕ with ϕ inside the gap with B_ϕ being stronger near the pole plates than in the median plane. This is then another reason for not using

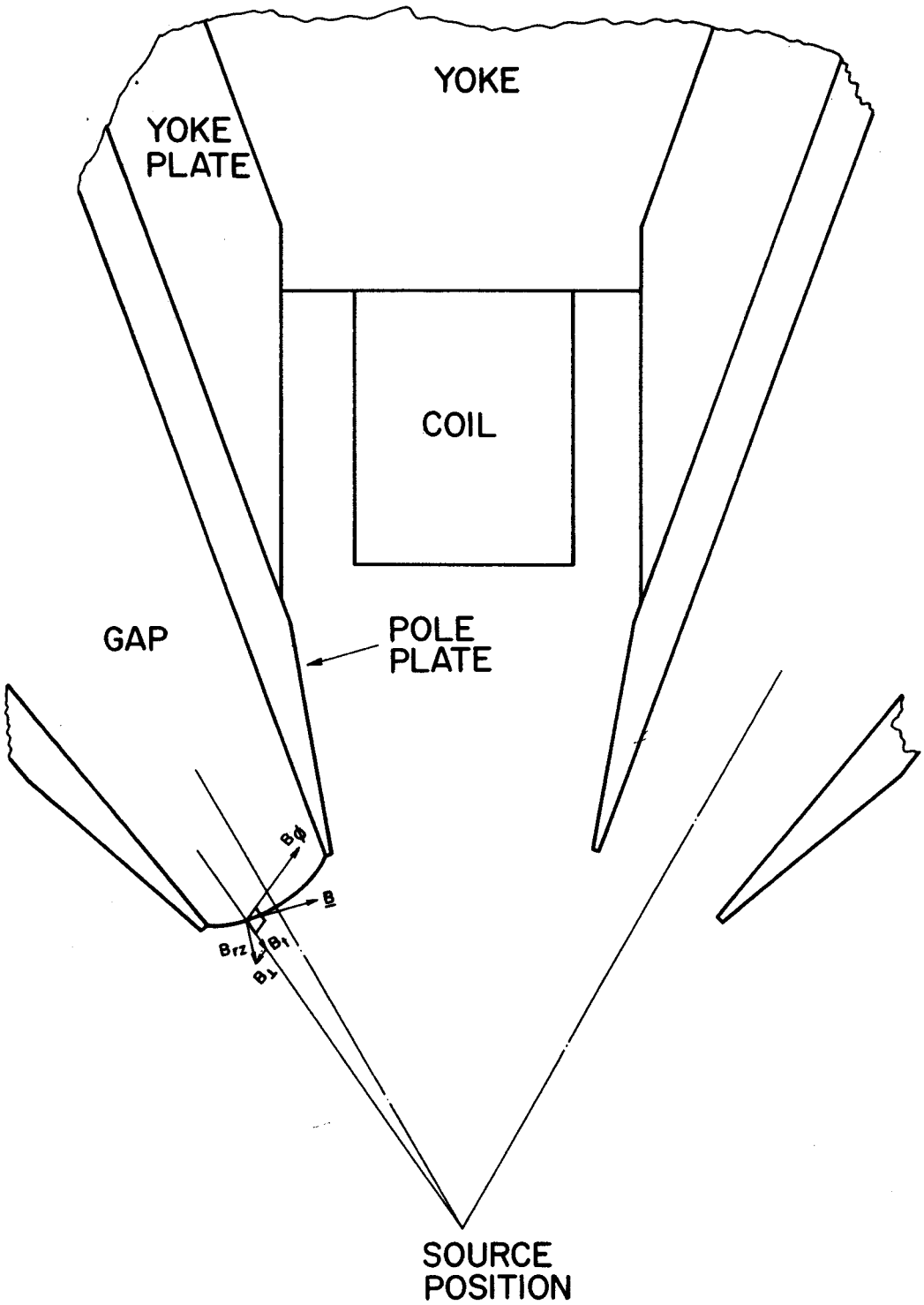

Figure 3. The central region of the spectrometer showing two of the six gaps, as viewed from above, along the symmetry axis. A typical fringing field line is also shown, and is decomposed into its various defocusing components.

those parts of the gap near the poles for the experiments requiring the best resolution.

Source Size. The theory of focusing is for point sources. However, sources of a 2 mm extent do not seriously affect the resolution unless detector slit widths of smaller dimensions are being employed.

Mechanical Alignment. In theory, the instrument should be constructed as 6 identical spectrometers working in unison with no problems involved in the focusing properties by the addition of the several gaps. In practice, this task is difficult to overcome.

As an example, the MSU spectrometer is a 1.0000 ± 0.0001 meter diameter circle. The pole plates are vertical to within $\pm 0.1^0$ and the radial alignment is better. Even a minor misalignment problem has been found to deteriorate the resolution by a significant factor.

2.B. The Michigan State University Multigap Spectrometer

The orange spectrometer is essentially the same design as that described by Bisgord[11]. However, enough innovations have been used to warrant a description here for the purpose of those who wish to use it in the future.

2.B.1. The Vacuum System

The vacuum tank for the present instrument measures approximately 48 inches in diameter and 22 inches high. It was constructed by rolling 1-1/8 inch thick aluminum plate into semicylinders and joining the two halves by a heliarc weld. An additional ribbon of aluminum 1-1/8" x 2" was welded around the outer upper and lower peripheries to provide larger vacuum gasket surfaces. The lid and base plate are of the same material with grooves constructed to accommodate vacuum gaskets. Six brass rods around the central detector ports maintain positive separation of the lid and base plate. Although considerable difficulties were encountered in welding such large volumes of aluminum, the tank shows no leaks when tested with a mass spectrometer leak detector.

The pumping system consists of 2 mechanical pumps, one of 15 cfm serving as a roughing pump and a second of 10 cfm used as a combination forepump and roughing pump. In addition, a 5 inch diffusion pump is available for those applications requiring high vacuum. The mechanical pumps, operating in parallel, evacuate the system to 100 μ in 13 minutes. The diffusion pump can produce a vacuum of 5×10^{-5} mm Hg in an additional 10 minutes, or 5×10^{-6} mm in an additional 30 minutes. The quoted pumpdown times are for the assembled spectrometer, not just the tank alone. No applications are foreseen where better vacuums will be necessary.

The pressure is measured by means of a thermocouple gauge in the low vacuum range or a discharge gauge at high

vacuum.

2.B.2. The Magnet System and Coil Design

The iron parts used in the Michigan State spectrometer were made from prints provided by Bisgord[44]. These parts were made of low carbon Swedish steel by Dansk Insudstri Syndikat, a Copenhagen firm. Thus, the magnet section is, in principle, identical to Bisgord's design. However, the coil design has been governed by two factors: 1) the maximum number of ampere-turns which can be produced by an existing power supply and 2) a shape reduction required in the dimension of the coils to provide space to allow the cyclotron beam to pass beside or over the coils, if desired. The latter problem was solved by using pre-insulated square copper tubing. The insulation is a double dacron-glass fiber tightly bonded with vitrotex resin†. The tube dimensions are 3/16" square outside with 1/8" diameter hole for internal water cooling. The material was supplied in 1200 foot lengths.

The final configuration of the coils is 12 layers of the tubing with 10 turns per layer. The total length of wire on each coil is about 250 feet. Each layer is electrically insulated from the previous by 1/16" layer of laminated fiberglass. The core is simply a segment of brass pipe machined to the desired dimension. After each coil was wound, it was placed in a mold, saturated with a low vapor pressure epoxy

†Obtained from Anaconda Wire and Cable Company.

and evacuated. This evacuation insured good penetration of the epoxy throughout the coil. They were then baked as prescribed by the manufacturer, producing an extremely rigid and durable package.

The procedure followed in winding the coils insured that the number of turns varied by less than 1/4 turn out of the 120 turns total. Resistance measurements were also carefully performed on each, and all were found to be within the variation produced by slight temperature changes, insuring that they contained no shorted turns. The cooling has been found to be very effective also. With a parallel flow of 1/4 gallon per minute per coil, there is a temperature rise of only 10° C at 50 amps. Of course, such a system construction requires deionized water, which is readily available in the Cyclotron Laboratory. This type of cooling is considered much more desirable than the external cooling of the coils of the previous instruments[11,41].

2.B.3. The Power Supply

The power supply is an all-transistorized constant current unit capable of producing 50 amps at 50 volts. The power source is a 208 V, 3 phase, motor driven auto-transformer whose output is a slight modification of that reported by Patlach[45]. The circuit diagram is shown in figs. 4 and 5. The reference voltage is provided by a network of resistors across a mercury cell as shown in fig. 6. The current has been found to be stable to better than 5 parts in 10^5 for short term periods

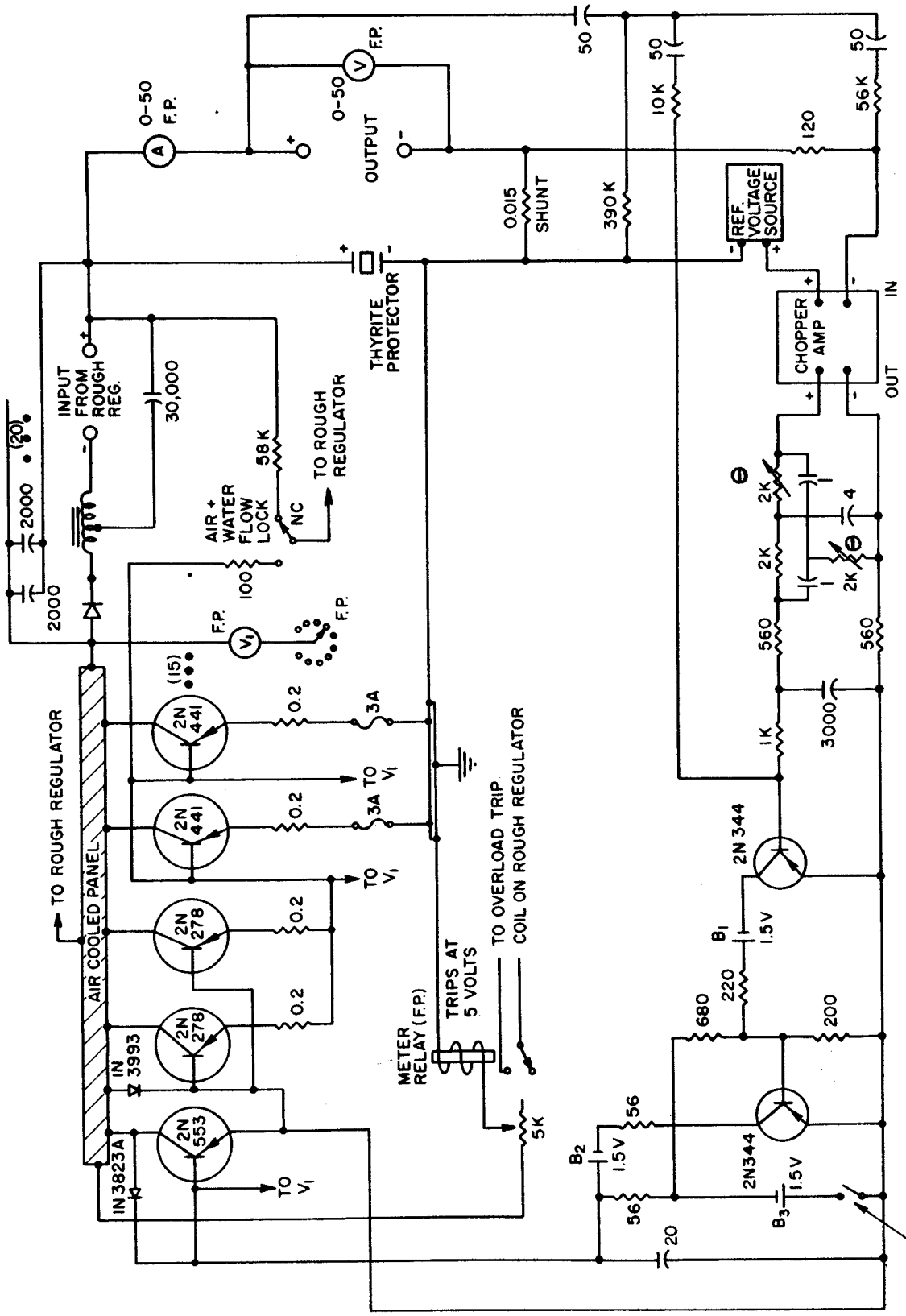

Figure 4. The circuit diagram of the fine current regulation system.

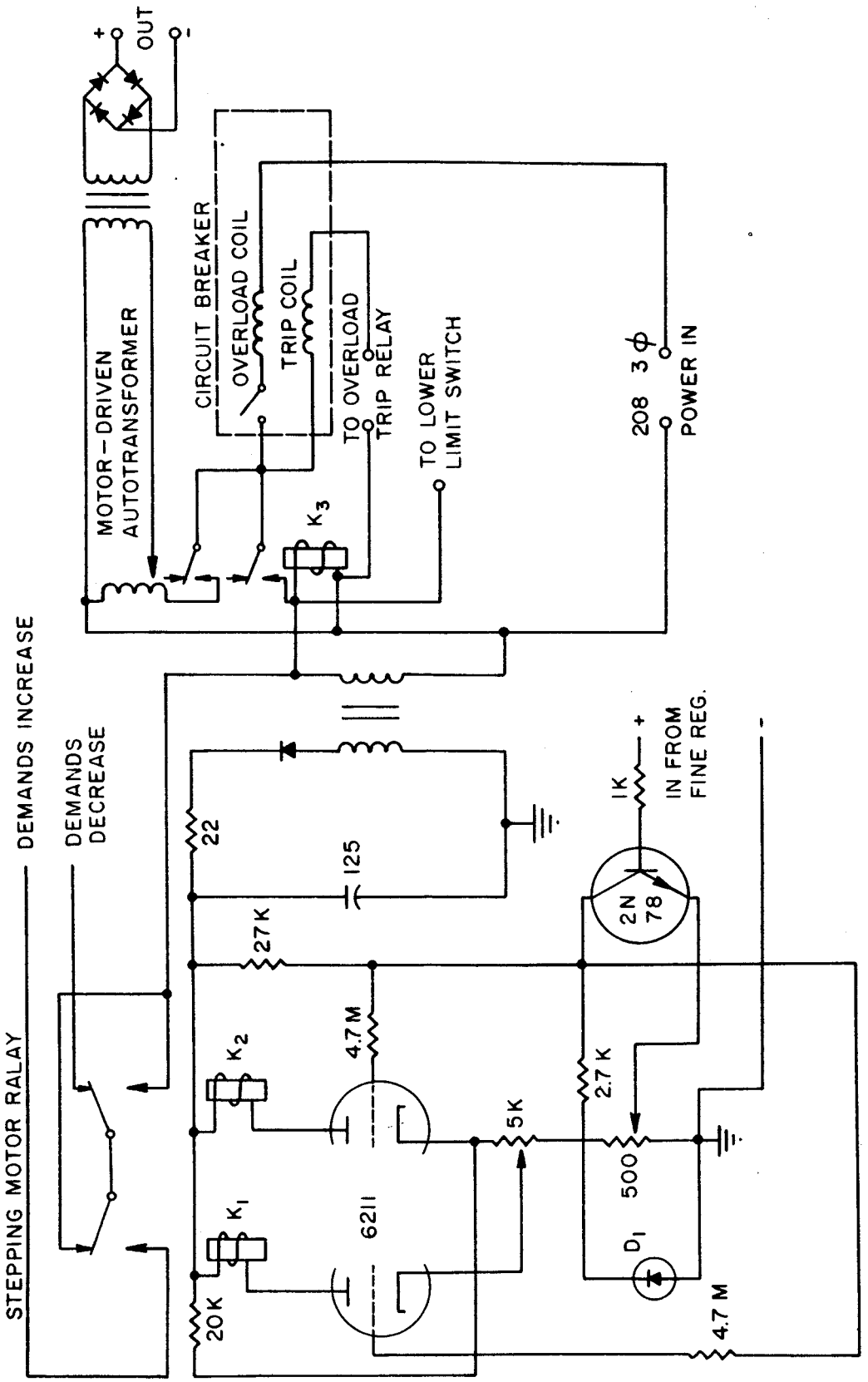

Figure 5. The motor driven transformer power source with coarse current regulation. The coarse current regulator drives the fine current regulator.

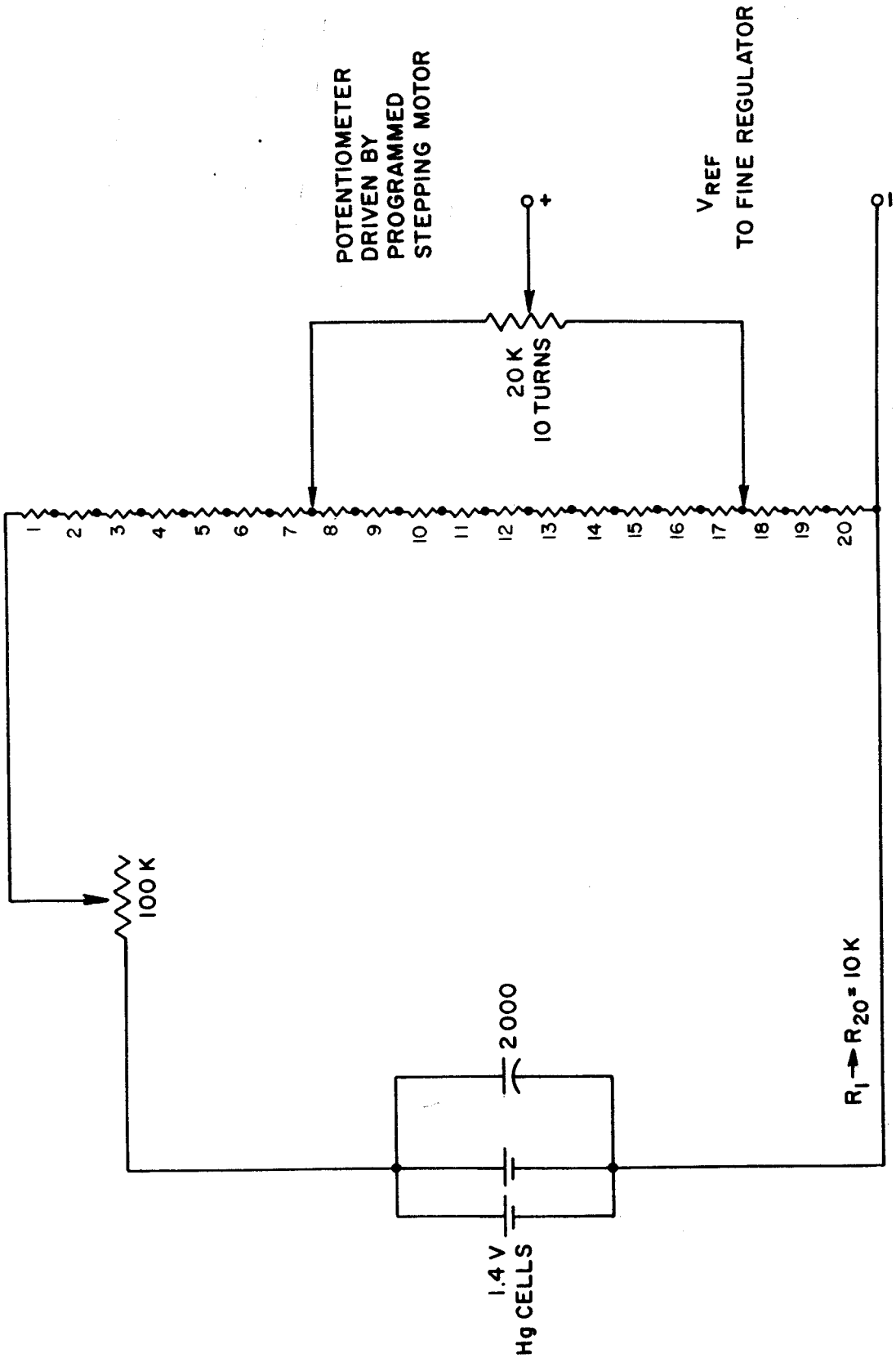

Figure 6. The reference voltage source whose output is controlled by a stepping motor driven potentiometer. The stepping motor is actuated by a programmable pulser unit which is coupled to the automation system.

(5 min.) with extreme drifts of $1/10^4$ over a period of a day. Although the regulation of the magnetic field itself, instead of the current, would give better regulation, the present system is very satisfactory for this type spectrometer and the achievable resolutions. It is felt that simply using better resistors and stabilizing the temperature of the power supply will give considerably better stabilities.

A very convenient feature of the power supply is the ability to check base-collector voltage drops of all the power transistors. Thus, in the event of a failure of one of the transistors, it can be located immediately by a quick meter check.

A simple, yet very effective automation system for stepping the power supply has been constructed. A block diagram of the system is shown in fig. 7. The principal components are a stepping motor driving a potentiometer, a programmed pulse system to step the motor, mechanical timers, and a printing scaler. The system is capable of counting times continuously variable from 4 seconds to 20 minutes and read-out times ranging from 2 sec. to 2 min. The current can be set at any value between 0.5 and 50 amps and can be stepped in increments as small as 5 ma over any 5 amp range and 50 ma, or larger, over the entire 50 amp (3.5 MeV) range. At the end of each counting period, the scaler is printed out and reset, the currents advanced, and, after a pre-set time, the counting begins again. Limit switches are provided on each limit of the 10 turn potentiometer to prevent overdriving. The automation system,

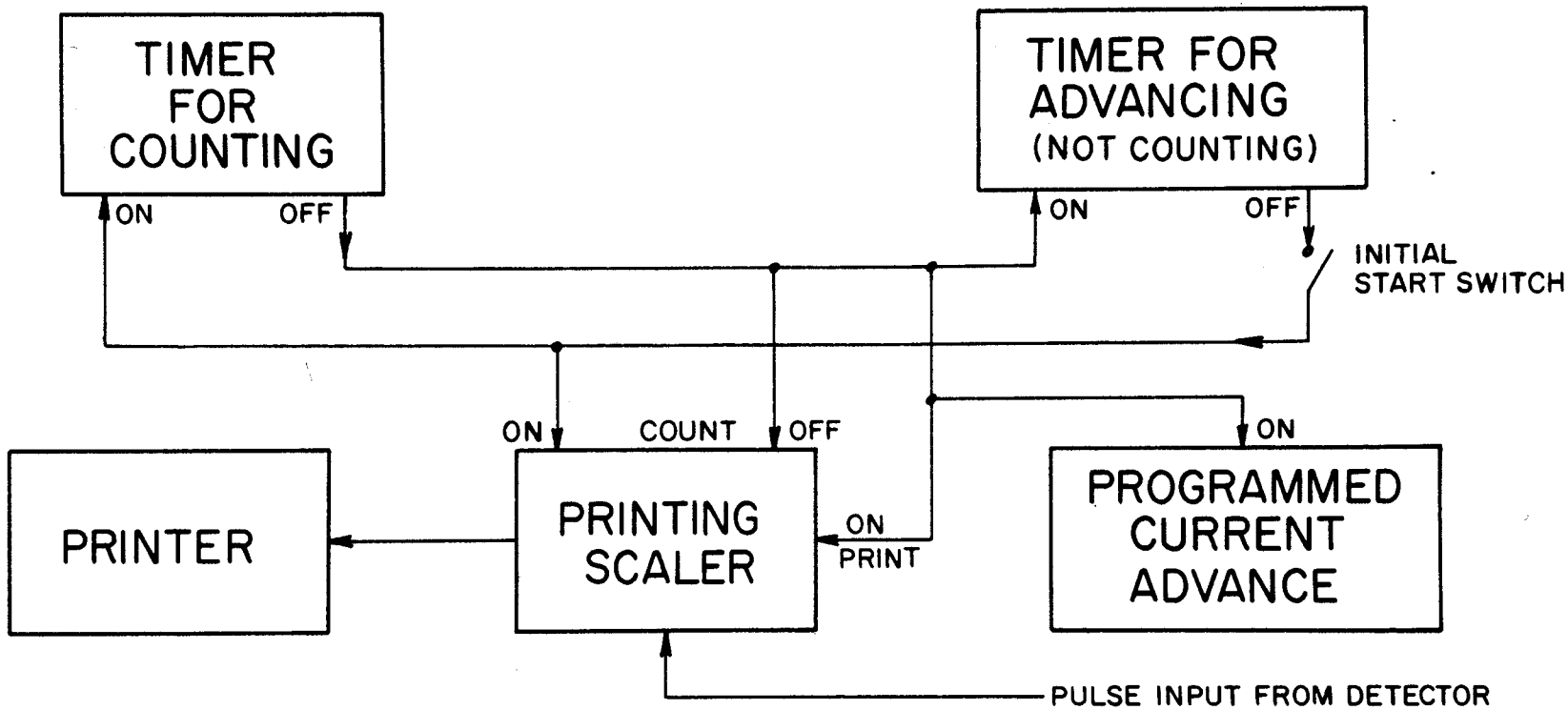

BLOCK DIAGRAM OF AUTOMATION SYSTEM

Figure 7. A block diagram of the automation system.

although partially constructed from outdated components, has proven both satisfactory and reliable.

2.B.4. The Detector System

The detector mechanism of this spectrometer incorporates the general features of that designed for Bisgord's instrument[11], but has been modified to incorporate a low noise system. The field free region in the center of the spectrometer makes it very convenient to use windowless scintillation detectors coupled to photomultiplier tubes. Anthracene and pilot B scintillators have been used. Although anthracene has the undesirable feature of slow decomposition in vacuo, its higher light output has been used to good advantage in the detection of low energy ($\lesssim$ 25 keV) electrons. Modifications in our detector mechanism allow the light output from the crystal to split into two light pipes which are coupled to two separate phototubes. A coincident signal is then required of both photomultiplier tube outputs in order that it be recorded as a true count. Since the noise pulses in each tube are uncorrelated with time, this technique enables one to efficiently detect low energy electrons without the high noise count rates that are usually associated with the required high voltage. With this system, 13 keV Auger electrons have been detected. No sources have been made thin enough to test the instrumentat lower energies. The power supply is capable of regulating on currents corresponding to focusing electrons of 2.5 keV energy.

2.B.5. Earth Field Compensation

Following the final assembly of the spectrometer, it was found that the electrons from the various gaps still did not focus at the same current. For the 624 keV conversion line of ^{137}Cs, the deviation was found to be as much as 1.2% for gaps located at 120° with respect to one another. A careful search of the focusing current vs. angle was found to very nearly follow a sine wave. Such a phenomenon arises from an added horizontal field in a particular direction, i.e., the horizontal component of the earth's magnetic field. Although the earth's field is only 0.1% that of the spectrometer for 624 keV electrons, the iron core concentrates it by a large factor in the spectrometer. Therefore, a compensating field is very necessary for even moderate resolution.

The problem has been circumvented satisfactorily by the construction of Helmholtz type coils. These compensating coils are 7 feet in diameter and 8 feet apart, thus deviating considerably from the Helmholtz condition. However, with a field produced by 75 amp-turns, the deviation in focusing currents for the various gaps deviates by less than $\pm$ 0.1%. East-west coils have also been constructed, but have been found unnecessary for conversion electrons of ^{137}Cs. They may prove to be of use for fine adjustment of the field for very low energy electrons. Coils to compensate the vertical component of the earth's field are not necessary. The lateral deflection produced by this field in the upper half of the orbit is reversed in the lower half.

Measurements have shown that the spectrum taken with six gaps, with the described external field, gives resolutions of about 0.7%. Under the same conditions, a single gap has a resolution of 0.6%. This is indeed a very satisfactory solution in view of the fact that without the external field, the six gap resolution was 1.3%.

2.B.6. The Performance of the Spectrometer

The Michigan State University orange spectrometer has been thoroughly checked in terms of transmission, resolution, and linearity. The basis for judgment of the performance has been to compare the results with those obtained by Bisgord with the prototype[11]. Figure 8 shows a comparison of the resolution vs. transmission curve in the two instruments for similar baffle openings. In this figure, the points are those obtained with the MSU spectrometer and the curve is from the work of Bisgord[11]. The source size in the present spectrometer, which is twice the width used by Bisgord[11], may affect the curve at the lower values. However, the ultimate single gap resolution which has been obtained in this instrument with a small source is 0.45%, while Bisgord has operated his machine at 0.3%. This may be some cause for concern that the machining of the pole tips was not as good as it should be. There are differences in the pole faces of the various plates that are easily visible. However, such effects may not deteriorate the focusing properties significantly when all 6 gaps are used to-

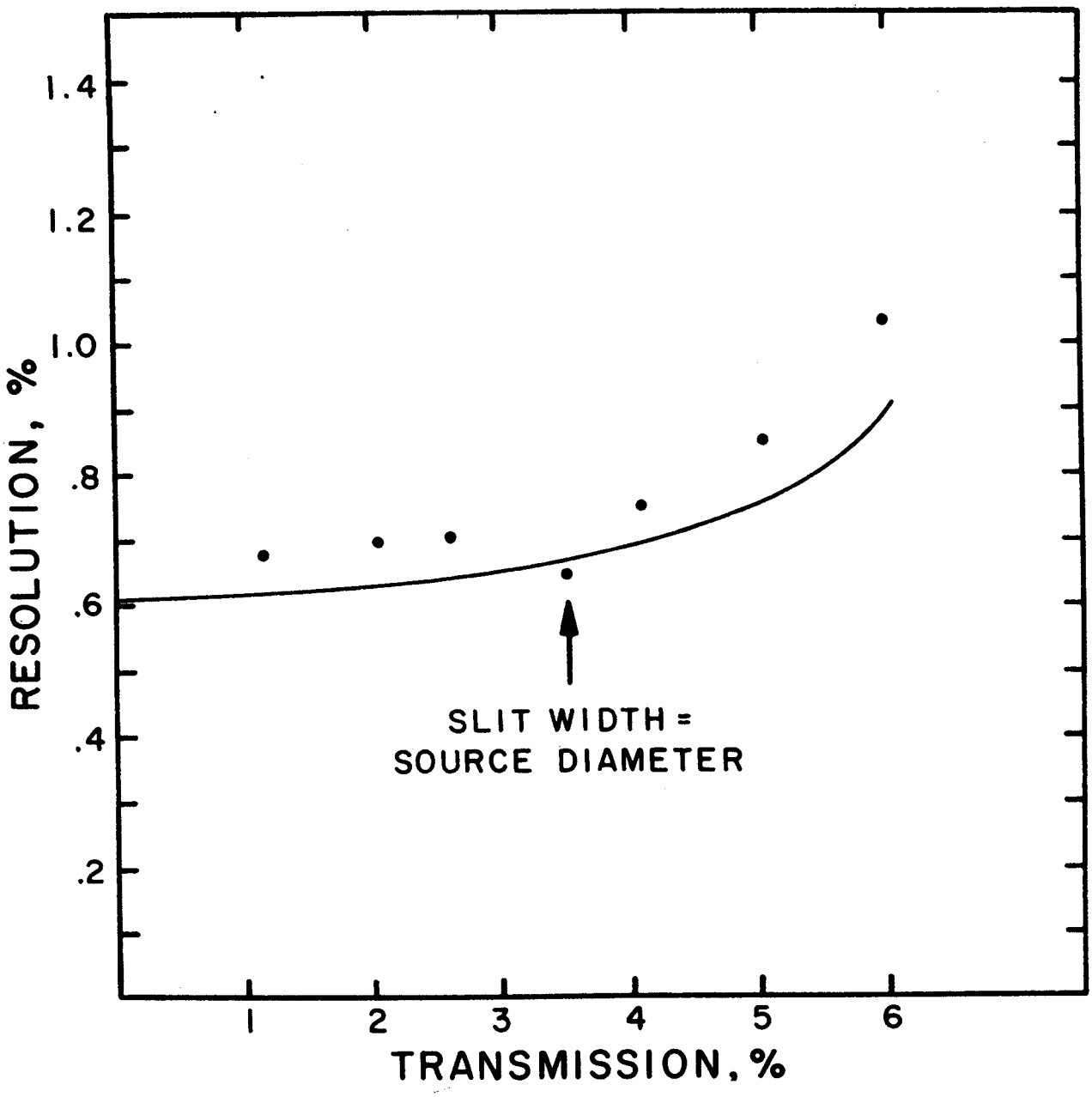

Figure 8. Comparison of the six gap resolution vs. transmission curve of the M.S.U. spectrometer with the prototype. The full curve is from ref. 11, while the experimental points have been obtained with this spectrometer.

gether and operating at much higher transmissions. In any event, the comparison of the two instruments is favorable.

The spectrometer has been found to be very linear when operating above 250 keV. The calibration equation is

$$B\rho = 270.2\ I$$

where $B\rho$ is measured in gauss-cm and I in amperes. Unless meticulous premagnetization procedures are followed[46], the $B\rho$ vs. I relation is non-linear for the lower energies. For example, the spectrometer constant is reduced from 270 to 245 when focusing 25 keV electrons. This effect is not considered to be a serious limitation of the effectiveness of the machine as long as the problem is known to exist. The energy measurements of the transitions are usually performed on high resolution Ge(Li) detectors. Fermi analysis of continuous spectra can be easily corrected for the non-linearity by the inclusion of a quadratic term in the calibration equation.

A typical spectrum of the type recorded with the spectrometer is shown in fig. 9. The source used was ^{137}Cs.

2.B.7. Comparison with Other Types of Spectrometers

Direct comparisons of the spectrometers of various types are difficult, if not impossible, because of the numerous factors involved. The spectrometer cannot compare with the resolution nor luminosity obtainable with the $\pi\sqrt{2}$ double focusing spectrometer. However, the transmission is much higher and the

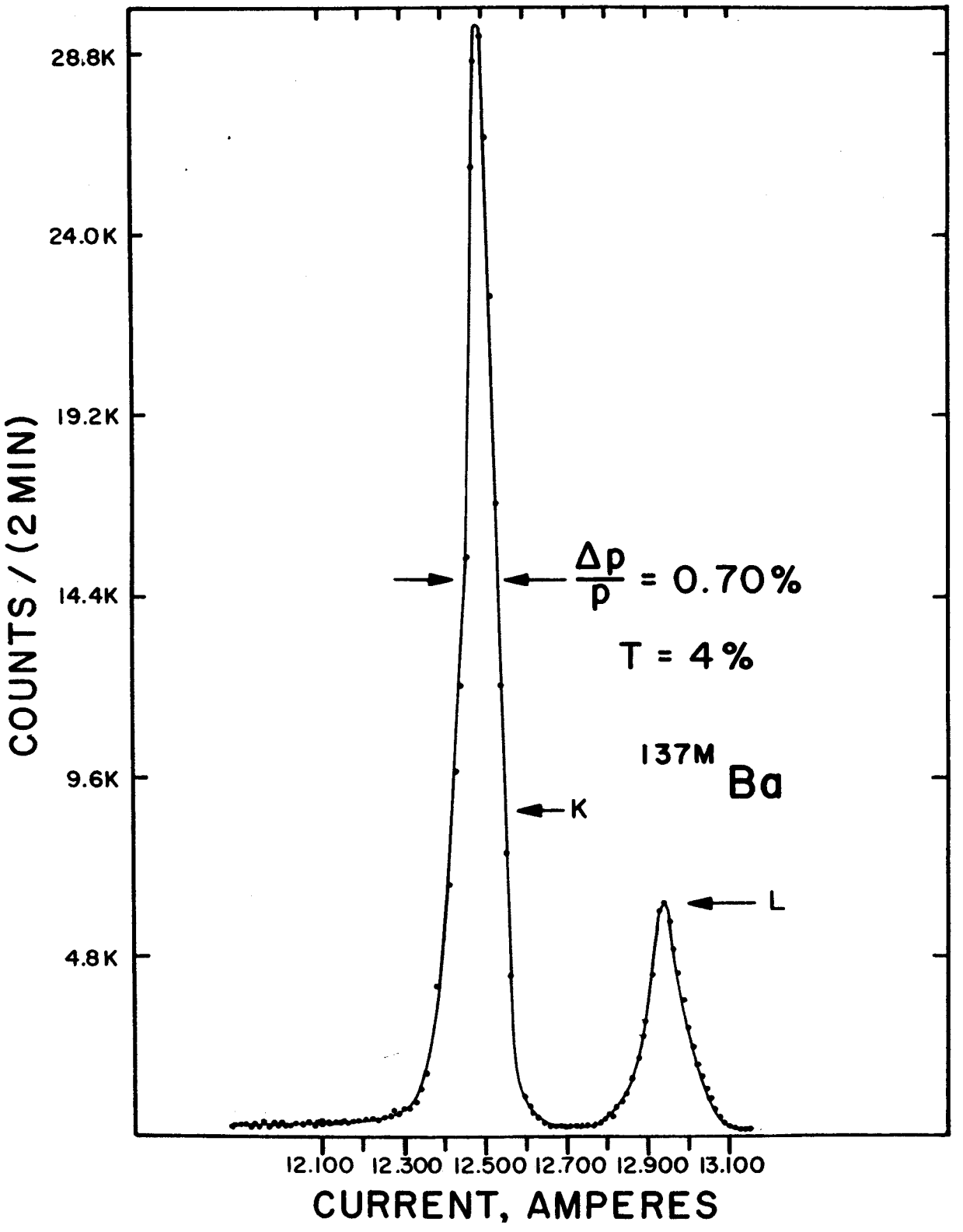

Figure 9. The K and (L + M) internal conversion electron lines of ^{137m}Ba, recorded with the MSU orange spectrometer.

cost much less. The 100 gap iron-free version of the orange spectrometer[47] is a superior instrument in resolution, luminosity, and transmission. However, the MSU instrument has been constructed at less than 3% of the cost of iron-free system. Other iron-free orange spectrometers have been constructed which actually have characteristics inferior to the iron machine[47]. However, these are usually designed for different purposes.

Probably the best comparison is with the lens spectrometer which has been very widely used. Both spectrometers are relatively easy to build and their costs are not excessive. Both have relatively good figures of merit, but suffer tremendously with source size. The theoretical limit for T vs. R in the lens spectrometer is $T^2 = 0.16R$, neglecting source size effects[44]. The corresponding equation for the orange spectrometer is[11] $T^2 = 1.25R - .0075$. Thus, the lens spectrometer is capable of attaining better resolutions as long as transmissions of less than 2% are involved. However, the luminosity, $L = AT$, for the 6 gap orange spectrometer is probably a factor of 10 better than for the lens type instrument. In addition, the optimum angle of emission for the lens spectrometer is 45°, which means that, in general, larger counters must be used in this instrument. This has the effect of increasing the background to true count ratio.

From these arguments, it may be concluded that the multigap spectrometer is, in reality, a very versatile instrument. It is capable of achieving both high resolution and high trans-

mission. It is ideal for e-γ coincidence counting experiments, and the single gap version is well suited for e-γ angular correlation studies. The geometrical arrangement is such that charged particle beams can be introduced without any serious instrumental modifications. Finally, the cost is small in comparison with other tools of nuclear research in use today. Once the instrument is constructed, the operating costs are indeed nominal. These consist mainly of replacing the anthracene detector which deteriorates in a vacuum.

CHAPTER 3

THE DECAY SCHEME OF ^{131m}Te: SYSTEMATIC TRENDS OF ODD MASS I ISOTOPES

3.A. Introduction

The study of the β and γ decay of the odd-mass ($127 \leq A \leq 133$) tellurium isotopes to iodine daughters presents an excellent opportunity for the examination of the systematic trends of the 53 proton levels as a function of (even) neutron number. With the exception of ^{133}Te, the isotopes are easily produced by thermal neutron capture. The half-lives of the isotopes are of sufficient duration to allow a fairly detailed study. In addition, the β decay of both $11/2^-$ and $3/2^+$ isomers can be observed. Therefore, a wide variety of spin-parity states are expected to be populated and not as many levels are missed as in many radioactive decay studies. The systematic trends in this region should thus be informative for comparisons with recent model calculations, such as those reported by Kisslinger and Sorensen[4] and by O'Dwyer and Choudhury[5].

The work reported here is primarily concerned with the decay of 30.5 hr ^{131m}Te, populating the states of ^{131}I. The states of ^{127}I and ^{129}I have recently been re-examined[48-50] and the states of ^{133}I are under investigation elsewhere[51].

Early investigation[52,53] of the internal and external conversion electron spectra of ^{131m}Te gave some indications of the complexity of the gamma spectrum. The beta endpoint

energy was measured to be 2.45 MeV and the existence of an isomeric transition of 182 keV energy between the $11/2^-$ and $3/2^+$ parent isomers was found to account for 18% of the decay of the $11/2^-$ state of the ^{131m}Te parent. Badescu, et al., later published a series of papers[54-56] over a period of several years, in which scintillation techniques as well as magnetic spectrometers were utilized. This group was able to arrive at a decay scheme which would place the most prominent transitions. Measured values for α_K indicated the presence of E1 transitions, leading to the assignment of part of the low energy states in the proposed decay scheme as negative parity states. That such a situation should exist is somewhat doubtful since all of the known low energy states of ^{127}I and ^{129}I have positive parity[48-50]. In addition, Badescu, et al., reported the strong 774 and 852 keV transitions to be in cascade[55] with a crossover transition of 1645 ± 1 keV. On the basis of energy sums, such a situation cannot exist, of course. These discrepancies, coupled with the fact that the high resolution Ge(Li) detectors were now available, warranted a reinvestigation of the decay scheme.

During the course of this investigation, Devare, Singru and Devare published a more comprehensive study using scintillation coincidence techniques, beta spectrometry, delayed coincidence techniques and some limited data recorded with a Ge(Li) detector[57]. Even though some of their data were quite informative, our technique of using a Ge(Li)-NaI(Tl) detector combination for coincidence experiments made it obvious that

their proposed decay scheme was in error. The investigation was continued in order to establish a more complete disintegration scheme of ^{131m}Te, as well as to find and remove errors which still existed.

3.B. Source Preparation

The sources of ^{131m}Te were produced by the irradiation for one week periods of 10 mg samples of tellurium metal, enriched to >99.5% ^{130}Te, in the ORNL ORR reactor. The thermal neutron fluxes were approximately 2 x 10^{14} n cm^{-2} sec^{-1}. Several sources were used during the course of the experiments. All of the sources were chemically purified[58] to remove contaminants, especially the ^{131}I daughter, silver and antimony activities. The chemical procedure entailed dissolving the metal target in aqua regia and transferring to a distillation flask. The ^{131}I activity was then distilled into an ice water bath or acetone, which dissolved the iodine gas. The solution was then boiled to near dryness three times to remove all the nitrate ions. Tellurium metal was precipitated from a 3N HCl solution with SO_2 gas and a trace of hydroxylamine hydrochloride, leaving any antimony in solution. The tellurium metal was again put into solution with HNO_3 and $AgNO_3$ carrier added. A drop of HCl then precipitated the silver activities.

The sources thus purified were prepared for gamma counting by drying the nitric acid solution that contained the

sample onto a thin glass microscope slide or mylar film. The samples were covered with mylar. Sources for singles counting were typically about 30 μc strength, while those used for coincidence counting were 150 μc.

The sources for the electron spectrometers were prepared by vacuum sublimation of the tellurium metal obtained in the SO_2 precipitation. These sources contained trace amounts of ^{110}Ag activity, but this did not interfere with the measurements performed.

The sources for the orange spectrometer were 2 mm diameter while those for the $\pi\sqrt{2}$ iron free spectrometer were 1 mm x 15 mm. The low specific activity made source thickness a limiting factor in the resolutions obtained with both spectrometers.

3.C. The Gamma-Ray Singles Spectrum

The singles spectrum has been recorded and analyzed with both NaI(Tl) and Ge(Li) detectors. The NaI(Tl) spectra were taken with a 7.6 cm x 7.6 cm crystal having approximately 8% resolution for the 662 keV gamma-ray of ^{137}Cs. The results do not differ significantly from the previous results of DSD[57] and are, therefore, not shown here. The high resolution data were recorded with a Ge(Li) detector with a sensitive volume 4 mm deep and 2 cm diameter which was made in our laboratory. The associated electronics consisted of a low noise preampli-

fier and a low noise RC pulse shaping amplifier coupled to a 1024 channel analyzer. Near the completion of the study, a room temperature field effect transistor preamplifier was used. The low energy portion of the spectrum shown in fig. 10 was recorded with this latter system.

The singles spectrum, shown in figs. 10 and 11, consists of 45 gamma-rays identified as belonging to the decay of ^{131m}Te. These range in energy from 81 to 2270 keV. The 159 keV gamma-ray belows to ^{123m}Te. Gamma-rays with energies 284.3, 364.5 and 638.4 keV belong to the decay of the ^{131}I daughter. The 80.2 and 723.8 keV transitions in ^{131}I are masked by the strong 80.9 keV peak and the high Compton distributions respectively.

The energies of the gamma-rays were determined by counting the source of ^{131m}Te, both simultaneously and consecutively, with a number of well-known standard sources[59]. The best results were obtained by making separate runs with the low and high energy portions of the spectrum, and recording the singles and calibration data simultaneously. The peak positions were found by first subtracting a third order least squares curve that had been fitted to several background channels on both sides of the peak and then calculating the centroids of the peaks. The centroids of the calibration peaks were then fitted to a least squares quadratic curve, thus accounting for non-linearities in the electronics. These calculations were performed on the Michigan State University CDC3600 computer. The energies of the calibration points typically

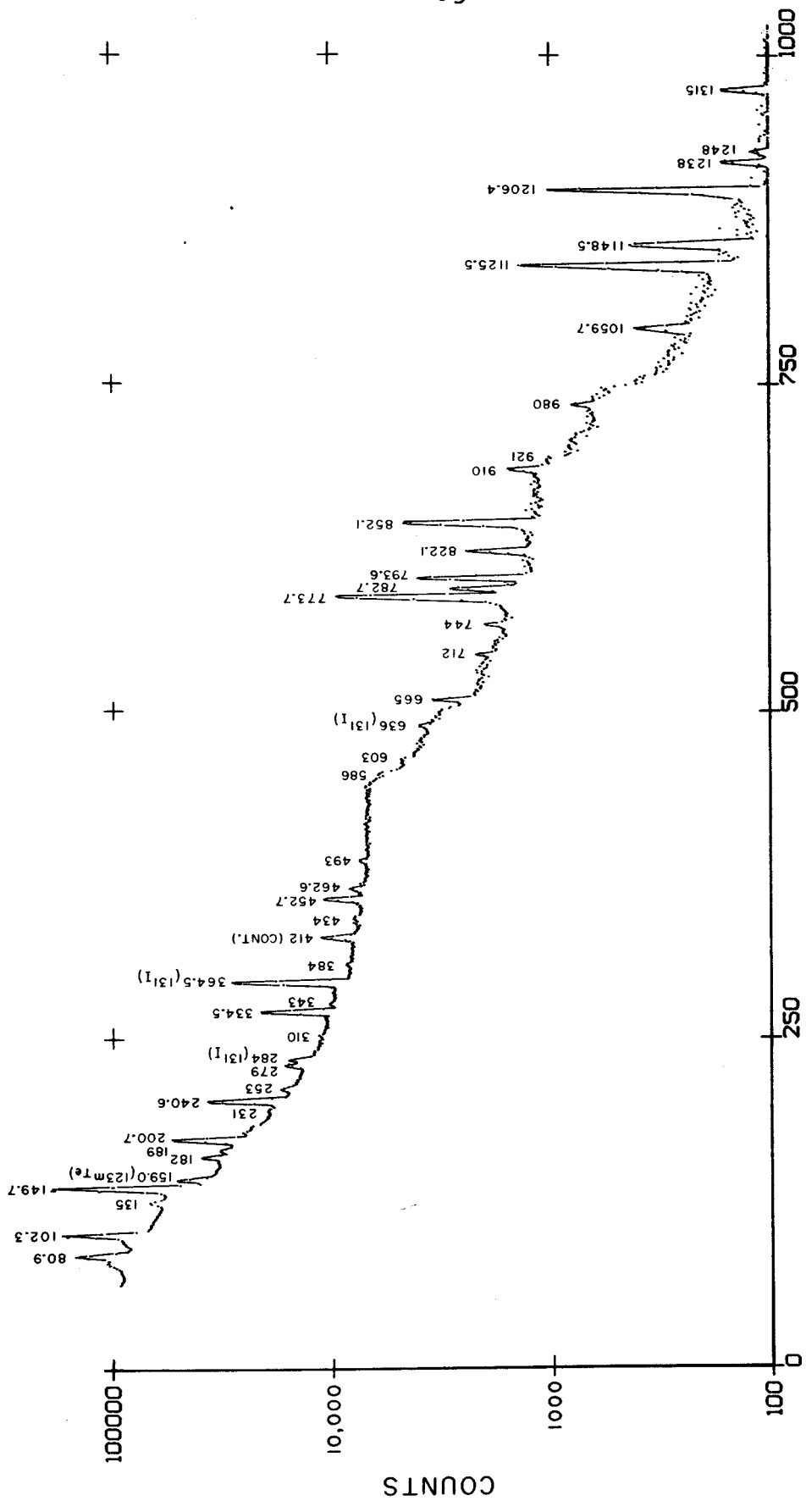

Figure 10. The low energy part of the ^{131m}Te gamma-ray singles spectrum taken with a 2 cm² x 4 mm deep (0.8cc) Ge(Li) detector and an FET preamplifier.

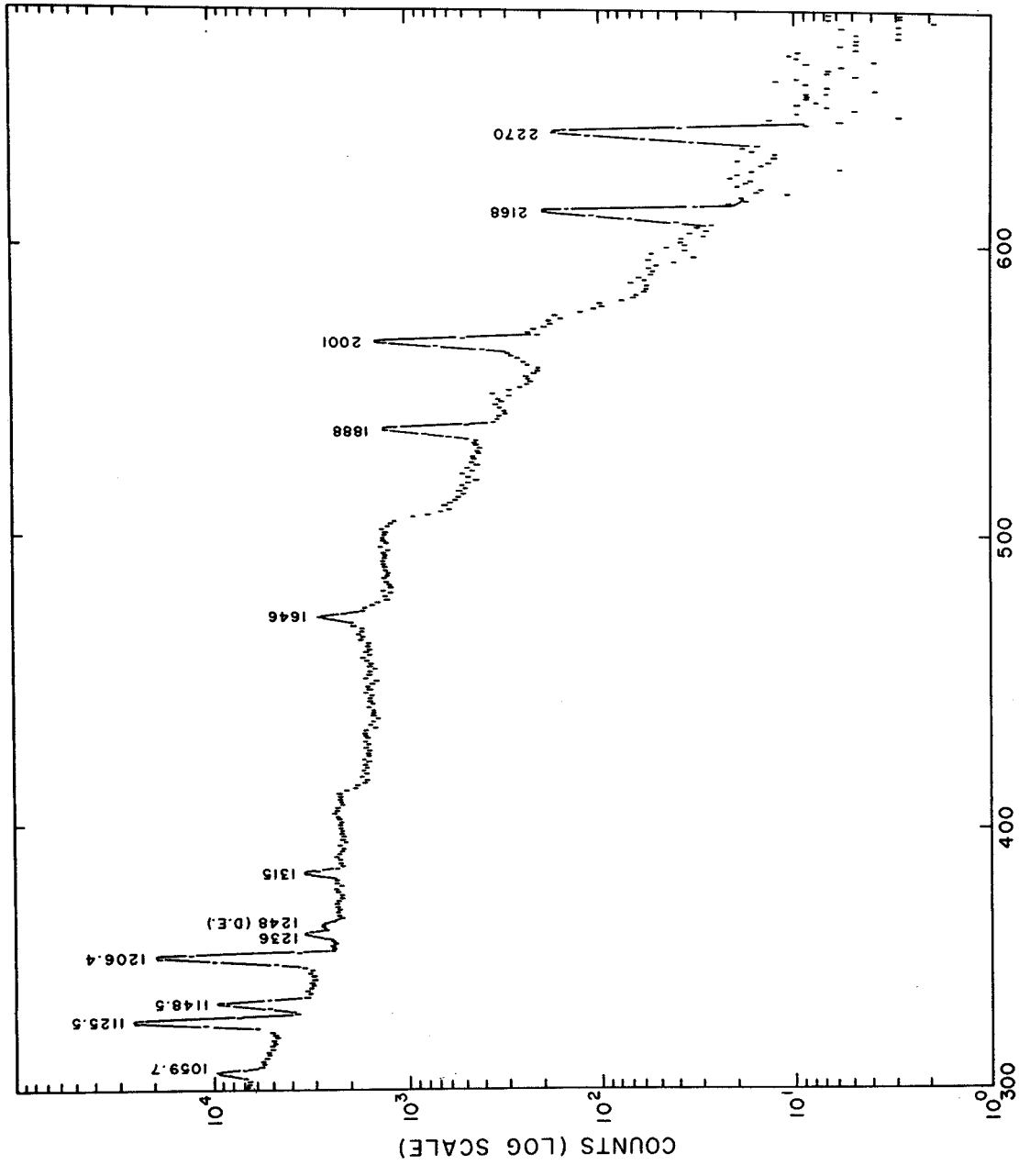

Figure 11. The high energy part of the ^{131m}Te gamma-ray singles spectrum, recorded using a 0.8cc Ge(Li) detector.

reproduced to within ± 0.15 keV or better, thus determining the energies of even the weakest gamma-rays to within ± 1 keV. Typical results of a linear vs. quadratic fit are shown in table 1. Gamma peak areas, in conjunction with the detector efficiency curve, were used to determine the relative intensities of the gamma-rays. A list of the ^{131m}Te gamma-ray energies and their relative intensities is given in table 2. The errors quoted are RMS deviations from average values.

3.D. Gamma-Gamma Coincidence Studies and the Construction of the Decay Scheme

3.D.1. The Present Coincidence Spectrometer and Its Advantages

One of the main difficulties in interpreting previous coincidence data has been due to the multiplet of seven gamma-rays in the region of 740-910 keV. This region of the spectrum accounts for a large fraction of the combined intensities of all gamma-rays and six of the gamma-rays are in coincidence with one or more of the remainder. The entire region is on top of the Compton distribution of the strong 1126 and 1207 keV gamma-rays, which are also in coincidence with the strongest gamma-ray in this region. A part of the difficulty in analysis has been removed by using a NaI(Tl)-Ge(Li) coincidence spectrometer. Although the pulse shaping requirements from the Ge(Li) detector to the coincidence circuit prevent optimum resolution, the coincidence spectra recorded with the

TABLE 1

Typical linear vs. quadratic least squares fit to calibration points

Source	Energy, keV	Linear fit, keV	Linear deviation, keV	Quadratic fit, keV	Quadratic deviation, keV
^{22}Na	511.006±0.005[a]	508.313	2.690	510.938	0.065
^{137}Cs	661.595±0.076[a]	660.329	1.266	661.730	-0.135
^{60}Co	1173.226±0.040[a]	1174.472	-1.246	1173.143	0.083
^{22}Na	1274.6 ±0.2[b]	1276.157	-1.557	1274.546	0.054
^{60}Co	1332.483±0.05[a]	1334.144	-1.661	1332.410	0.073
ThC"(D.E.)	1592.46 ±0.10[a]	1594.56	-2.10	1592.62	-0.16
ThC"	2614.47 ±0.10[a]	2611.86	2.607	2614.46	0.01

Linear equation

$$\text{Energy (keV)} = 7.187 + 2.582\ (\text{Channel})$$

Quadratic equation

$$\text{Energy (keV)} = 15.195 + 2.549\ (\text{Channel}) + .000027\ (\text{Channel})^2$$

a) Ref. 14

b) Ref. 18

Table 2

^{131m}Te gamma ray energies and relative intensities.

Present Work		Devare, et al.[a]	
Energy[b] (keV)	Rel.Int.[c] (Gamma)	Energy (keV)	Rel.Int. (Gamma)
80.9 ± 0.4	48	81.1	23
102.3 ± 0.4	107	102.1	56
115 ± 1.5	2		
135 ± 1.0	10		
149.7 ± 0.2	280	149.7	209
183 ± 1.0	18		
189 ± 1.0	3		
200.7 ± 0.4	79	200.5	80
215 ± 1.5	3		
231 ± 1.0	8		
240.6 ± 0.4	91[d]	241.5	82
254 ± 1.0	12		
279.5 ± 0.5	26[d]	278	37
310 ± 1.0	3		
334.5 ± 0.4	100	335.8	100[e]
343 ± 1.0	7[d]		
354 ± 1.0	6		
384 ± 1.5	5		
434 ± 1.5	7		
452.7 ± 0.4	59	452	66
462.6 ± 0.4	23		
493 ± 0.8	11		

Table 2 (cont.)

^{131m}Te gamma ray energies and relative intensities.

Present Work		Devare, et al.[a]	
Energy[b] (keV)	Rel.Int.[c] (Gamma)	Energy (keV)	Rel.Int. (Gamma)
586 ± 1.5	10		
603 ± 1.0	10	602	17
665 ± 1.0	33	650-665	28
712 ± 1.0	11		
744 ± 1.0	14	740	7
773.7 ± 0.4	380	775	370
782.7 ± 0.6	80	786	33
793.6 ± 0.4	130	797	63
822.1 ± 0.4	55	831	47
852.1 ± 0.4	210	854	190
870 ± 1.0	D.E.	869	
910 ± 1.0	35	915	46
922 ± 2.0	5		
980 ± 1.0	D.E.		
		995	
1059.7 ± 0.5	11	1050-1065	17
1125.5 ± 0.4	120	1126	102
1148.5 ± 0.5	38	1145	29
1206.5 ± 0.5	95	1206	100 ± 20
1238 ± 1.0	5		
1248 ± 1.0	D.E.		

Table 2 (cont.)

^{131m}Te gamma ray energies and relative intensities.

Present Work		Devare, et al.[a]	
Energy[b] (keV)	Rel.Int.[c] (Gamma)	Energy (keV)	Rel.Int. (Gamma)
1315 ± 1.0	9	1340	11
		1583 }	
1646 ± 1.0	14	1629 }	9
1888 ± 1.0	15	1860	9
2001 ± 1.0	20	1965	19
2168 ± 1.0	3	2130	4
2270 ± 1.0	3	2240	5
		2330	2

a) Ref. 12.

b) Errors are based on rms deviations from the mean value of several runs and include the quoted errors of the standard energies.

c) Uncertainties in relative intensities are estimated to be ± 10% or less, except for peaks of intensity less than 15 on the present scale. In these cases the uncertainties are greater.

d) This peak is considered to be a possible doublet.

e) Normalization point for relative intensities. In the original work, relative intensities were normalized to I(774) + I(783) + I (793) = 100.

germanium detector are, in general, quite satisfactory.

In addition to the detectors previously mentioned, the coincidence spectrometer consisted of conventional fast-slow coincidence circuitry, resolving time ≈40 nsec, and a 1024 channel analyzer. The analyzer was operated in the automatic chance-coincidence subtract mode described previously[60]. Thus all spectra (with the exception of the 150 and 1126 keV coincidence spectra) have been corrected for chance coincidence contributions. In the cases where peaks were well separated, coincidence spectra were recorded with separate gates, set first on and then off the peak in order to correct for underlying Compton distributions. Usually the NaI(Tl) detector was used for the gate. Figures 12 through 15 show the majority of these coincidence spectra. In some cases, such as those shown in fig. 16, the Ge(Li) detector was used as the gate in order to eliminate interference from photons of comparable energy. The counting geometry was generally 90°, with some runs recorded at 180°. The spectra shown in figs. 12 through 15 have been gain shifted by the computer for the ease of comparison in this presentation.

3.D.2. Evidences for Levels at 150, 603 and 1060 keV

With the NaI(Tl) crystal gating the analyzer on the 150 keV peak, gamma-rays of energies 453 and 910 keV are especially prominent, as shown in fig. 12. The peak areas have been measured and compared to the peak areas of the photons

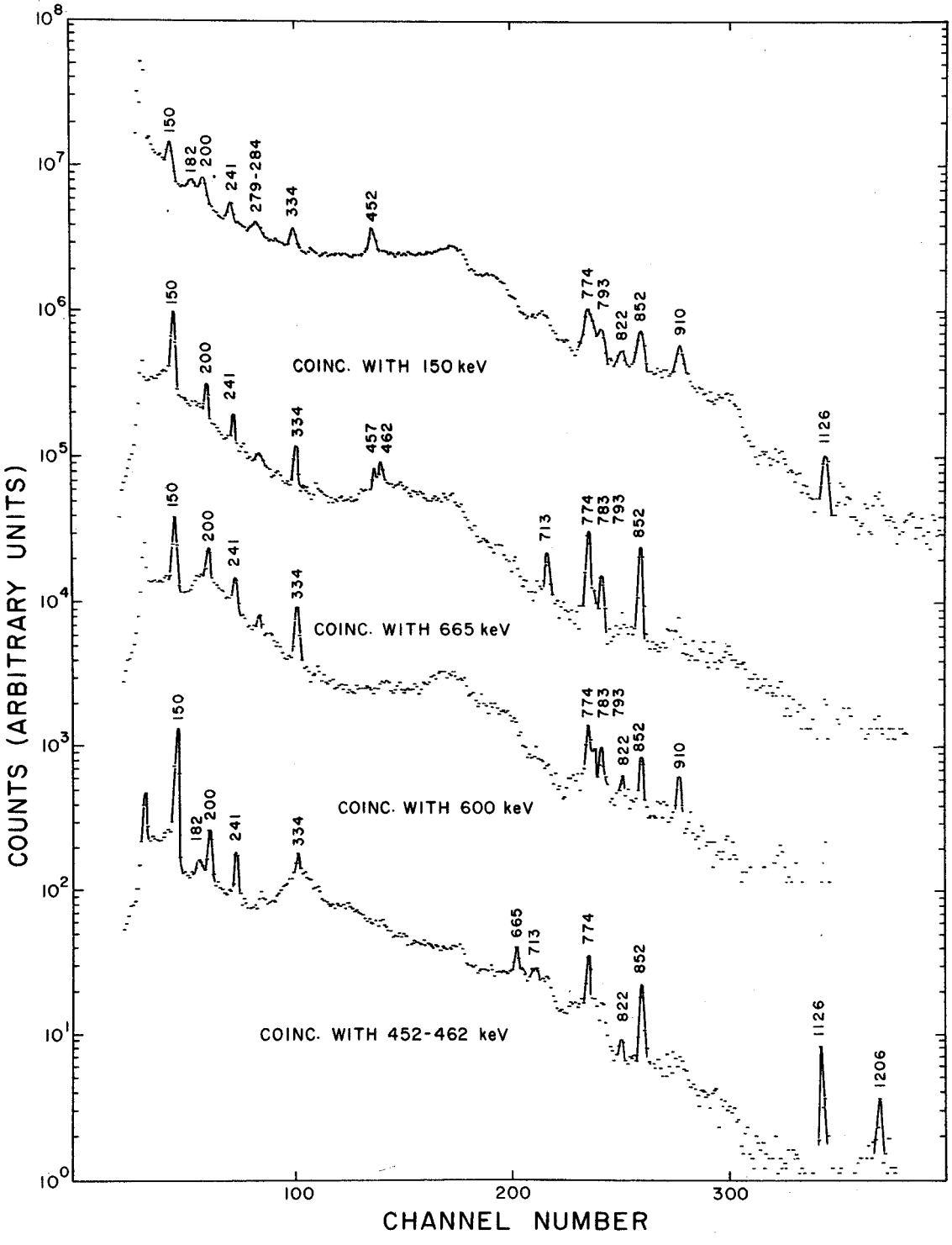

Figure 12. The ^{131m}Te coincidence spectra recorded with a Ge(Li) detector of 0.8 cm^3 active volume, gated by a 7.6 cm x 7.6 cm NaI(Tl) detector on the peaks indicated below each spectrum in the figure:

a) NaI(Tl) gate on the 150 keV photopeak
b) NaI(Tl) gate on the 665 keV photopeak
c) NaI(Tl) gate on the 600 keV photopeak
d) NaI(Tl) gate on the 452 and 462 keV photopeaks

recorded by gating on the high energy side of the 150 keV peak. The 453 and 910 keV gamma-rays are enhanced by a factor of 2 more than the other gamma-rays that are present in both runs. The 453 keV photons have been reported previously[52-56,61,62] as depopulating the 603 keV level in ^{131g}Te to the 150 keV level. The 603 keV level is also fed in the decay of ^{131m}Te via the isomeric transition and, as shall be shown in section 3.D.3, from the higher energy states. The 910-150 keV coincidence is interpreted as evidence for the placement of a level at 1060 keV and is complemented by the existence of a 1060 keV photon seen in the singles spectrum. The remainder of the peaks in this spectrum, as well as those not discussed explicitly in the following spectra, are due to coincidences with underlying Compton distributions.

3.D.3. Evidences for States at 852 and 1315 keV

The results of runs taken with the analyzer gated on the 665 keV peak and the Compton distribution in the region of 600 keV are shown in figs. 12b and 12c, respectively. With the 665 keV gate, gamma-rays of energies 150, 453, 462, 712 and 852 keV were observed. The remaining transitions were found to be due to underlying Compton distributions by comparing relative peak areas with those in coincidence with the 600 keV Compton region. Due to the low efficiencies of the Ge(Li) detectors, higher energy photons are difficult to observe. However, using NaI(Tl)-NaI(Tl) coincidence tech-

niques, DSD have observed a transition of about 1300 keV in coincidence with the 665 keV gamma-ray[57]. This result is consistent with our similar measurements. There is a level at 1980 keV which can depopulate to a level at 1315 keV via a 665 keV transition. (This level is discussed further in section 3.D.4.) The 1315 keV level, in turn, depopulates via the 462 and 712 keV transitions to levels at 852 and 603 keV, respectively, as well as by a crossover transition. As a consistency check, a coincidence spectrum was recorded with the 452-462 keV region in the gate. The results are shown in fig. 12d. The 150 keV peak was greatly enhanced due to the 452 keV photopeak, as expected. Also, the 852 keV gamma is enhanced by a factor of 4 above that seen in coincidence with the 600 keV gate, while the ratios of intensities of the 852 keV quanta are comparable with those obtained with the 462 and 665 keV coincident gates. The peak at 910 keV in fig. 12c is explained in section 3.D.7.

3.D.4. Evidences for the 1646 and 1980 Levels

In previous works on the decay of ^{131m}Te, the intense 774 and 852 keV photons have been placed as a cascade depopulating a level of approximately 1626 keV, along with a crossover transition of the same energy[55,57]. In each instance, the 334 keV gamma-ray has been shown to be in coincidence with the crossover transition and has been substantiated in this study. However, our energy measurement of

the photon is 1646 ± 1 keV which rules it out as a crossover for an 852-774 keV cascade. Thus, a coincidence run was recorded, gating on the 334 keV region of the spectrum. The results, fig. 13a, show the 793 and 852 keV quanta to be enhanced. Evidence for such a cascade is supported by the energy sum 852.1 + 793.6 = 1645.7 keV, which agrees with the measured crossover energy to within experimental error. Thus, the 334 keV transition depopulates a level at 1980 keV to one at 1646 keV, which, in turn, depopulates via a crossover transition and a 793 keV photon to a level at 852 keV. The conclusion that the state must be at 852 keV rather than at 793 keV is based on intensity considerations as well as on the evidence for the 462-852 keV coincidence presented in section 3.D.3.

3.D.5. Evidences for the 1556, 1596, 1797 and 1900 keV Levels

The coincidence data recorded with the 81 and 102 keV regions of the spectrum are shown in figs. 13b and 13c, respectively. Peaks of energies 102, 200, 241, 774, 793, 822, 852 and 1126 keV are found to be enhanced in the 81 keV coincidence run. With the exception of the 102 and 1126 keV gammas, the same peaks show equal enhancement with the 102 keV gate. The 81 keV transition does not show in this figure, but another measurement, with a lower analyzer threshold setting, also showed it to be in coincidence with the 102 keV photon. The existence of the 102 and 1126 keV peaks in fig.

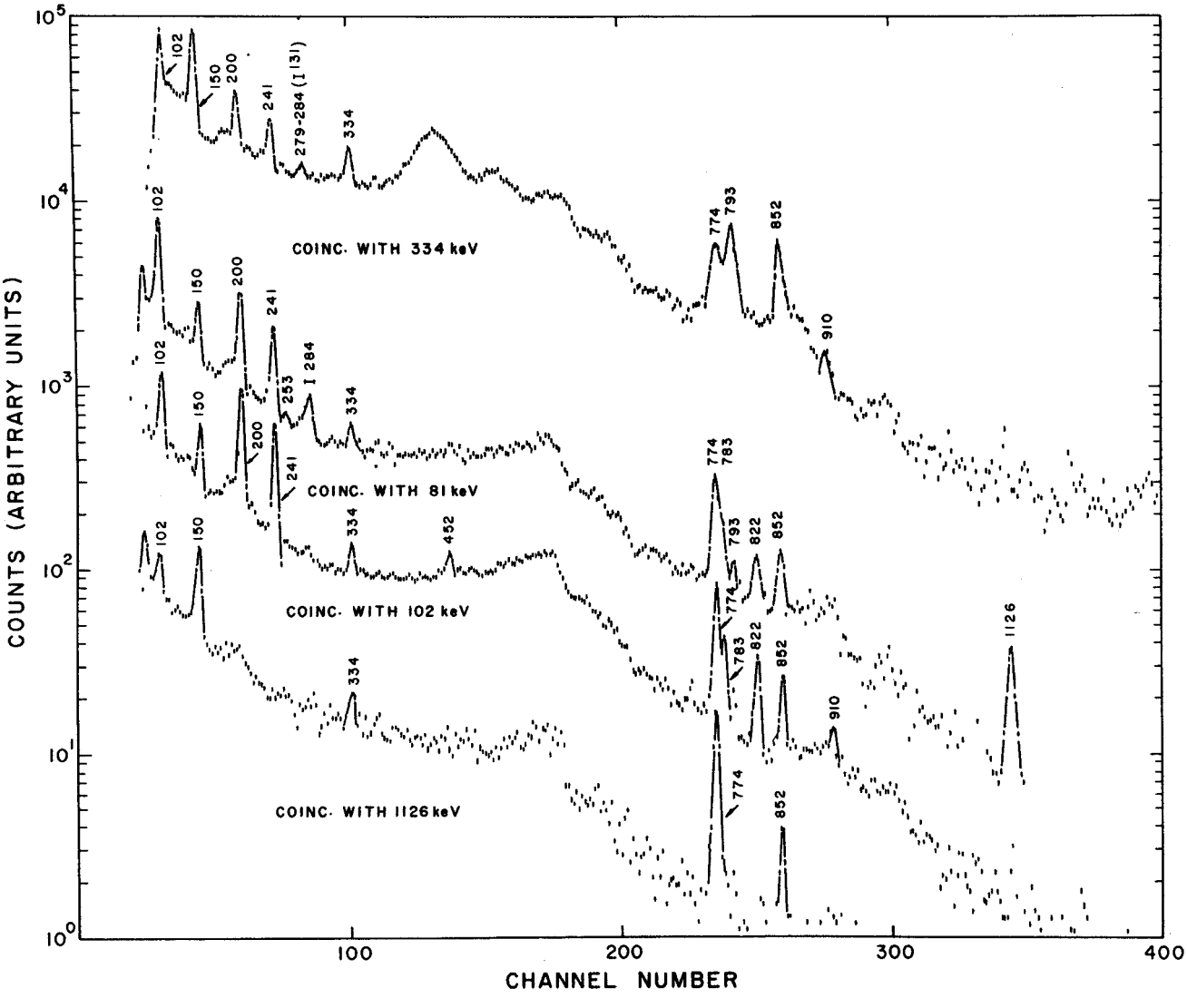

Figure 13. The ^{131m}Te coincidence spectra recorded with a Ge(Li) detector of 0.8 cm^3 active volume, gated by a 7.6 cm x 7.6 cm NaI(Tl) detector on the peaks indicated below each spectrum in the figure:

a) NaI(Tl) gate on the 334 keV photopeak
b) NaI(Tl) gate on the 81 keV photopeak
c) NaI(Tl) gate on the 102 keV photopeak
d) NaI(Tl) gate on the 1126 keV photopeak

13c is attributed to the incomplete resolution of the 81 and 102 keV peaks in the NaI(Tl) detector. The coincidence spectrum recorded with the 1126 and 1148 keV quanta in the gate, is shown in fig. 13d. The 81 and 774 keV peaks are enhanced by coincidences due to the 1126 keV photon, while the 852 keV peak is attributed to a 852-1148 keV coincidence. The conclusions based on these data are then as follows: The 81 keV transition depopulates a level at 1980 keV to an 1899 keV level. The 1899 keV level, in turn, depopulates via the 1126 keV transition to the 774 keV level and the 102 keV gamma to a level at 1797 keV. The latter level can feed levels of energy 1596 and 1556 keV via the 200 and 241 keV quanta. This ordering of the 81, 102, (200-241) keV cascade is in agreement with the delayed coincidence evidence of DSD[57]. The levels at 1556 and 1596 keV are further supported by the coincidence data and energy sums presented in the next section. The weak peak at 253 keV and the possibility of a peak at 343 keV in fig. 13b, taken with the gate set on the 81 keV peak, is consistent with the proposed level scheme.

3.D.6. Further Evidence for the 1556, 1596, 1646, 1797, 1899 and 1980 keV levels

The data shown in figs. 14a and 14c are coincidence spectra recorded with the 200 and 241 keV photons in the gate, respectively, while fig. 14b was recorded with the gate set

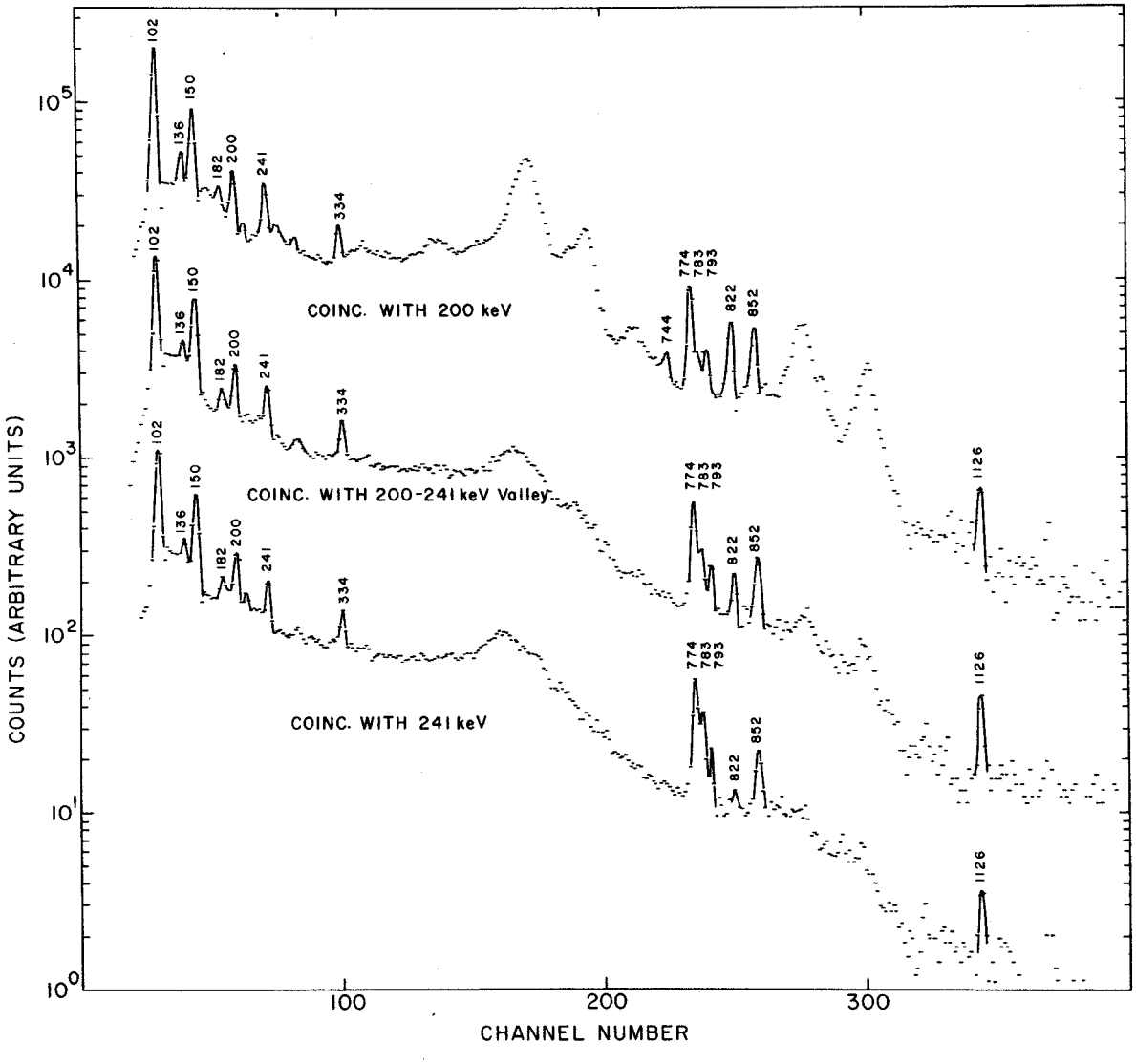

Figure 14. The ^{131m}Te coincidence spectra recorded with a Ge(Li) detector of 0.8 cm^3 active volume, gated by a 7.6 cm x 7.6 cm NaI(Tl) detector on the peaks indicated below each spectrum in the figure:

a) NaI(Tl) gate on the 200 keV photopeak
b) NaI(Tl) gate on the 200–241 keV valley
c) NaI(Tl) gate on the 241 keV photopeak

between the two peaks. Besides the (81 and) 102 keV transition, the 744, 774, 822 and 852 keV transitions are enhanced in the 200 keV coincidence spectrum while the 783 keV transition is more intense in the spectrum recorded with the 241 keV gate. Again, there was considerable overlap in the peaks of the 200 and 241 keV photons in the NaI(Tl) gate as well as the underlying Compton distributions. However, by taking a third gate between the two peaks and comparing photopeak areas in all three runs, the results just stated were clearly verified. Thus the 1596 keV level depopulates via 744 and 822 keV transitions to the 852 and 774 keV levels, respectively. The 1556 keV state depopulates by a 783 keV transition to the 774 keV level. The corresponding energy sums agree to within experimental error.

In order to complement the data presented above, a series of NaI(Tl)-Ge(Li) coincidence spectra were taken gating on small regions across the intense 740-850 keV region of the spectrum. The results are shown in figs. 15a-15e. Due to the poor resolution of the sodium iodide detector, one cannot accurately determine the relative intensity of each transition in the gate. However, a definite trend can be observed as the gate is moved across the region in small increments. The principal contributions to the gates are those given on fig. 15. The results are seen to confirm the data presented above, i.e. coincidences between 744-852, 783-774, 793-852 and 822-774 keV transitions.

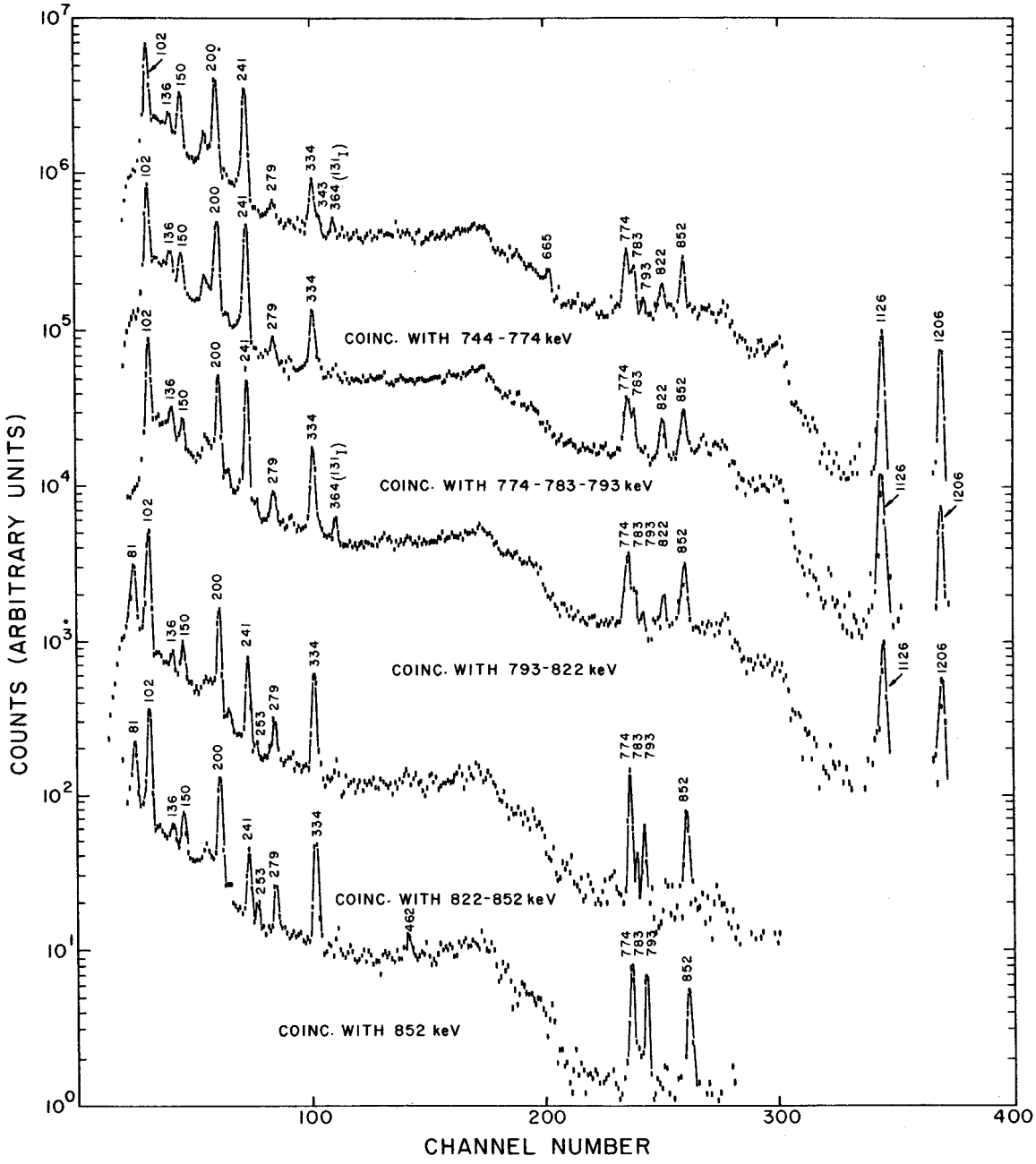

Figure 15. The ^{131m}Te coincidence spectra recorded with a Ge(Li) detector of 0.8 cm^3 active volume, gated by a 7.6 cm x 7.6 cm NaI(Tl) detector. The gates are taken in small increments across the 800 keV region, the major contributions being that indicated below each spectrum in the figure.

3.D.7. Evidence for the Placement of the Other Gamma Transitions

Further coincidence studies were performed on the 910 and 1060 keV photons, as shown in figs. 16a-16d. The spectra, in this case, were taken with a large volume germanium detector* as the gating crystal, while recording the NaI(Tl) spectrum in coincidence. The higher resolution facilitates separating information of interest from underlying Compton distributions by gating on the peak in one run and on the neighboring Compton distribution in a second run. Thus, coincidence information was obtained on the weak 910 and 1060 keV photons without the interference of the strong gamma-rays that were within 60 keV of each. However, due to the low efficiency of the Ge(Li) detector, good statistics were difficult to obtain. By comparing the spectrum with the gate on the peak to the one with the gate on the Compton distribution, photons of energy 150, 586 and 920 keV are seen to be in coincidence with the 910 keV gamma-ray. By the same method, the 586 and 920 keV gamma-rays are seen to be in coincidence with the 1060 keV photon. The 910-150 keV coincidence is taken as evidence for a 1060 keV level, while the 920-910 and 920-1060 keV coincidences are interpreted as arising from a 920 keV transition between the 1980 and 1060 keV levels. The 586 keV gamma is then a transition between the 1646 and 1060 keV levels. A summary of all the coinci-

*A 12 cm^3 Ge(Li) detector obtained from Nuclear Diodes, Inc.

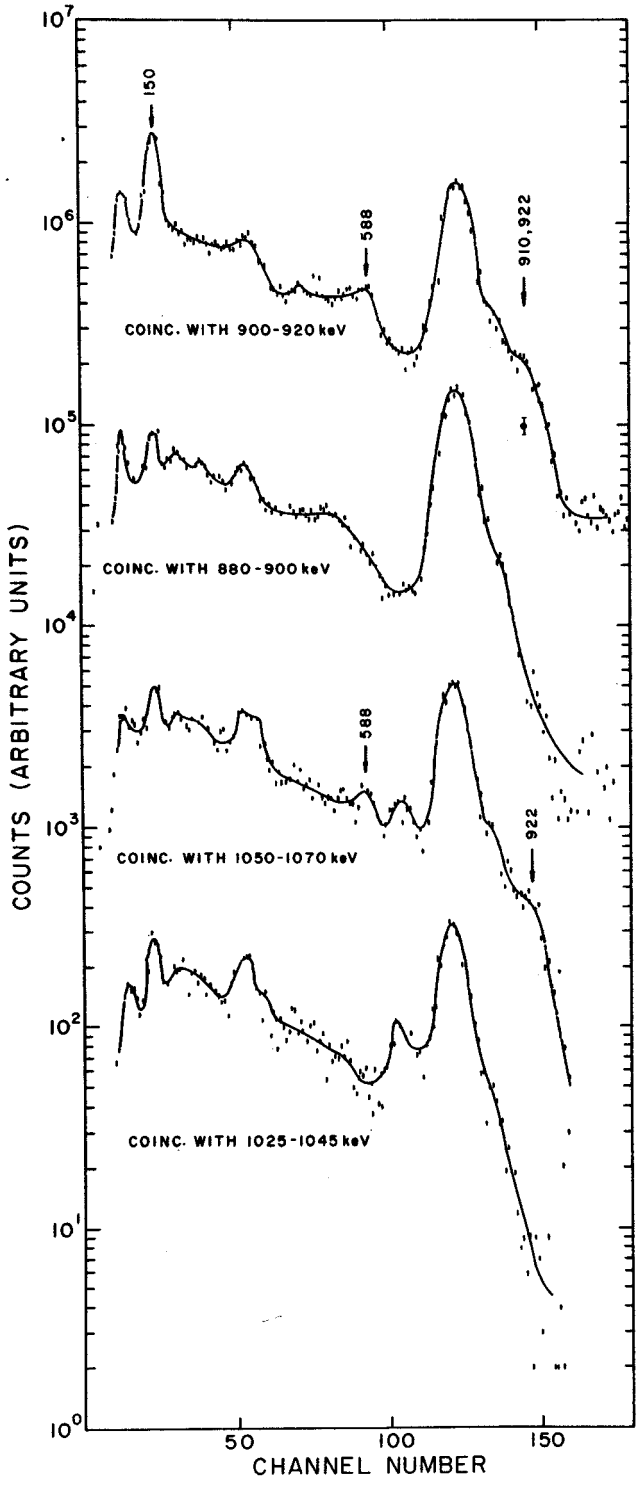

Figure 16. The ^{131m}Te coincidence spectra recorded with a 7.6 cm x 7.6 cm NaI(Tl) detector and gated by a Ge(Li) detector with 12 cm^3 active volume. The energy range included in the gate is indicated below each spectrum in the figure.

dence results is presented in table 3.

3.E. The Internal Conversion Spectrum

The internal conversion electron spectrum has been investigated with the orange spectrometer described in chapter 2 and with the Michigan State University iron-free $\pi\sqrt{2}$ spectrometer[63]. The spectrum from 45 to 240 keV recorded with the orange spectrometer is shown in fig. 17. The K conversion line of the 334.5 keV transition, recorded on the same instrument, is shown in fig. 18. The K and L conversion lines of the 149.7 keV ground state transition, recorded with the high precision $\pi\sqrt{2}$ spectrometer[63] are shown in fig. 19. Additional lines corresponding to the K conversion lines of the 452.6 and 773.7 keV transitions have also been observed in both instruments. The relative gamma-ray and conversion electron intensities thus being known, the internal conversion coefficients can be calculated if the conversion coefficient is known for one of the transitions. This number has been obtained by assuming that a correct value for α_K of the 149.7 keV transition can be derived from the theoretical conversion coefficients[10] and the experimental K/L ratio. This can be done using the expression

$$\frac{A_1}{A_2} = \frac{(K/L)\alpha_L(E2)-\alpha_K(E2)}{\alpha_K(M1)-(K/L)\alpha_L(M1)}$$

Table 3

Results of ^{131m}Te gamma-gamma coincidences.

Gate (keV)	Photons in coincidence (keV)
81	102, 200, 241, 774, 783, 822, 852, 1126
102	81, 200, 241, 774, 783, 822, 852
150	452, (665)[a], (713)[a], 910 (922)[a]
200	81, 102, 744, 774, 822, 852
241	81, 102, 774, 783
334	774, 793, (1646)[a]
452, 462	150, 665, 713, 852
550-600	150, 334, 910
665	150, 452, 462, 713, 852
774	81, 102, 200, 241, 334, 783, 822, 1126, (1206)[a]
852	(81)[a], (102)[a], 200, 334, 462, 744, 783, 1148[b]
1060	586, 922
1126	81, 774
>1600[b,c]	81, 102, 189, 231, 279, 334, 353

a) The peak may be too weak to be seen in this particular run or is masked by coincidences with underlying Compton distributions, but evidence exists from other runs.

b) The data are not shown.

c) The gate includes sum peaks.

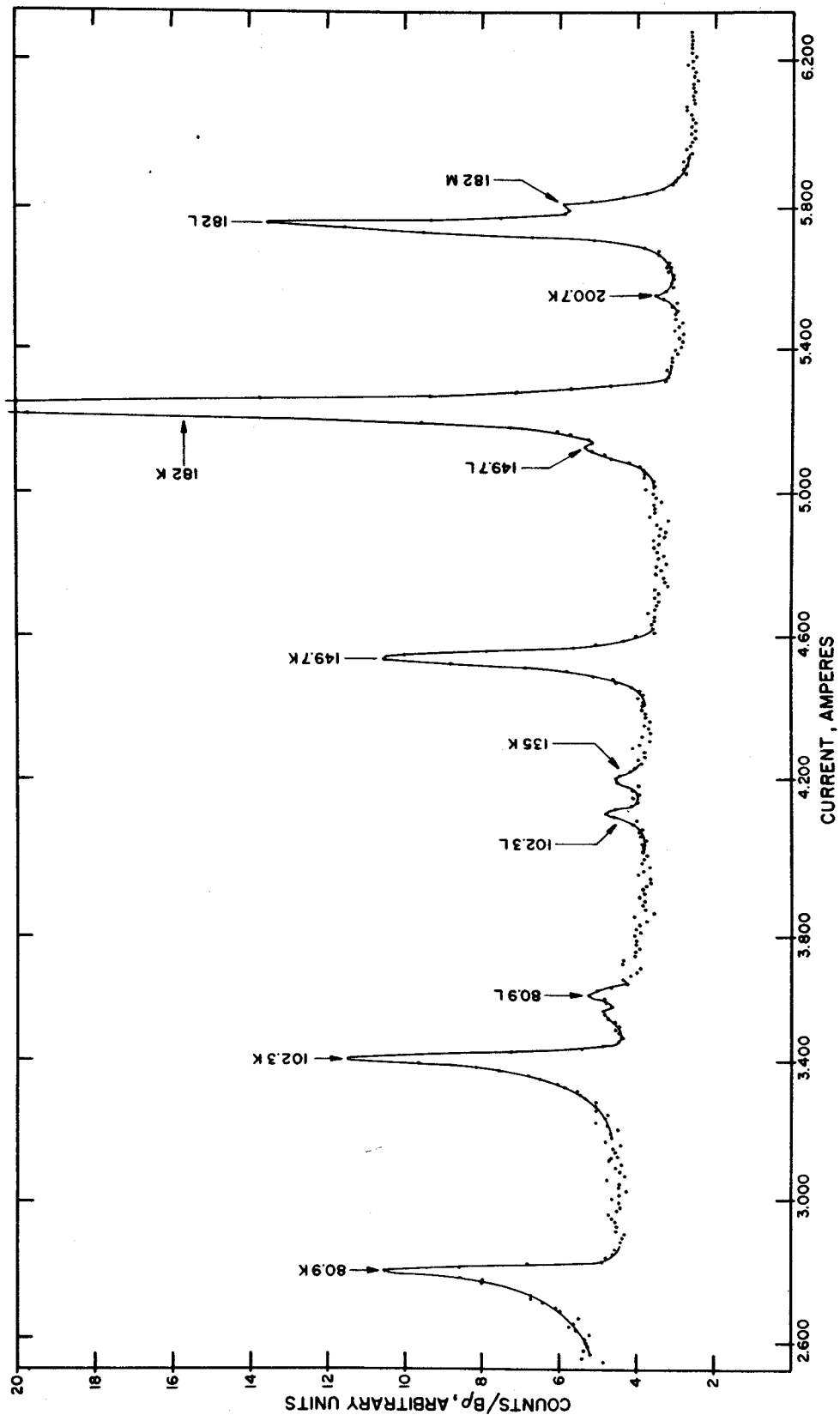

Figure 17. The ^{131m}Te internal conversion electron spectrum measured from 45 to 240 keV. This was recorded with the orange spectrometer.

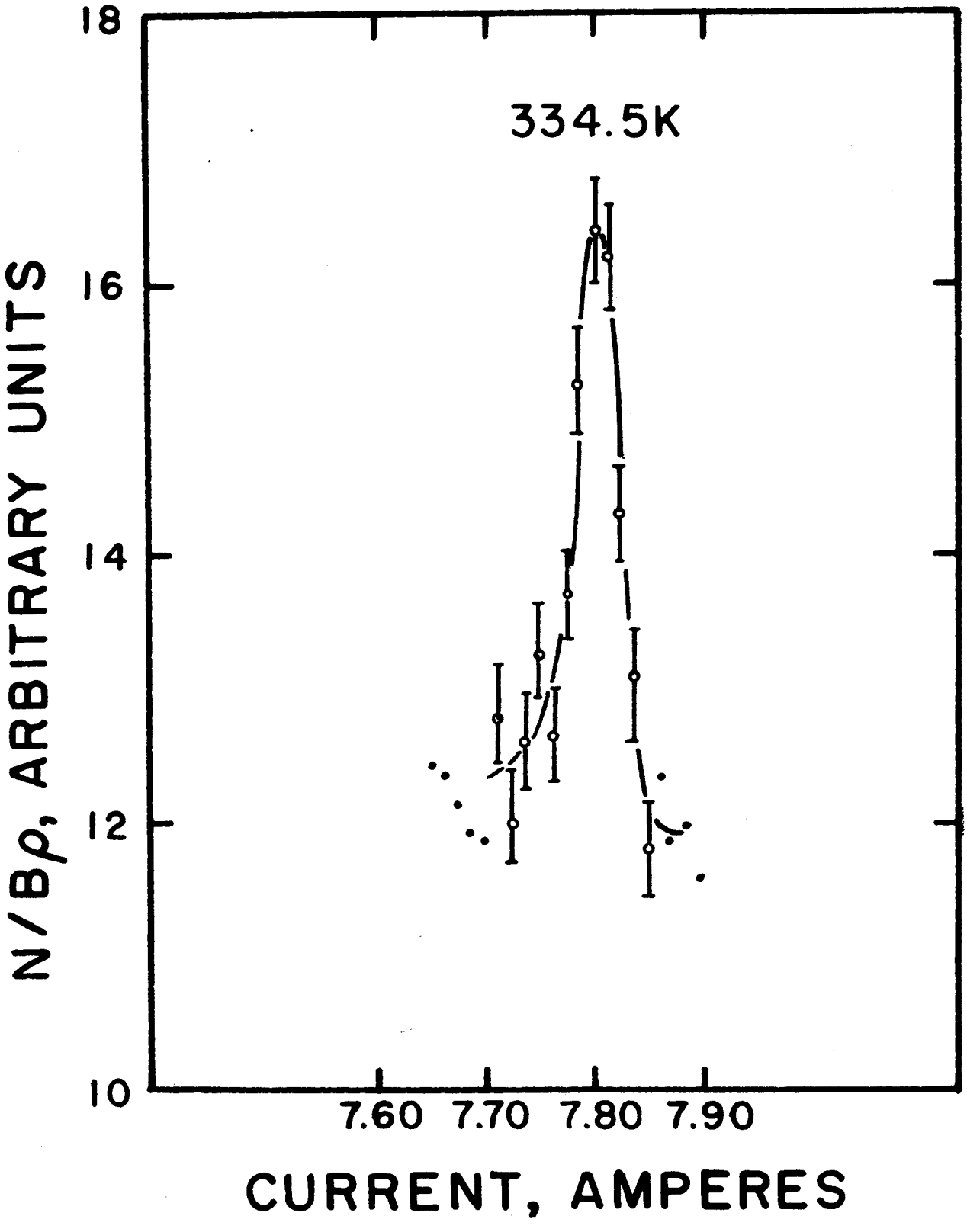

Figure 18. The K conversion line of the 334 keV photopeak of ^{131m}Te. This was recorded with the orange spectrometer.

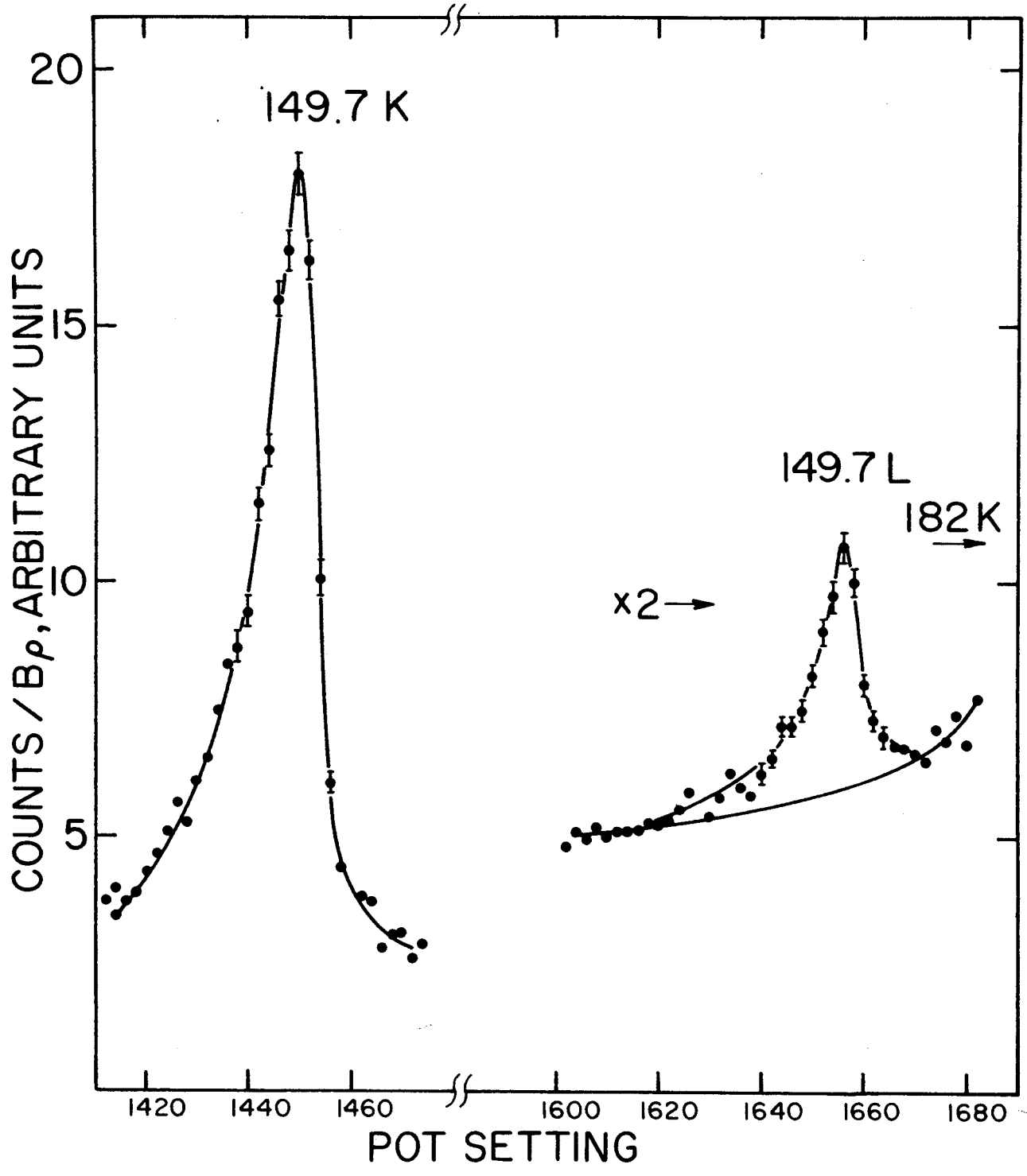

Figure 19. The K and L conversion lines of the 149.7 keV transition of ^{131m}Te. This was recorded with the $\pi\sqrt{2}$ spectrometer.

where K/L is measured, α's are taken from the tables[10], and A_1 and A_2 are the percentages of M1 and E2 multipole mixtures in the transitions, respectively.

The results of the data analysis are summarized in table 4, as well as the theoretical values of the conversion coefficients for the various possible multipole orders. The data do not differ significantly from the results of Devare et al.[57]. The most important aspect of the data is that they confirm the E1 assignment for the 201 and 241 keV transitions, indicating the presence of negative parity states in ^{131}I. The results still do not indicate which of the levels have negative parity. However, a measurement of the multipolarity of the 822 keV transition, when coupled with the information already determined, would allow the assignment of the parities to the levels at 1556, 1596, 1646, 1797, 1899 and 1980 keV. Unfortunately, it was not possible for us to measure the conversion coefficient for the 822 keV transition. Because of the very small energy difference between the 793.6 L and 822.1 K lines, such a measurement would require operating a spectrometer at 0.05% resolution with mass separated sources. In the discussion which follows, the 822.1 keV transition has been assumed to be an E2 + M1 transition.

3.F. The Proposed Decay Scheme and Discussion

A proposed decay scheme, based on the extensive results of the coincidence measurements and energy sums, is presented

Table 4

The results of conversion electron measurements of ^{131m}Te

E (keV)	electron intensity (K149.7 ≡100)	I_γ (I149.7 ≡100)	α_k a) (expt)	α_k (theoretical) b)			K/L (expt)	K/L (theoretical) b)				Multipole Assignment c)
				E1	E2	M1		Rose		Sliv		
								M1	E2	M1	E2	
80.9	K 103±10	17	1.25±.1(0)	3.2(0)	2.3(0)	1.2(0)	9±3	8.4	2.0	7.6	1.8	M1
	L 11± 4											
102.3	K 108±10	38	5.8±.5(-1)	1.7(-1)	1.1(0)	6.2(-1)	9±3	8.4	2.8	7.6	2.7	M1
	L 12 ± 4											
149.7	K 100+	100	2.1±.1(-1)	5.6(-2)	3.3(-1)	2.1(-1)	7.9±.4	8.4	4.1	7.6	2.9	M1, 10% E2
	L 12.6±.6											
200.7	K 3.8±.5	28	2.6±.4(-2)	2.6(-2)	1.2(-1)	9.6(-2)						E1
240.6	K 3.0±1.0	32	1.8±.6(-3)	1.5(-2)	6.7(-2)	5.8(-2)						E1
334.5	K 4.5±.5	36	2.6±.3(-2)	6.6(-3)	2.3(-2)	2.4(-2)						M1,E2
452.7	K 1.4±.5	21	1.4±.5(-2)	3.1(-3)	9.7(-3)	1.1(-2)						M1,E2
773.7	K 1.2±.6	135	1.8±.9(-3)	9.4(-4)	2.4(-3)	3.1(-3)						E2, 20% M1

a) The number in parenthesis is the appropriate power of 10, i.e., 1.25±0.1(0) means (1.25±0.1) x 10^0.

b) Reference 5).

c) The conversion coefficients are in good agreement with the results of Devare, et al. 2).

in fig. 20. The levels and transitions presented with dashed lines are those for which no direct coincidence evidences exist, but are indicated on the basis of energy sums. However, these photons are all very weak and the principal features of the decay scheme are not dependent upon their placement.

The spin-parity assignments are based on log ft values calculated from the measured gamma-ray intensities and on the measured internal conversion coefficients. The ground state of ^{131}I is known to be $7/2^+$ from microwave absorption and magnetic moment measurements[1]. The 150 keV state is assigned a spin of $5/2^+$ on the basis of the M1 predominance of the 150 keV transition, and the allowed nature of the beta transition from the $d_{3/2}$ ground state of ^{131g}Te[61]. The assignment is also consistent with the shell model systematics in this region[1]. The $3/2^+$ spin assignment to the 493 keV state is obtained from the study[61] of ^{131g}Te. The 603 keV state can only be $3/2^+$ or $5/2^+$ since it de-excites to both the $7/2^+$ and $5/2^+$ states, and the beta transition from the $3/2^+$ parent state is allowed[61]. The conversion coefficient of the 452 keV transition indicates an M1 + E2 transition and confirms the parity assignment. On the basis of the systematics of the other known odd mass iodine isotopes, the $5/2^+$ assignment is favored.

The 774 keV transition is predominately E2 on the basis of the measured conversion coefficient. The log ft value of 9 indicates the beta transition to the 774 keV level is proba-

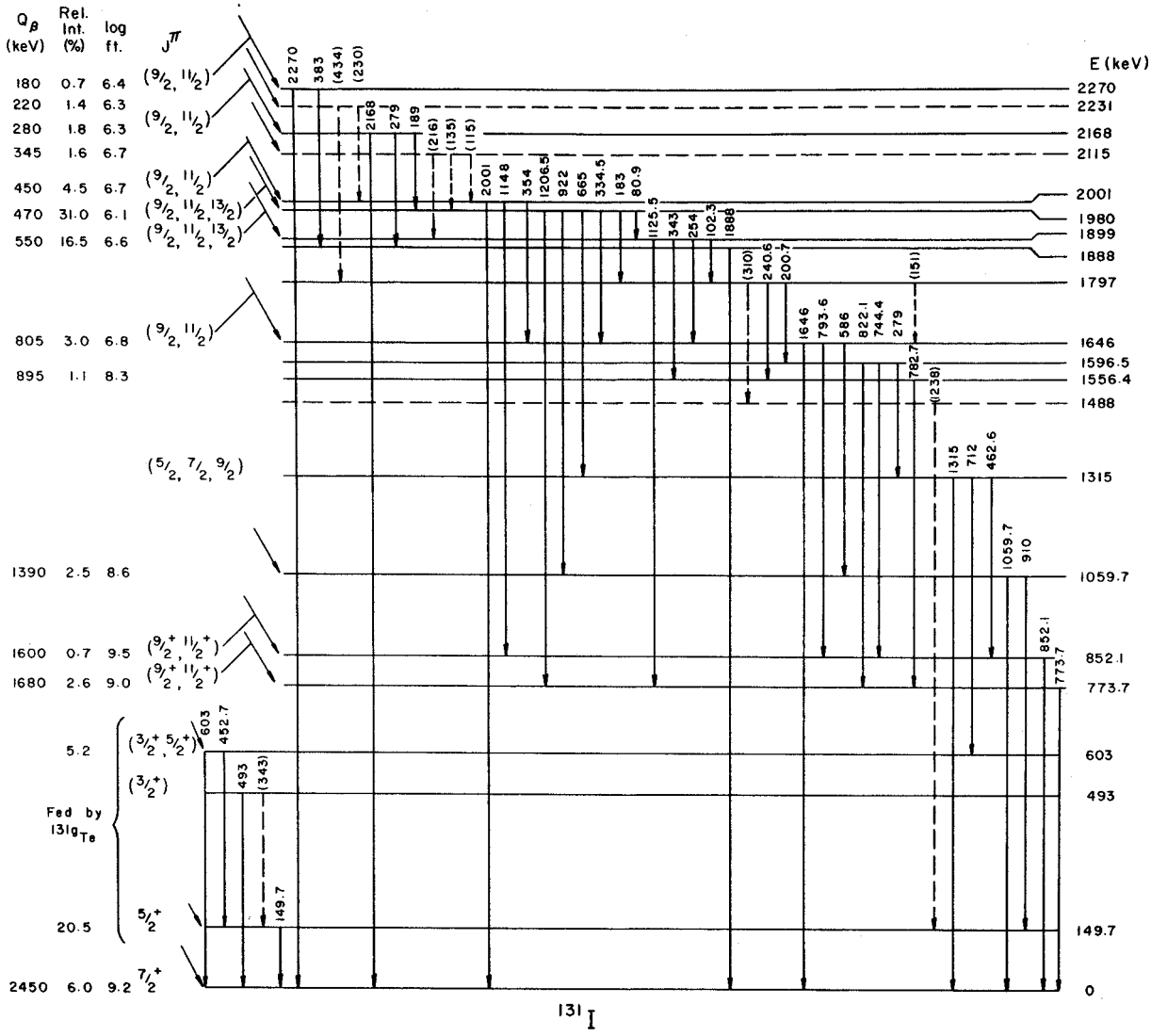

Figure 20. The proposed energy level scheme for ^{131}I as seen in the decay of 30.5 hour ^{131m}Te.

bly first forbidden. The spin of the level is then limited to $9/2^+$ or $11/2^+$. Similar arguments apply to the same spin parity assignment to the 852 keV state.

The log ft value of the beta transition to the 1060 keV level is 8.6, so the parity is positive. The level depopulates to both the $7/2^+$ ground and $5/2^+$ first excited state. Assuming both transitions to be M1 + E2 mixtures, the level has $7/2^+$. The 1315 keV state is $7/2^+$ or $9/2^+$ when the assignment is based on the same arguments as for the 1060 keV state.

The M1 character of the 81 and 102 keV transitions, the E1 character of the 201 and 241 keV transitions, and the M1 + E2 mixture of the 334 keV photon define a parity difference in the higher excited states. The 1556 and 1596 keV levels must be of one parity, while the 1646, 1797, 1899 and 1980 levels are opposite. The log ft values of the higher energy group range from 6.1 to 6.8, possibly indicating allowed beta transitions and negative parity states. The log ft values to the 1556 and 1596 states are high, but probably not high enough for second forbidden beta transitions. They are probably first forbidden transitions, leading to positive parity states. Furthermore, if the 1556 and 1596 keV levels were not positive parity, the 744, 783 and 822 keV transitions would have to be of E1 character. This is indeed an unlikely situation. Finally, Singru and Devare[64] have measured the g factor of the 1797 level and found it to be small and negative. They interpret their results as indicating the level to be a three quasi-particle state, with

$(g_{7/2}^{p}, d_{3/2}^{n}, h_{11/2}^{n})$ or $(d_{5/2}^{p}, d_{3/2}^{n}, h_{11/2}^{n})$ configurations possible. This measurement may not be conclusive, but it at least lends additional support to the evidence presented above.

The positive parity assignment to the 1556 and 1596 keV levels are indeed plausible with respect to the core coupling model: The 774 keV state would correspond to a one phonon excitation of the core, while the 1556 and 1596 keV levels would arise from two phonon excitations. The average energy of this pair, 1576 keV, is 2.0 times the 774 keV one phonon energy, as the model predicts. It should be noted, however, that no weighting factors have been used in this simple averaging procedure. The absence of crossover transitions and the high log ft values may be another indication of the collective nature of the states.

Another interesting feature of the decay scheme is the 852 keV level and the transitions to it. If the 774 keV level is a one phonon excitation of the core coupled to the ground state, one would actually expect a multiplet of levels in this vicinity which would arise from the coupling of the 2^{+} phonon with the $g_{7/2}$ quasi-particle state. The 852 keV level is thus a very good candidate. However, upon examining the decay scheme, it is noted that those levels which account for 95% of the gamma-ray feeding to the 852 keV level also give rise to ground state transitions. Such a situation could arise from phonon-quasi-particle admixtures in the wave functions of the excited states. One possibility would be

that the 852 keV state is a one-phonon coupling with the ground state, while the 1315, 1646 and 2001 keV states arise from two phonons admixing with the same $g_{7/2}$ single quasi-particle state. The center of gravity of this multiplet is 1.94 times the 852 keV energy. The large splitting of the levels could arise from the stronger coupling between the quasi-particle and phonons involved.

In addition, one can conclude from such arguments that the 774 keV state is probably $11/2^+$ and the 852 keV state $9/2^+$, since the 774 keV photon may be pure E2, and the 852 keV photon probably is an M1 + E2 admixture.

3.G. Systematics of Odd Mass Iodine Isotopes

An illustration of the presently known levels of the odd A iodine isotopes that are populated by the decay of both the $3/2^+$ and $11/2^-$ tellurium isomers[48-50,61,65] is given in fig. 21. Figures 22 and 23 show the results of recent theoretical predictions of Kisslinger and Sorensen[3], and O'Dwyer and Choudhury[4]. Although there is insufficient experimental information available concerning the properties of the states to allow a detailed quantitative comparison with the predictions of transition rates and lifetimes, it is interesting to make some qualitative comparisons and to note systematic trends.

The calculations of Kisslinger and Sorensen, as discussed in chap. 1, are based on pairing plus quadrupole

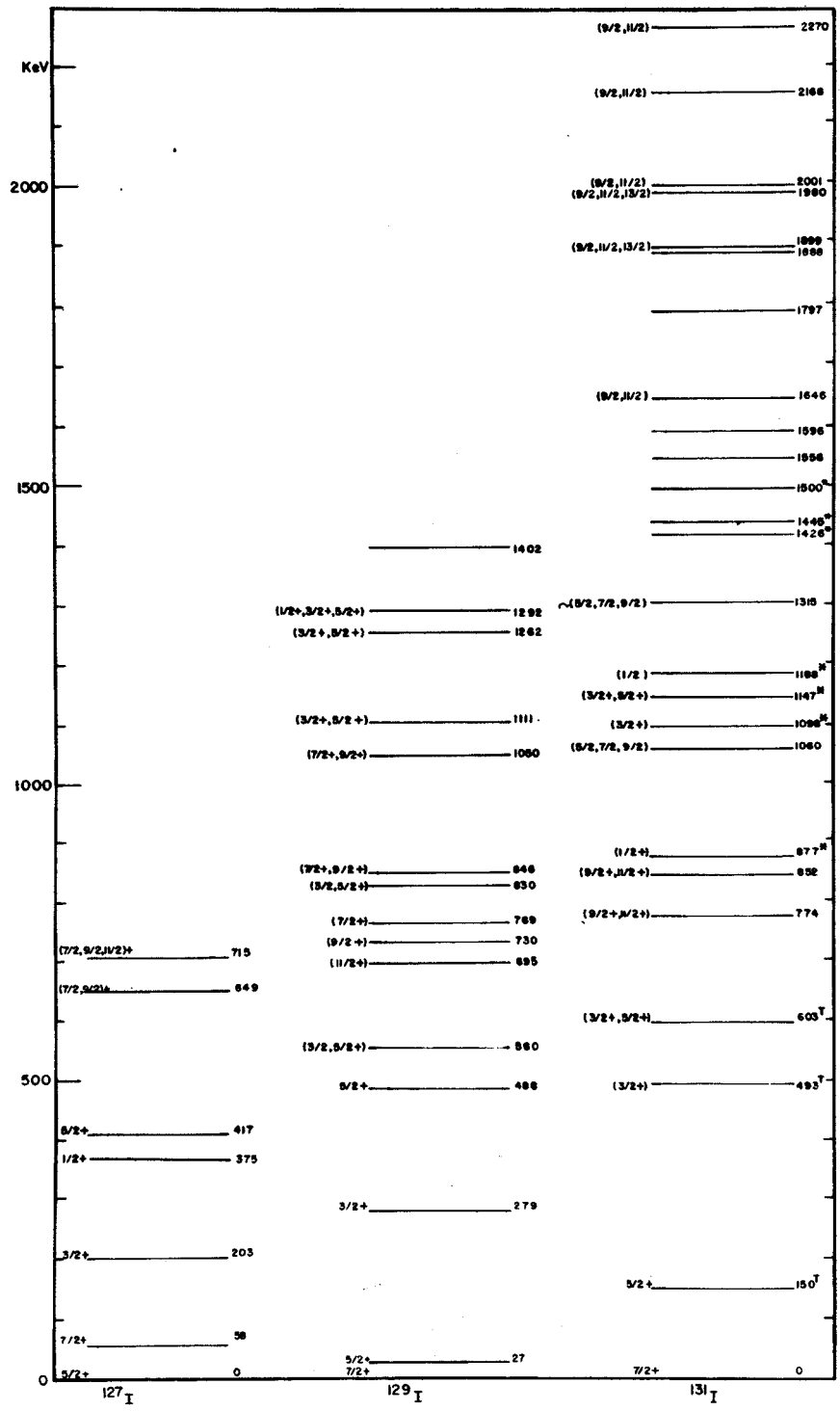

Figure 21. A comparison of the experimentally determined energy states in ^{127}I, ^{129}I, and ^{131}I.

*) Populated by the decay of ^{131g}Te only

†) Populated by the decay of both ^{131g}Te and ^{131m}Te

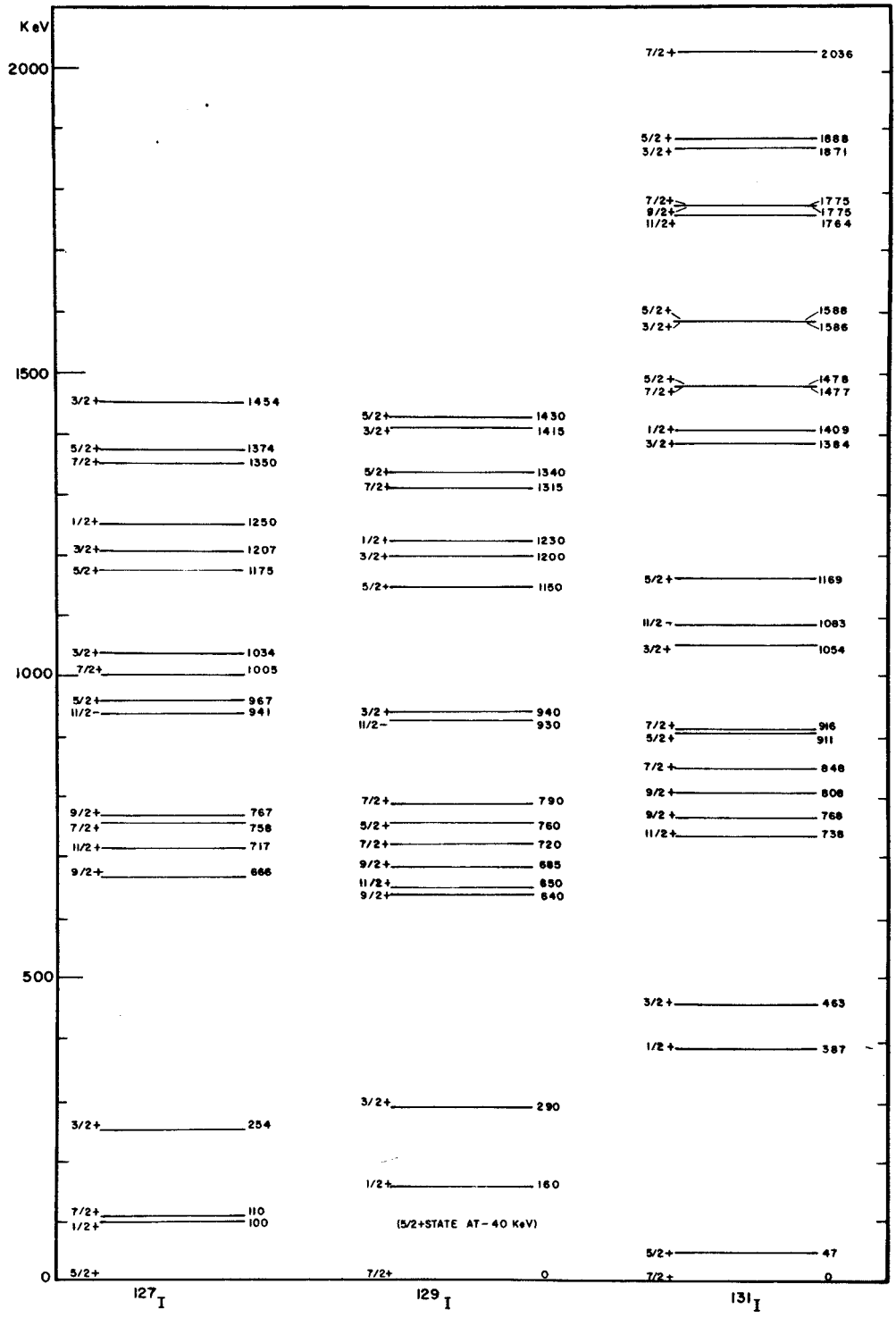

Figure 22. The states of ^{127}I, ^{129}I, and ^{131}I as calculated by Kisslinger and Sorensen.[3]

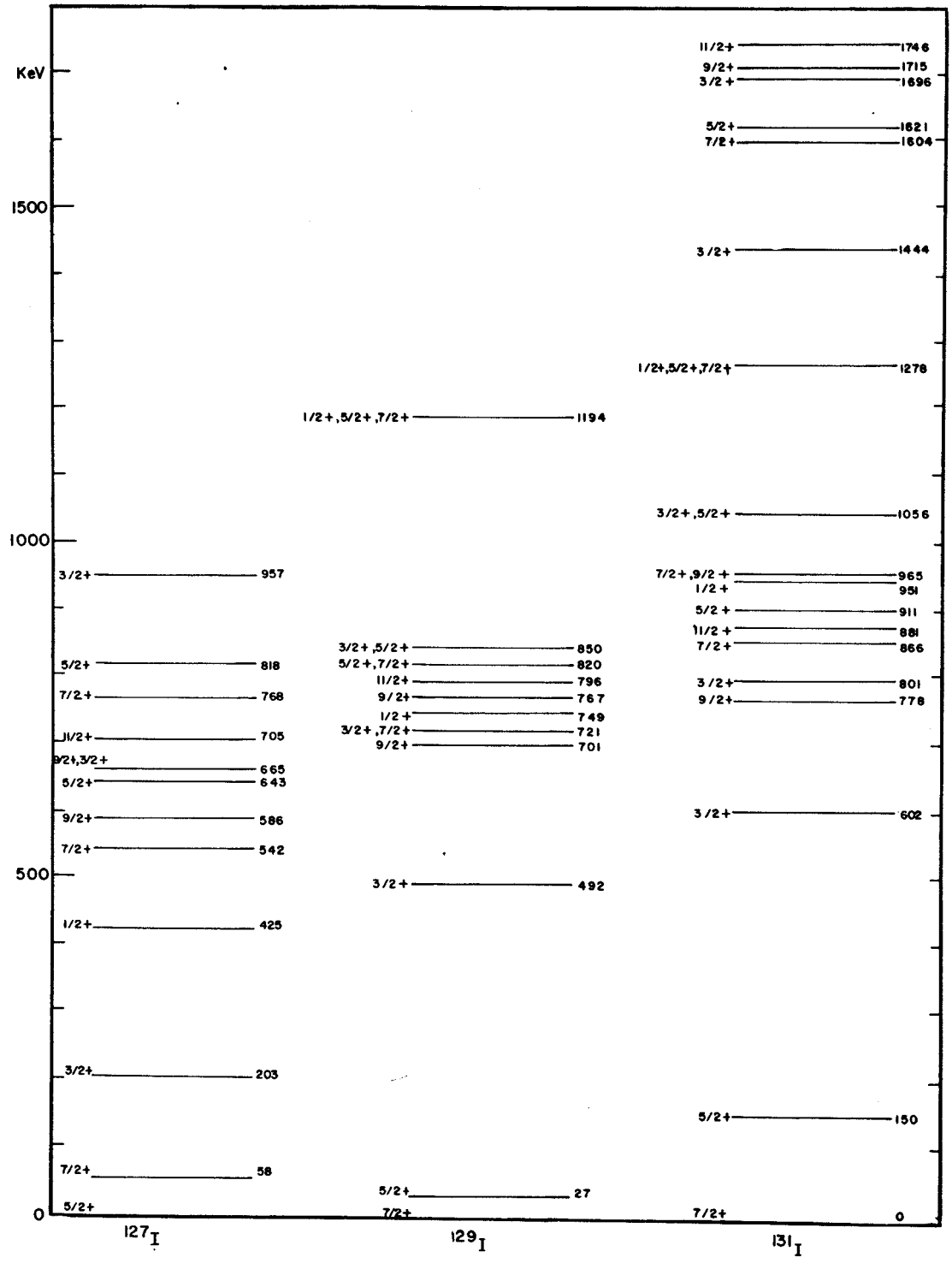

Figure 23. The energy states of ^{127}I, ^{129}I, and ^{131}I as calculated by O'Dwyer and Choudhury.[4]

forces. The pairing interaction tends to couple like nucleons to zero angular momentum, producing a spherical shape, while the long range quadrupole force tends to correlate the motion of the nucleons, giving rise to collective features in the energy spectrum. The application of this model to the iodine isotopes is successful in predicting the low lying single quasi-particle states of spin $5/2^+$ and $7/2^+$, corresponding to the $d_{5/2}$ and $g_{7/2}$ shell model states. It also predicts $1/2^+$ and $3/2^+$ states below 500 keV, $7/2^+$, $9/2^+$ and $11/2^+$ states in the vicinity of 700 keV, and a large energy gap between the first and second $5/2^+$ states. Although the actual energy values of the calculated states differ considerably, the predicted systematic trends are remarkably accurate. In addition, Kisslinger and Sorensen explicitly state that the $1/2^+$ state is mainly of phonon character[3]. Experimentally, the $1/2^+$ state at 877 keV is very weakly populated by the negatron decay of the tellurium parent having a spin and parity $3/2^+$. On the basis of spin differences alone, this should be an allowed transition. This may then be an experimental indication that the $1/2^+$ state is actually collective in nature.

The calculations of O'Dwyer and Choudhury predict the energy levels arising from phonons coupling to $g_{7/2}$, $d_{5/2}$ and $d_{3/2}$ single particle states[4]. In these calculations, the phonon energy $\hbar\omega$, the single particle energies ε_j, and the coupling strengths ξ are used as adjustable parameters to optimize the fit of the predicted states with the known

experimental levels. In the case of ^{129}I, the 488 keV state, rather than the 279 keV state was assumed to be the $3/2^+$ level in these preliminary calculations. The more recent experimental results suggest that the 488 keV state in this nucleus corresponds to the 417 keV $5/2^+$ state in ^{127}I. The position of the $3/2^+$ state in ^{131}I is as yet uncertain, but the 493 keV state is more likely to be the $3/2^+$ state than the 603 keV state used in the above calculations. As in the case with many core coupling calculations[33,35], a multitude of states are predicted, all of which may not be populated by radioactive decay. Reaction type experiments may be a more sensitive test of this model. The correspondence of the predicted 778 keV $9/2^+$ and 881 keV $11/2^+$ with the experimental 774 and 852 keV states is tempting, but may be fortuitous.

Both models predict states of $9/2^+$ and $11/2^+$ in the 600-800 keV region. These states probably lie at 649 and 715 keV in ^{127}I, 696 and 730 keV in ^{129}I, and 774 and 852 keV in ^{131}I, although the ordering is not certain. Insufficient information is known about the higher energy states to afford even a qualitative comparison.

Perhaps the most interesting phenomenon observed in this study of systematic trends is shown in fig. 24. The energy level separation of the $1/2^+$, $3/2^+$ and $5/2^+$ states, with respect to the $7/2^+$ states have been plotted as a function of neutron number for the iodine isotopes. A least squares quadratic fit has been performed on each curve for the known ex-

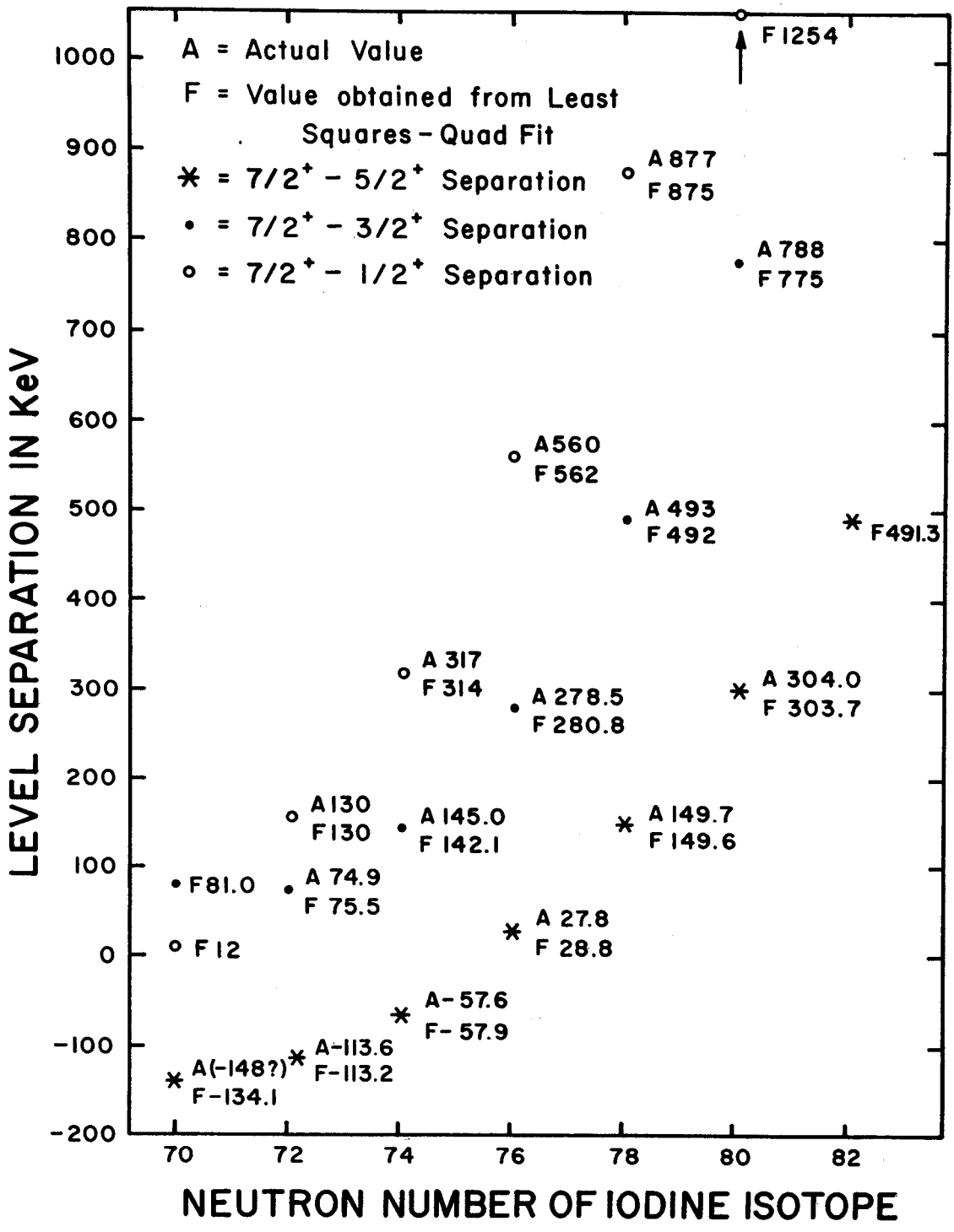

Figure 24. A comparison of the systematic energies of separation of the low lying levels of odd mass iodine isotopes with the values obtained from a least squares quadratic fit of the data points. All values marked A except the $5/2 - 7/2$ value for ^{123}I and the $3/2 - 7/2$ value for ^{133}I have been included in the least squares fit. The values marked F are those obtained from the fitted equation.

perimental points. As can be noted from the figure, the fit is exceptional. The curves have been extrapolated to the neighboring isotopes (i.e. to ^{123}I and ^{133}I), effectively predicting the energy levels expected. In the case of ^{133}I, the extrapolated curve gave very good agreement with some new experimental investigations being performed at MIT[66]. This same type of analysis technique has now been applied to low energy levels of Sb isotopes, with equally good results[67].

CHAPTER 4

CONVERSION ELECTRON AND POSITRON MEASUREMENTS OF 34.5hr ^{83}Sr

4.A. Introduction

The study of the decay scheme of ^{83}Sr has been undertaken for two reasons. First, using an effective configuration interaction in shell model calculations, Talmi and Unna[5] have predicted some of the energy levels of ^{83}Sr. The ground state spin and parity of the parent ^{83}Sr can be inferred from the experimental study, thus serving as an initial test of the calculations. Second, the energy levels of $^{83}_{37}$Rb are obtained, extending the study of the systematic trends of the low lying levels of the Rb isotopes to the more neutron deficient side of the stable isotopes. This is an interesting region of the periodic table in which to obtain systematics, since there are subshell closures at Z = 38 and 40. Hence, there should be low energy shell model states available for particle-hole configurations on both sides of the subshell closures. A wide variety of spin-parity states are expected from such a situation.

Previous to the recent study by Etherton, Beyer, Kelly and Horen[69], very little was known about the decay scheme of ^{83}Sr. Previous investigations had determined the half-life, the existence of the strong conversion lines of the 42.3 keV transition, and the positron end point energy[70,71]. Some groups had reported studies of the gamma-ray spectrum

using scintillation techniques[72-74] but conclusions about the intense 42.3 keV transition remained in question. In addition, the decay scheme was known to be incomplete and thus no conclusions could be reached about the ground state spin-parity assignment for the ^{83}Sr parent. Internal conversion electron studies were thus undertaken in order to complement and extend the coincidence studies of Etherton et al.[69]. A search has also been made for the presence of the isomeric state in ^{83}Sr that was predicted by Talmi and Unna[5].

The decay scheme of Etherton, et al. is presented in fig. 25. Although the coincidence arguments for the decay scheme constitute an entirely independent study, the final decay scheme depends very sensitively on the M2 multipolarity assignment of the highly converted 42.3 keV transition. Because of the requirements of intensity balance in the decay scheme, the level structure below 805 keV would be quite different if the 42.3 keV transition had another character, e.g. E2.

4.B. Source Preparation

The sources of ^{83}Sr utilized in this study were produced by a ^{85}Rb(p,3n)^{83}Sr reaction using natural RbCl targets. Proton energies from 34 to 42 MeV from the Michigan State University cyclotron were used with different targets. With careful carrier-free chemical procedures, at least one source

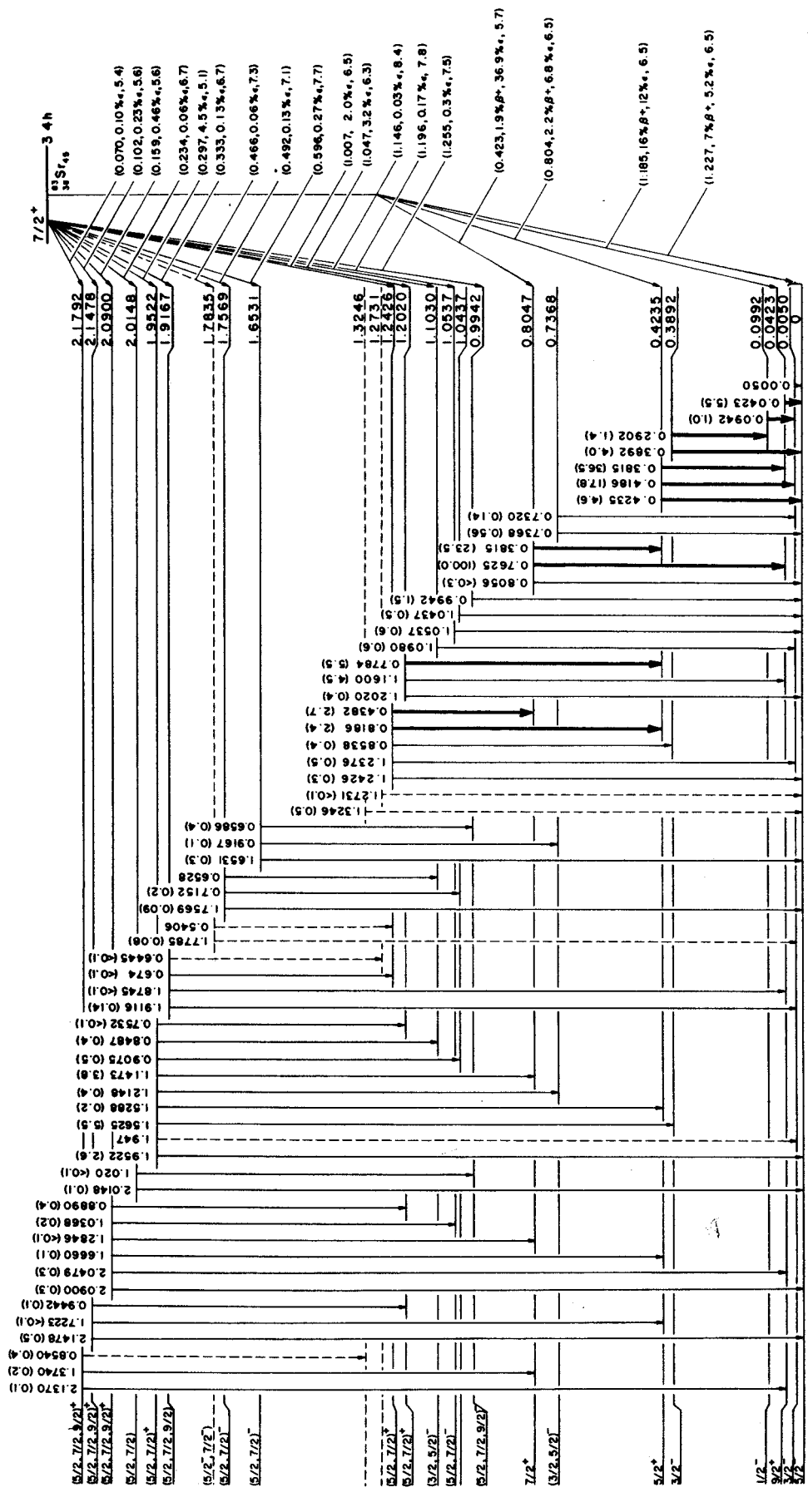

Figure 25. The proposed decay scheme of ^{83}Sr. The transitions indicated by the more intense lines in the drawing are those for which the internal conversion coefficients were measured.

of sufficient specific activity was obtainable for the spectrometer studies from each bombardment.

Two entirely different chemical procedures were used to separate the strontium fraction from the RbCl target. The first involved the standard precipitation procedures of strontium in fuming nitric acid[75]. The target was dissolved in a minimum amount of distilled water and transferred to a centrifuge tube immersed in an ice water bath. To this solution was added a few milligrams of $BaCl_2$ in water solution. Chilled fuming nitric acid was added in sufficient quantity to bring the solution to at least 70% concentration. The solution was allowed to digest for 30 minutes at ice water temperature and then centrifuged. The $Ba(NO_3)_2$ precipitates under these conditions, carrying the strontium fraction with it while the rubidium remains in solution. The barium-strontium precipitate was dissolved in a few drops of 0.1N HCl and the fuming nitric acid precipitation repeated to remove the trace amounts of the rubidium remaining. The final precipitate was dissolved in a few ml 0.1 NHCl and then saturated with dry HCl gas in an ice bath. The $BaCl_2$ will precipitate under these conditions, leaving the strontium fraction in solution. This solution was found to be radiochemically free from ^{83}Rb, ^{84}Rb and ^{86}Rb which were also produced in the bombardments. However, complete removal of the barium was difficult to achieve.

The second procedure involved a slightly modified version of the extraction technique that was originally reported

by Kiba and Mizukami[76,77]. The RbCl target was dissolved in a few milliliters of a 0.5 M buffer solution composed of acetic acid and ammonium hydroxide, adjusted to pH 8. This solution was transferred to a separatory funnel, to which was added an equal volume of an organic solution consisting of 0.05M TTA (o-thenoyl triflouroacetone) in hexone (methyl isobutyl ketone). After shaking the vessel for a few minutes, the phases were allowed to disengage. The aqueous phase was drained into a second separatory funnel and re-extracted with the same organic solution. The two organic phases were combined and again extracted with the buffer solution to remove any rubidium carried down in the first operation. The resulting organic solution was found to contain greater than 90% of the ^{83}Sr produced in the activation, and radiochemically free of rubidium contaminants.

This organic solution is very convenient for preparing gamma sources, since it can be evaporated to dryness very easily. However, for an electron source free of the large TTA molecules, it was found very easy to back extract the strontium activity into a very small amount of 0.2N HNO_3 solution. When the resulting solution was evaporated to dryness in a centrifuge tube, a small amount of mass still remained. This residue was driven off by simply heating over a flame. A few drops of water will then take up the strontium activity, leaving one with the desired source of high specific activity in a neutral solution. This extraction procedure has been used exclusively from the time of its per-

fection. It offers the obvious advantage of being very rapid as well as avoiding the use of potentially hazardous fuming nitric acid. In addition, electron sources are easier to prepare because the solution is not corrosive to the thin aluminum foils used in mounting. Furthermore, vacuum evaporation is easier with $Sr(NO_3)_2$ than with $SrCl_2$. In one series of experiments designed to search for a short lived isomer of ^{83}Sr, the chemistry was performed and counting begun within two minutes of the time the target was removed from the beam pipe.

4.C. Apparatus

The internal conversion electron spectrum of ^{83}Sr was measured with the "orange" spectrometer, described in Chap. 2. The baffles and detector slit were set for resolution of 0.8% and about 5% transmission. Some measurements on the 42.3 keV transition were recorded with the Michigan State University iron free $\pi\sqrt{2}$ spectrometer[63]. The baffles were set for resolution of $\leq$ 0.2%, but, in actuality, the source thickness determined the resolution of these low energy lines.

Photon spectra have been recorded with Ge(Li) crystals ranging in size from 0.8 to 7 cc, as well as with NaI(Tl) crystals. The low energy portion of the spectrum is shown in fig. 26 and the remainder in fig. 27. Table 5 lists the results of energy and relative intensity measurements.

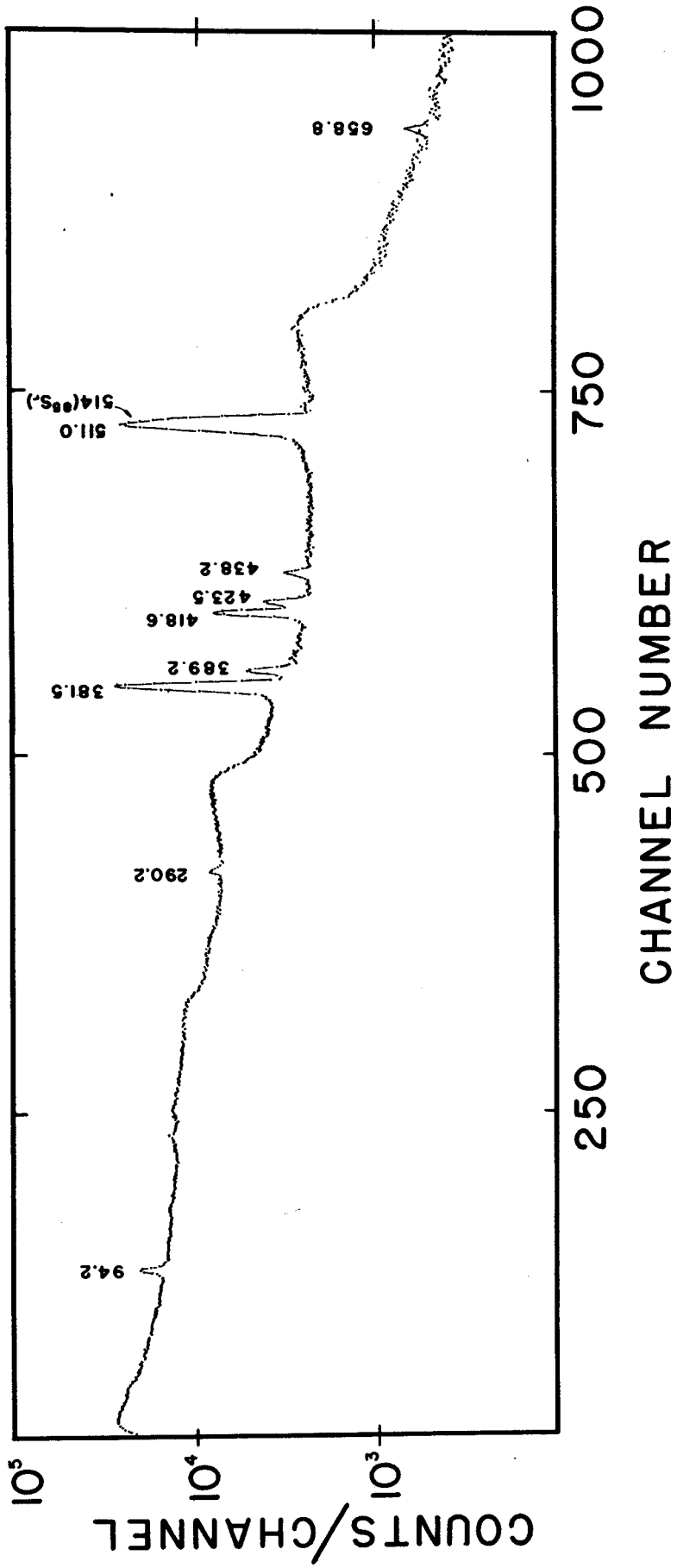

Figure 26. The low energy part of the gamma-ray singles spectrum of ^{83}Sr recorded with a 7 cm^3 Ge(Li) detector.

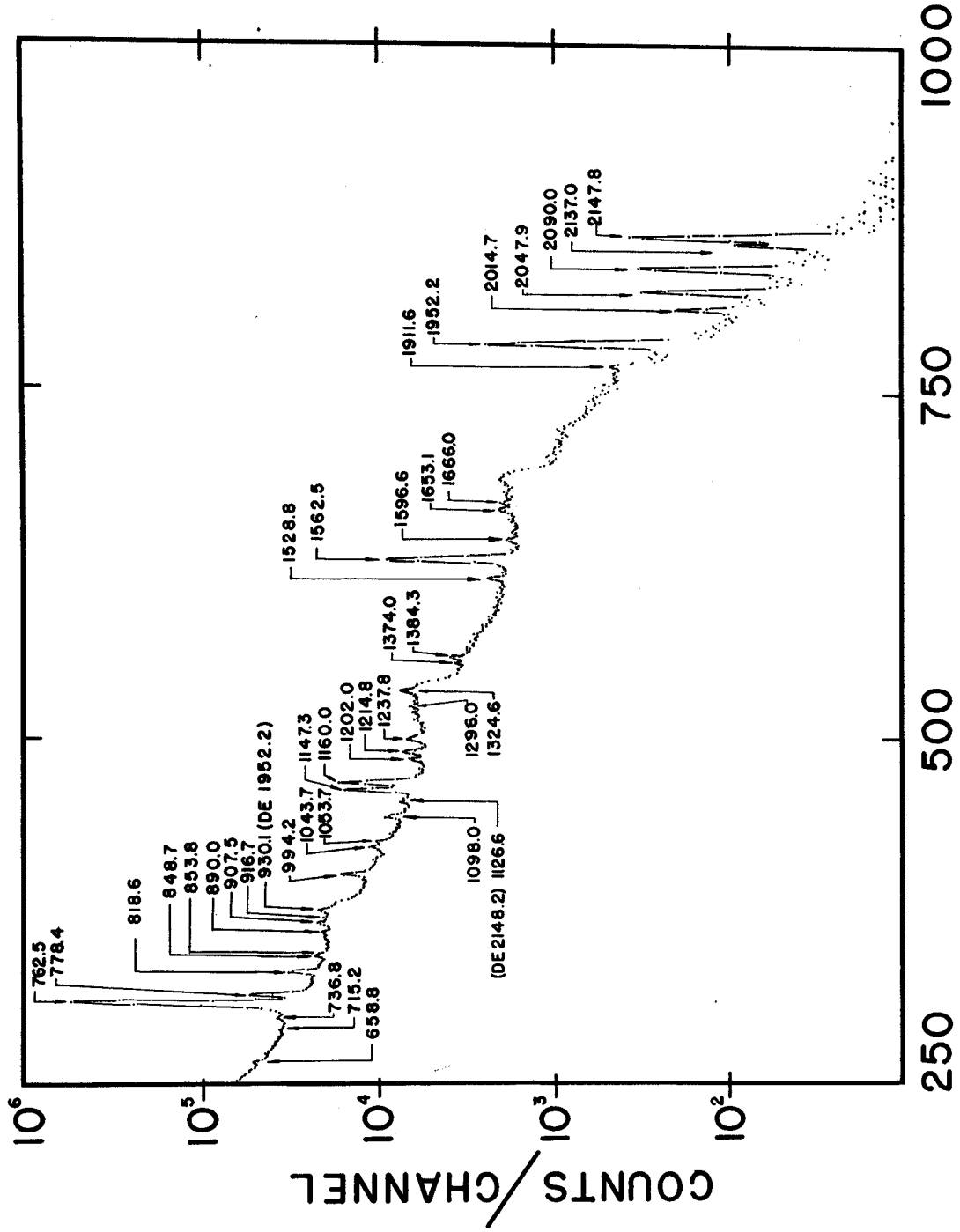

Figure 27. The high energy part of the gamma-ray singles spectrum of ^{83}Sr recorded with a 7 cm^3 Ge(Li) detector.

Table 5

The ^{83}Sr gamma ray energies and relative intensities

Energy[a] (keV)	Relative[b] Intensity	Energy (cont.)	Relative Intensity (cont.)	Energy (cont.)	Relative Intensity (cont.)
5.0		805.6	weak	1296.0	0.4
42.3	5.5	818.6	2.4	1324.6	0.5
94.2	1.0	848.7	0.4	1339.5	weak
290.2	1.4	853.8	0.4	1374.0	0.2
381.5[c]	23.5	889.2	0.4	1384.3	0.3
381.5[c]	36.5	907.5	0.5	1396.0	weak
389.2	4.0	916.7	0.1	1528.8	0.2
418.6	17.8	944.2	0.1	1562.5	5.5
423.5	4.6	994.2	1.5	1596.6	0.07
438.2	2.7	1020.1	weak	1653.1	0.3
511.0	163.2	1037.8	0.2	1666.0	0.1
540.6[d]	weak	1043.7	0.5	1710.3	weak
559.4	weak	1053.7	0.6	1722.3	weak
565.2	weak	1069.4	weak	1749.1	0.08
644.5	weak	1087.2	weak	1756.5	0.09
652.8	weak	1098.0	0.6	1778.5	0.08
658.6	0.4	1147.3	3.8	1795.7	weak
674.0	weak	1160.0	4.5	1874.5	weak
714.2	0.2	1202.0	0.4	1911.6	0.14
732.0	0.15	1214.8	0.4	1952.2	2.6
736.8	0.55	1237.6	0.5	2014.7	0.1
753.2	weak	1242.6	0.3	2047.9	0.3
762.5	100	1273.1	weak	2090.0	0.3
778.4	5.5	1284.6	weak	2137.0	0.1
				2147.8	0.5

These gamma ray data are taken from a more complete discussion which will be reported elsewhere[69].

4.D. Conversion Coefficients and Multipolarities

4.D.1. The 42.3 keV Transition and the Search for an Isomer in ^{83}Sr

It is well known that the isotopes ^{87}Sr and ^{85}Sr possess isomeric states, arising from the large spin difference of the $1/2^-$ excited state and the $9/2^+$ ground state. In addition, Talmi and Unna[5] predict the same type structure for ^{83}Sr, so an isomeric state was expected in this latter isotope. The absence of transitions in prompt coincidence with the 42.3 keV photon initiated the question as to whether this might be a transition in the parent. In order to answer this question, as well as to determine the multipolarity and the accurate energy of the transition, the conversion electron spectrum was studied in the $\pi\sqrt{2}$ spectrometer[63]. The K, L and M electron spectra that were obtained are shown in fig. 28. When compared to the x-ray binding energies[8], the measured K-L and K-M energy differences were found, however, to deviate by only 0.07 keV from the values for Rb, as shown in table 6. Thus, the 42.3 keV transition occurs in ^{83}Rb. Several different experiments were then performed to specifically search for an isomeric state in ^{83}Sr. No evidence has been found to indicate its existence. The fast chemical pro-

These gamma ray data are taken from a more complete discussion which will be reported elsewhere[69].

4.D. Conversion Coefficients and Multipolarities

4.D.1. The 42.3 keV Transition and the Search for an Isomer in ^{83}Sr

It is well known that the isotopes ^{87}Sr and ^{85}Sr possess isomeric states, arising from the large spin difference of the $1/2^-$ excited state and the $9/2^+$ ground state. In addition, Talmi and Unna[5] predict the same type structure for ^{83}Sr, so an isomeric state was expected in this latter isotope. The absence of transitions in prompt coincidence with the 42.3 keV photon initiated the question as to whether this might be a transition in the parent. In order to answer this question, as well as to determine the multipolarity and the accurate energy of the transition, the conversion electron spectrum was studied in the $\pi\sqrt{2}$ spectrometer[63]. The K, L and M electron spectra that were obtained are shown in fig. 28. When compared to the x-ray binding energies[8], the measured K-L and K-M energy differences were found, however, to deviate by only 0.07 keV from the values for Rb, as shown in table 6. Thus, the 42.3 keV transition occurs in ^{83}Rb. Several different experiments were then performed to specifically search for an isomeric state in ^{83}Sr. No evidence has been found to indicate its existence. The fast chemical pro-

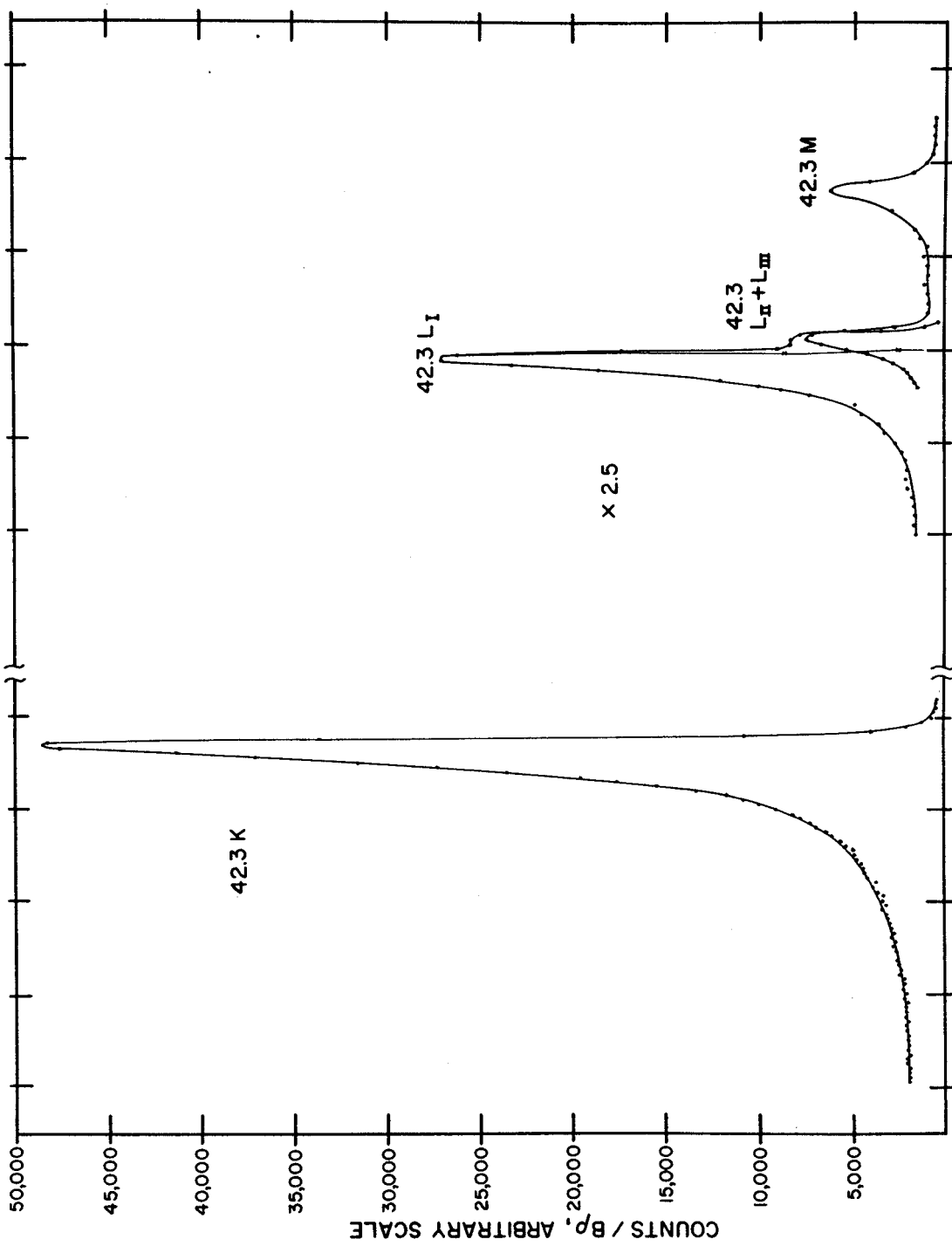

Figure 28. The K, L, and M conversion electron lines of the 42.3 keV transition in ^{83}Rb. This spectrum was recorded with the MSU iron free $\pi\sqrt{2}$ spectrometer.

Table 6

A. Experimental results of the internal conversion electron measurements on the 42.3 keV transition.

E_γ (keV)	$E_x - E_{L_I}$ (keV)	$E_K - E_M$ (keV)	α_K	K/L	$L_I/(L_{II} + L_{III})$	K/M
42.3 ± 0.05	13.20 ± 0.03	15.0 ± 0.1	29.3 ± 3.5	5.5 ± 0.1	2.8 ± 0.2	30 ± 2

B. Electron binding energies, demonstrating that the 42.3 keV photon is a transition in rubidium.

Nucleus	$E_K - E_{L_I}$ (keV)	$E_K - E_M$ (keV)
Sr	13.89	15.80
Rb	13.13	15.0
Experimental measurement	13.20 ± 0.03	15.0 ± 0.1

C. Theoretical conversion coefficients for the 42.3 keV transitions in rubidium, as a function of multipolarity[10].

K				K/L				$L_I/(L_{II} + L_{III})$			
E_1	E_2	M_1	M_2	E_1	E_2	M_1	M_2	E_1	E_2	M_1	M_2
1.06	16.2	1.52	32.9	9	3.2	8.6	5.6	3.4	0.36	13.4	3.4

cedures described in section 4.B. have been utilized to place an upper limit of 2 minutes on the half-life of any existing short-lived isomeric state. (If the half-life of an isomer was long relative to the 35 hour ground state, it would have been detected in the gamma-ray studies[69]. There is, of course, the remote possibility of comparable lifetimes for the two states in question. Final "evidence" for the absence of the $1/2^-$ isomeric state stems from the fact that a consistent decay scheme can be constructed without the presence of such a $1/2^-$ state.)

In addition to the K-L and K-M energy differences, an absolute value of 42.30 ± 0.05 keV was obtained for the transition energy.

The measured K/L, $L_I/(L_{II} + L_{III})$ and K/M ratios for the 42.3 keV transition are listed in table 6, along with the theoretical predictions[10]. An absolute value for the K internal conversion coefficient α_K, has also been obtained on the orange spectrometer by comparing electron and photon relative intensities. The technique is that that is explained in section 4.D.2. The measured value of α_K is in good agreement with the M2 multipolarity assignment based on the above K/L and L subshell ratios. Thus the 42.3 keV transition appears to proceed from an excited state of $9/2^+$ (or $1/2^+$) spin and parity to the ground state of ^{83}Rb, which has been measured[78,79] as $5/2^-$. If the spin is $9/2^+$, such a state would be analogous to the 514 keV state in ^{85}Rb.

The values for the theoretical conversion coefficients

must, of course, be interpolated between the energies listed. As is pointed out by Rose[10], a plot of log α versus log k is very close to a straight line for a given Z. In order to obtain better accuracy for the interpolated α's, the computer has been used to make a least squares fit of log α versus log k. A first order equation will indeed give reasonable results for the higher energy points, but screening effects tend to pull down the values of α at lower energies. However, it has been found that a fourth order equation will reproduce the tabulated values to within 0.5% over the entire energy range for all multipolarities. The theoretical internal conversion coefficients listed for all the transitions have been calculated from the fourth order least squares routine.

The M conversion coefficient has not been compared with the theoretical values[10] because Coulomb screening effects have not been included in the calculations. It has been shown that, as a result of neglecting this correction, the tabulated values are not realistic[82]. An attempt was made to apply the semi-empirical correction of Chu and Perlman to obtain a good value, but it was prevented by an interpolation error in Rose's calculations[83].

4.D.2. The 762.5 keV Transition

The absolute conversion coefficient measurements can be performed very satisfactorily by making an absolute measurement of a single transition, then comparing electron and

photon relative intensities of the remaining transitions. The 762.5 keV transition conversion electron line, shown in fig. 29, has been chosen as the standard line and its absolute α_K measured via the mixed source technique. The internal conversion line of the 661.6 keV transition in ^{137m}Ba has been used in conjunction with relative gamma-ray intensity measurements performed with a 7 cc Ge(Li) detector of 3.4 keV FWHM resolution. The relation

$$\alpha_K(762.5 = \alpha_K(661.6) \frac{I_e(762.5}{I_e(661.6)} \frac{I_\gamma(661.6)}{I_\gamma(762.5)}$$ with the measured quantity[80] $_K(661.6) = 0.0894$ yields the desired result directly.

As shown in table 7, the measured value of $\alpha_K = (9.5 \pm .5) \times 10^{-3}$ for the 762.5 keV transition in ^{83}Rb fits equally well for a pure E2 or an admixture of 70% E1 + 30% M2. The K/L ratio, although not a very sensitive test of the multipolarity in this case, was unattainable because of the incomplete resolution of the 762.5 keV L and the 778.4 keV K lines of the internal conversion spectrum. In order to arrive at a consistent set of results, based on the log ft values and spin assignments of the 42.3 keV state and the ^{83}Sr ground state, the 762.5 keV transition must be an E2. In any event, the E1 + M2 mixture is very unlikely.

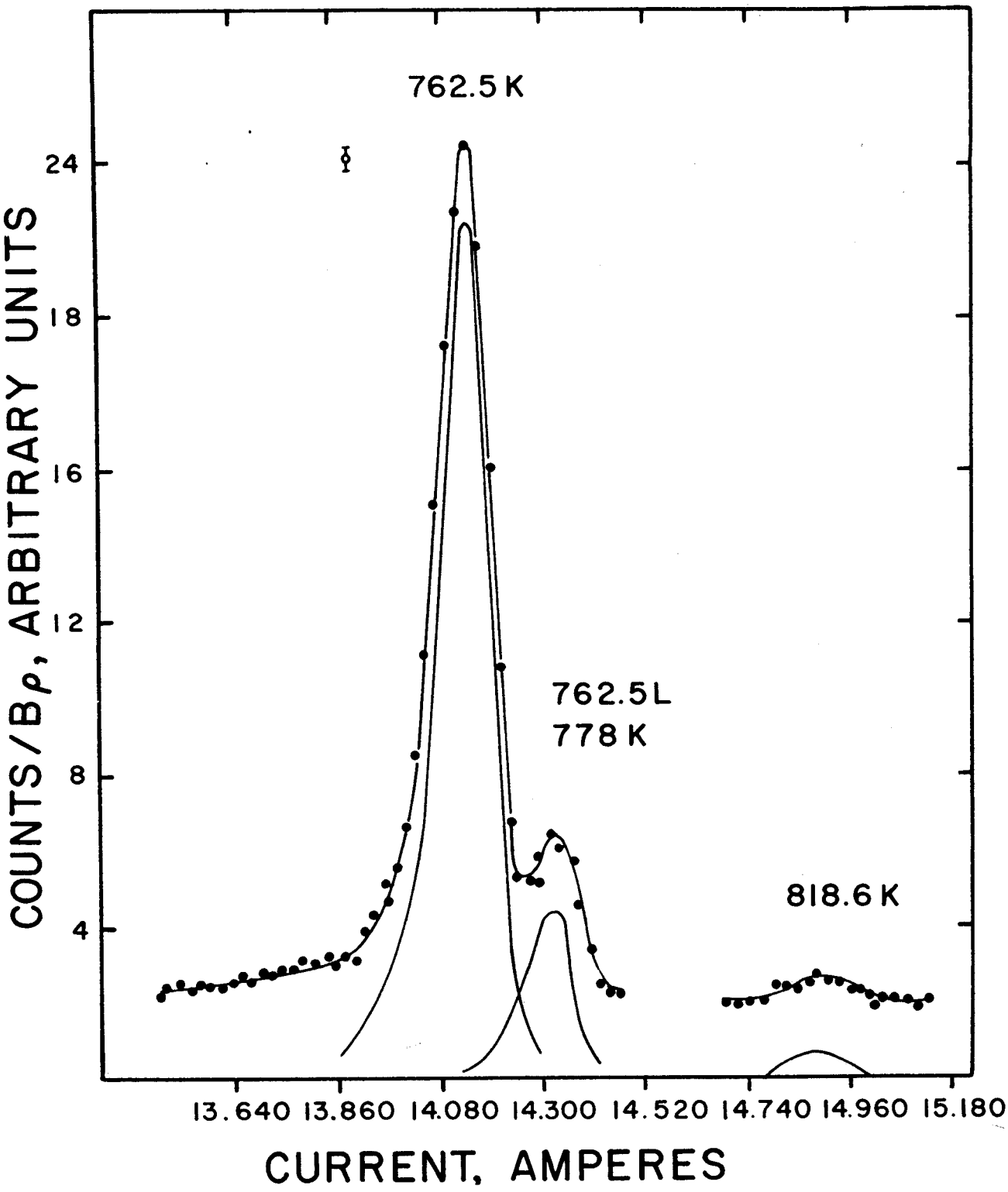

Figure 29. The internal conversion electron spectrum of ^{83}Sr spanning the 740–830 keV region recorded with the orange spectrometer.

Table 7

Multipole Order of transitions in ^{83}Rb, based on measured values of the internal conversion coefficients

E (keV)	Relative electron intensity I(762K)≡100	Relative gamma-ray intensity I(762.8)≡100	α_K a) (expt)	E_1	E_2	M_1	K/(L+M) (expt)	E_1	E_2	M_1	Multiple order
94.2	K 230	1.0	2.2±0.2(-1)	1.0(-1)	1.0(0)	1.5(-1)			6.5	8.7	M1, ≤10% E2
290.2	K 21 L+M 2.1	1.4	1.4±0.2(-2)	3.9(-3)	1.8(-2)	7.9(-3)	10±2		8.6	9.0	35% M1, 65% E2
381.5 b)	K 440 L+M 60	23.5 36.5 60.0 c)	7.1±0.3(-3)	1.9(-3)	7.2(-3)	4.1(-3)	7.4	9.6	8.9	9.2	E2, ≤10% M1 b)
389.2	K 27 L+M 3.2	4.0	6.5±0.5(-3)	1.8(-3)	6.7(-3)	3.9(-3)	8±2				E2, ≤20% M1
418.6	K 26	17.8	1.4±0.2(-3)	1.5(-3)	5.3(-3)	3.3(-3)					E1
423.5	K 7.8	4.6	1.6±9,4(-3)	1.4(-3)	5.1(-3)	3.2(-3)					E1
438.2	K 7.7	2.7	2.7±0.4(-3)	1.3(-3)	4.6(-3)	2.9(-3)					M1
762.5	K 100	100	9.5±0.5(-4)	3.6(-4)	9.3(-4)	8.8(-4)			8.7	9.3	E2
778.4	K 5.5	5.5	9.6±2 (-4)	3.4(-4)	8.8(-4)	7.9(-4)					M1, E2
818.6	K 2.7	2.4	1.1±0.4(-3)	3.1(-4)	7.8(-4)	7.0(-4)					M1, E2

a) The number in parenthesis is the appropriate power of 10, i.e., 2.2±0.2(-1) means (2.2±0.2) x 10^{-1}.

b) The 381.5 keV transition is a doublet, as described in section 4.D.3.

c) The division of intensities of the 381.5 keV doublet are based on the coincidence results of ref. 69.

4.D.3. The 381.5 keV Transitions

The conversion electron spectrum encompassing the region from 350 to 440 keV is shown in fig. 30. The peak corresponding to a 381.5 keV transition has been shown by Etherton, et al.[69] to be a cascading doublet on the basis of coincidence results, the upper member having about 60% of the intensity of the lower one. The transitions are so nearly equal in energy that no visible broadening of the peak has occurred in either the gamma-ray or conversion electron spectra. Thus, the α_K obtained for this peak must be considered as a composite. However, since the transition cascades between the 804, 423 and 42 keV positive parity states, their multipolarities are already limited to M1 or E2, or mixtures thereof. The conversion coefficient of the composite peak has been measured in an effort to determine whether either of the transitions is predominantly M1.

The value of α_K has been determined independently by both the mixed source technique and by comparison with the 762.5 keV α_K measurement. The former yields the result $\alpha_K = (7.2 \pm 0.3) \times 10^{-3}$. Assigning $\alpha_K = 9.5 \times 10^{-4}$ for the 762.5 keV transition, the value $\alpha_K = (7.0 \pm 0.3) \times 10^{-3}$ was obtained for the 382 keV composite transition from their gross relative electron and photon intensities. A simple average of $(7.1 \pm 0.3) \times 10^{-3}$ has been taken as the accepted value. As is shown in table 7, this is in good agreement with the theoretical E2 value[10] of 7.2×10^{-3}. If the

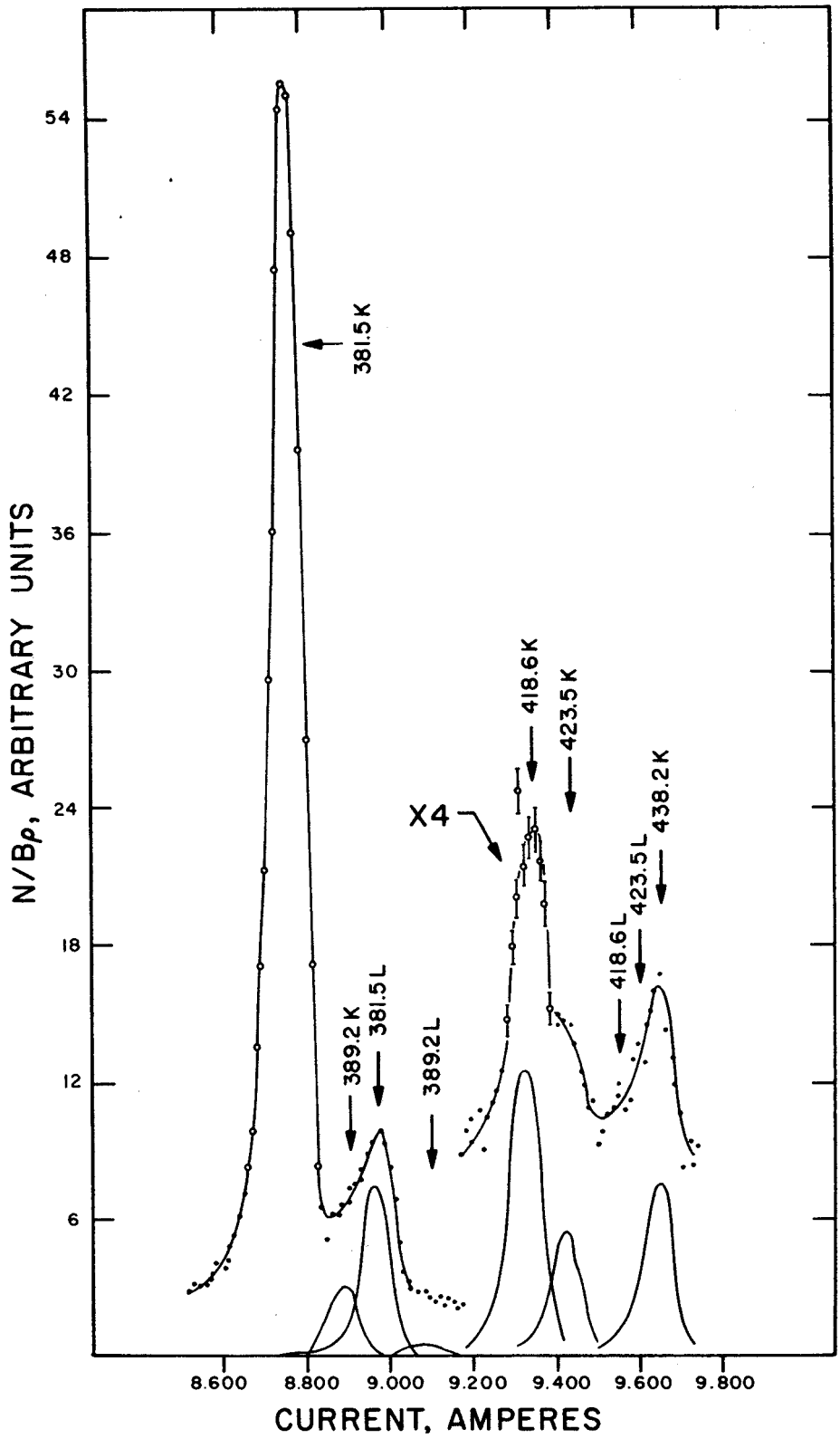

Figure 30. The internal conversion electron spectrum of ^{83}Sr spanning the 350–440 keV region. This was recorded with the orange spectrometer.

lower limit of α_K is taken as 6.7×10^{-3}, and all of the M1 admixture is attributed to the weaker of the pair, a maximum value of 40% M1 is attainable. On the other hand, if the weaker member is pure E2, and upper limit of 20% M1 admixture is possible for the stronger transition.

The 381.5 keV L + M and 389.2 K lines are unresolved. The measured K/(L+M) ratio of 7.4 ± 0.5 for the 381.5 keV transition has been obtained by the standard stripping process, whereby counts from the unresolved 389 keV K line were removed. The theoretical K/L ratio[10] for an E2 transition is 8.9. Application of the semi-empirical method of Chu and Perlman[82] to the M shell yields a value 1.7×10^{-4} for the total M conversion coefficient. Thus, the theoretical K/(L+M) ratio = 7.4 for an E2 transition, in good agreement with the experimental results.

4.D.4. The 389.2, 418.6, 423.5 and 438.2 keV Transitions

The K conversion lines corresponding to the 389.2, 418.6, 423.5 and 438.2 keV transitions have been analyzed using standard stripping techniques, as shown in fig. 30. The results of the analysis are given in table 7. The K conversion line of the 381.5 keV transition was used for the standard line shape. The conversion coefficients have been calculated by comparing the measured electron and gamma-ray relative intensities with the 381.5 keV transition, and using the measured value of $\alpha_K(381.5)$. The resulting conversion

coefficients indicate the 389.2 transition to be predominately E2, while the 418.6 and 423.5 keV transitions are E1. The 438.2 keV K line is not completely resolved from the 418.6 and 423.5 L lines. However, the theoretical K/L ratio of 10 for these latter two transitions indicate that the majority of the intensity of this composite line arises from the 438.2 K conversion line. The resulting comparisons with the theoretical coefficients indicate that the 438.2 keV transition has an M1 multipole order.

4.D.5. The 94.2 and 290.2 keV Transitions

Figure 31 shows the K conversion line of the 94.2 keV transition and the K and L lines of the 290.2 keV transition. A summary of the results is given in table 7. The K conversion coefficient for the 94.2 keV transition has been measured by comparing electron intensities with both the 42.3 and 381.5 keV K lines. A consistent result of $\alpha_K = (2.2 \pm 0.2) \times 10^{-1}$ is obtained which corresponds to an M1 transition. An admixture of $\lesssim$ 10% E2 is possible within the experimental accuracy. The transition is not strong enough to allow a reliable K/L measurement, but a lower limit of 8 could be derived from the data. This is another indication that the transition is not a pure E2, which would have K/L = 6.5.

The 290.2 keV transition is probably 65% E2 + 35% M1 on the basis of the measured α_K. This value has again been obtained by comparison with the 381.5 keV K conversion line.

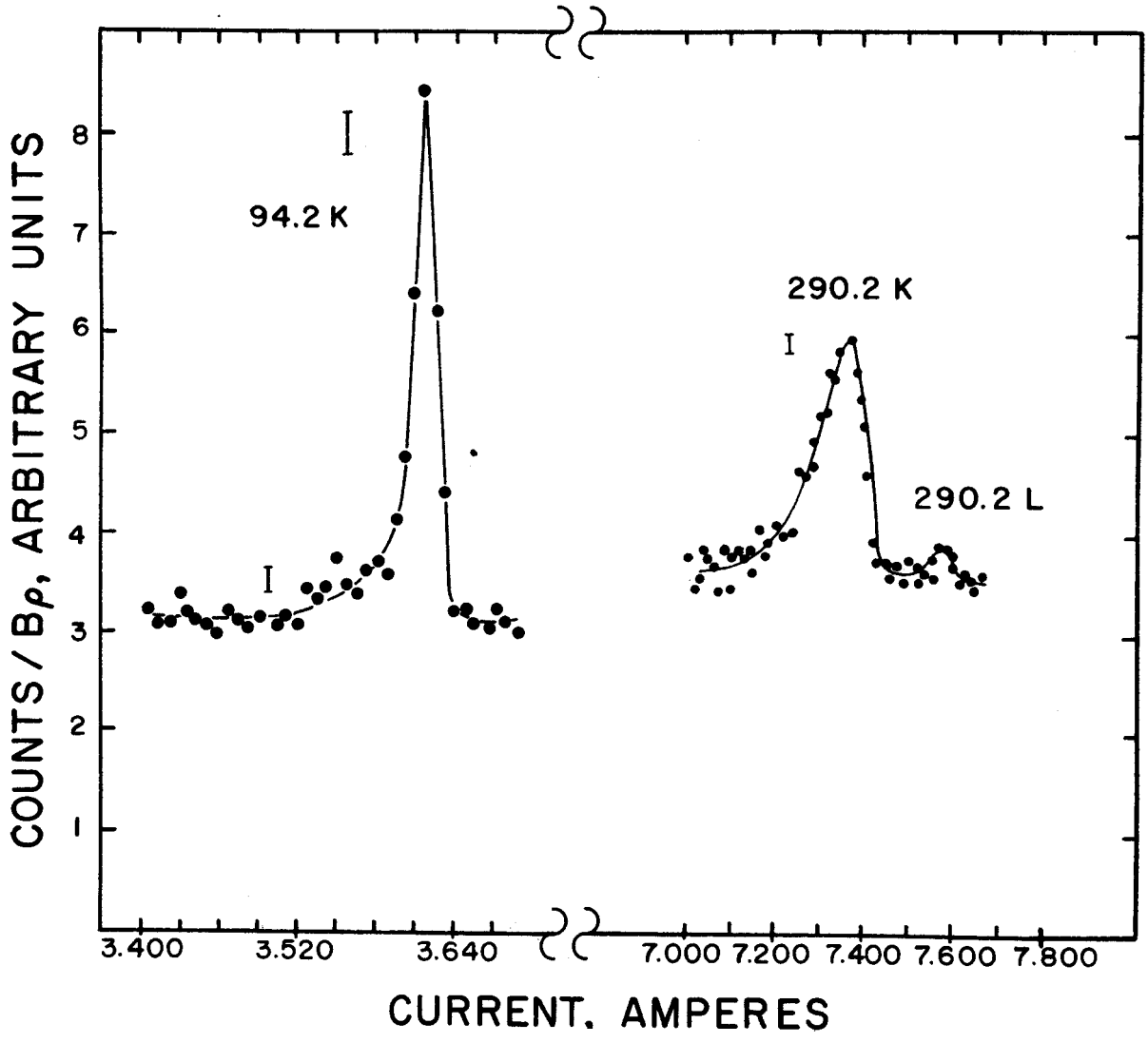

Figure 31. The internal conversion lines of the 94.2 and 290.2 keV transitions in the decay of ^{83}Sr. Different sources were used for the two lines. The 290.2 K conversion line was recorded using a source thick enough to cause line broadening. These were recorded with the orange spectrometer.

The measured value of K/L = 10 $\pm$ 2 lends little additional information since the theoretical K/L ratio for M1 and E2 transition are very close for energies above 250 keV.

4.D.6. The 778.4 and 818.6 keV Transitions

The conversion electron spectrum from 740 to 870 keV is shown in fig. 29. The intensity of the 778.4 keV K electron line was obtained by subtracting from the total counts in the 762.5 L and 778.4 K composite line, an amount for the 762.5 keV L line based on the assumption that it is a pure E2 transition. The resulting α_K, listed in table 7, for the 778.4 keV transition indicates an M1 + E2 mixture. However, nothing can be said about the mixing ratio within the experimental accuracy of the measurement.

The K conversion line of the 818.6 keV transition is very weak. The measured value for α_K is slightly high as compared to the theoretical M1 and E2 coefficients[10] as is shown in table 7. However, they agree to within experimental accuracy.

4.E. The Positron Spectra

The positron spectra have been measured on the orange spectrometer. The detector slit width was opened to produce a higher positron count rate relative to counts registered

from the positrons annihilating in the material surrounding the detector. Under these circumstances the resolution was 2%. The resulting Fermi plot is shown in fig. 32, which indicates three principal groups. The high energy group is assumed to be an unresolved composite, feeding the ground, 5.0 and 42.3 keV states. The second and third groups then feed the 423.5 and 804.7 keV states, respectively. The stripping procedure was accomplished by making successive first order least squares fits to the high energy fraction of the Fermi plots. The resulting analysis indicates 84.7% of the positrons are contained in the high energy group. There is 9.2% and 6.1% feeding, respectively, to the 423.5 and 804.7 keV states, in good agreement with expectations based on gamma intensities. These numbers, coupled with K/β^+ and E_K/E_L capture ratios[8,84] have been used to fix the total amount of feeding to each of the states indicated in the decay scheme, fig. 25. The division of the positron feeding between the ground and 42.3 keV states has been fixed by the requirements of intensity balance of the 42.3 keV state, i.e. the number of transitions to the state must balance the number leaving the state. Knowing the number of gamma-ray and conversion electron transitions into and out of the state, the required amount of β feeding to the level was then determined.

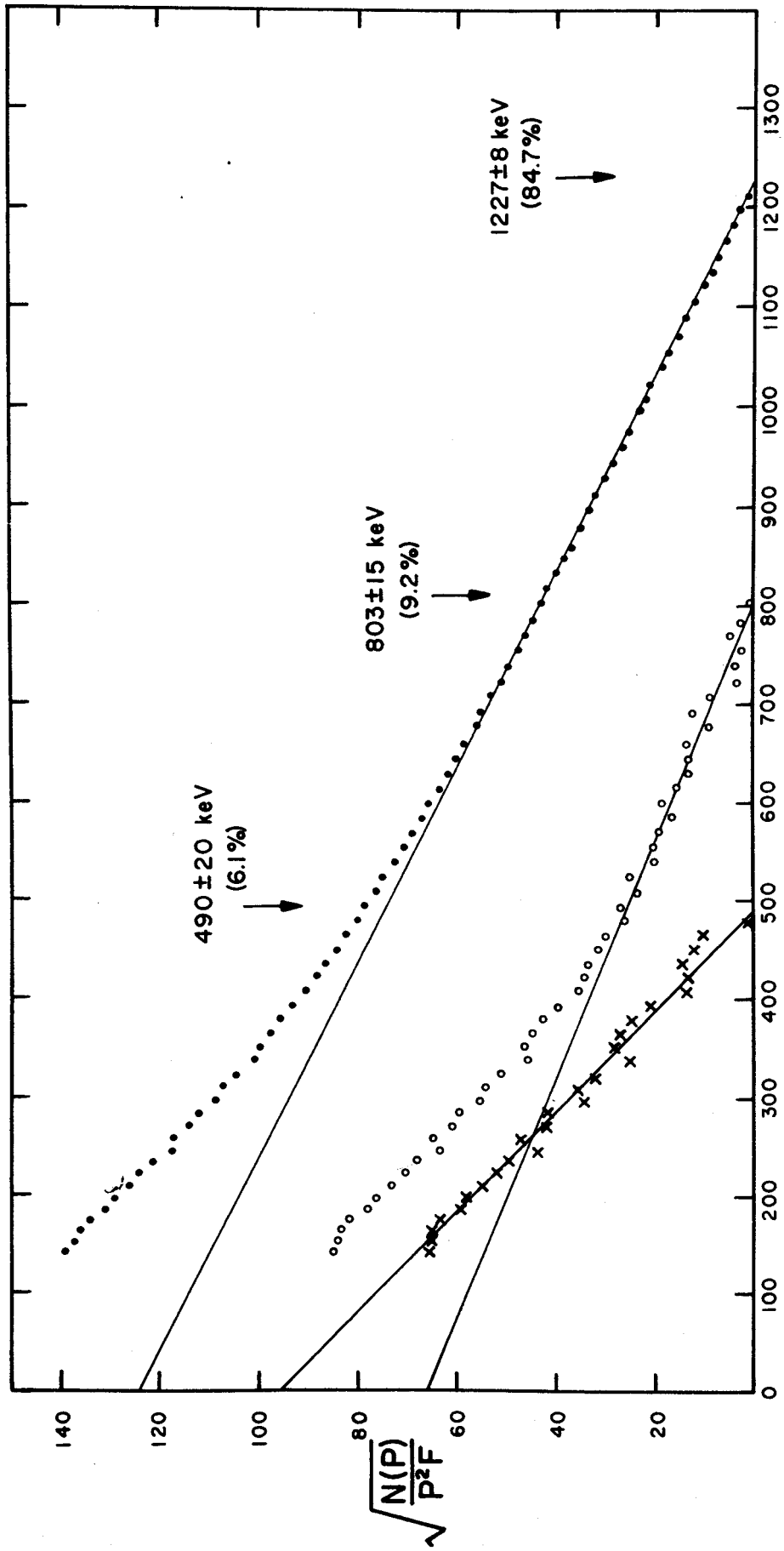

Figure 32. The Fermi analysis of the positrons emitted in the decay of ^{83}Sr. These data were recorded with the orange spectrometer.

4.F. Spin-Parity Assignments for the Levels of ^{83}Rb and the Ground State of ^{83}Sr

The transitions in ^{83}Rb for which internal conversion coefficients have been measured are shown as the more intense lines in the proposed decay scheme[69], fig. 25. The log ft values shown in the decay scheme, fig. 25, have been calculated on the basis of the Fermi plot analysis and gamma transition intensities. The spin-parity assignments presented here are based primarily on the internal conversion coefficient measurements with the log ft values being considered as confirming evidence.

4.F.1. The 42.3 keV State of ^{83}Rb

The ground state spin and parity of ^{83}Rb is known to be $5/2^-$ [78,79]. The measured α_K, K/L ratio and $L_I/(L_{II} + L_{III})$ ratio of the 42.3 keV transition indicate an M2 assignment. Thus the 42.3 keV state must either be $9/2^+$ or $1/2^+$. Although the $1/2^+$ assignment would be difficult to understand on the basis of shell model configurations available in this region of the periodic table, this alternative has been considered. A consistent interpretation of all the data was not possible with such an assignment. Hence, the spin and parity of $9/2^+$ for the 42.3 keV state is considered well established.

4.F.2. The 423.5 and 5.0 keV States of ^{83}Rb and the Ground State of ^{83}Sr

The 423.5 keV state decays to the $5/2^-$ ground state via an E1 transition, and to the $9/2^+$ 42.3 keV state via a 381.5 keV transition which is predominantly E2. Thus, the 423.5 keV level must have spin and parity $5/2^+$ or $7/2^+$. Any M1 admixture in the 381.5 keV transition would limit the spin to $5/2^+$.

The E1 character of the 418.6 keV transition from the $5/2^+$ or $7/2^+$ 423.5 keV state to the 5.0 keV state limits the latter to any value in the range from $3/2^-$ to $9/2^-$. If the 5.0 keV state were $7/2^-$ or $9/2^-$, it would be expected to be populated by a 37.3 keV E1 transition from the 42.3 keV state. A search for the K conversion line of such a transition was performed in the orange spectrometer, with the result that, if such a line exists, its total intensity is less then 1% of that of the 42.3 keV transition. Hence, it would be retarded by a factor of 10^5 over the single particle Weisskopf estimate[8]. Likewise, a $5/2^-$ assignment can be cast in doubt, since an M2 transition between the 42.3 and 5.0 keV states would be expected to compete favorably with the 42.3 keV transition. It is therefore concluded that the most probable spin-parity assignment for the 5.0 keV state is $3/2^-$. This assignment also fixes the spin-parity of the 423.5 keV state to be $5/2^+$.

The ground state of the parent ^{83}Sr is expected to be $1/2^-$, $9/2^+$ or $7/2^+$ on the basis of the systematics and shell

model configurations available in this region of the periodic table[1,16]. The $1/2^-$ possibility is ruled out immediately because of the relatively large amount of positron feeding to the $9/2^+$ 42.3 keV state. The allowed or first forbidden nature of the log ft values of the beta transitions to the $9/2^+$, $5/2^+$ and $5/2^-$ states in ^{83}Rb favors an assignment of $7/2^+$ to the ^{83}Sr ground state. Additional support for the $7/2^+$ assignment arises from the negative results obtained in the search for the presence of an isomer: The lifetime of a $1/2^-$ level in $^{83}_{38}Sr_{45}$ would be much less if the ground state is $7/2^+$ rather than $9/2^+$. As an example, the 190 keV $1/2^-$ state in $^{81}_{36}Kr_{45}$ decays via an E3 transition to the $7/2^+$ ground state, with a half-life of 13 seconds[1].

4.F.3. The 99.2 and 389.2 keV States

The M1 + E2 character of the 94.2 keV transition, in conjunction with the $3/2^-$ assignment of the 5.0 keV state, limits the 99.2 keV state to $1/2^-$, $3/2^-$, or $5/2^-$. The $5/2^-$ possibility is ruled out on the basis of the high log ft ($\geq$9) value for the decay to this level[69]. The $1/2^-$ assignment is considered to be the more probable of the remaining possibilities because of the lack of transitions to this level from the higher energy states whose spin-parity is $\geq 5/2^+$.

The M1 + E2 character of the 290.2 and 389.2 keV transitions, in conjunction with the above assignments, fixes the

389.2 keV state as $3/2^-$. This assignment is in agreement with the log ft value of ≥ 8 for this state[69].

4.F.4. The 804.6 keV State

The 762.5 keV E2 transition to the 42.3 keV $9/2^+$ state, and the 381.5 keV E2 transition to the $5/2^+$ state, limit the 804 keV state to have spin-parity $5/2^+$, $7/2^+$, or $9/2^+$—all of which are consistent with the allowed nature of the log ft value of the level. The $5/2^+$ possibility is very doubtful because of the absence of any transition from this level to any of the lower energy $1/2^-$ or $3/2^-$ states. Etherton, *et al.* have presented arguments[69] based on the gamma feeding to the 804 keV state from the higher energy states, which favor the $7/2^+$ assignment.

4.F.5. The 1202 and 1243 keV States

The probable M1 + E2 character of the 778 keV transition, coupled with the log ft value of the 1202 keV state, indicate a positive parity assignment, with spins 5/2 or 7/2 possible. The fact that this level decays to states of spin-parity $5/2^+$, $9/2^+$, and $5/2^-$ implies that the 1202 keV state is $7/2^+$.

The 1242.6 keV state decays via the 438.2 keV M1 transition to a $7/2^+$ level and via the 818.6 keV M1 + E2 transition

to the $5/2^+$ 423.5 keV level. The state is thus limited to a $5/2^+$ or $7/2^+$ assignment, in agreement with the log ft value for the level. The weak 1237 keV transition to the 5.0 keV $3/2^-$ state favors a $5/2^+$ assignment.

4.G. Discussion

The above results, based primarily on the transition multipolarities obtained from conversion electron measurements, are in good agreement with the spin-parity assignments from log ft values if the ground state of $^{83}_{38}Sr_{45}$ is assigned as $7/2^+$. This assignment does not coincide with the calculations of Talmi and Unna[5] which predict a $7/2^+$ state 320 keV and a $1/2^-$ state 170 keV above a $9/2^+$ ground state. However, the $7/2^+$ assignment is not surprising on the basis of systematics. Even though $^{85}_{38}Sr_{47}$ and $^{87}_{38}Sr_{49}$ have ground state spins of $9/2^+$, other 45 neutron even Z nuclei, $^{77}_{32}Ge_{45}$, $^{79}_{34}Se_{45}$, and $^{81}_{36}Kr_{45}$ have $7/2^+$ ground states[85]. These correspond to $(g_{9/2})^7_{7/2}$ shell model configurations[16]. The $^{83}_{38}Sr_{45}$ ground state probably has the same configuration.

In ^{83}Rb, the ground state ($5/2^-$), the 5.0 ($3/2^-$), the 42.3 ($9/2^+$) and 99.2 ($1/2^-$) keV states probably arise from shell model proton configurations $(f_{5/2})^{-1}$, $(p_{3/2})^{-1}$, $(g_{9/2})^1$ and $(p_{1/2})^1$, respectively. However, the extremely close spacing of these levels may indicate an appreciable amount of a more complex configuration mixing. The low lying $3/2^-$ state is expected since the $(p_{3/2})^{-1}$ and $(f_{5/2})^{-1}$ configurations are

in competition for the ground state of rubidium isotopes, the former prevailing for ^{81}Rb and ^{87}Rb, the latter for ^{83}Rb and ^{85}Rb[16]. The $9/2^+$ states in ^{81}Rb and ^{85}Rb probably correspond to the same type configuration assigned for ^{83}Rb. The $9/2^+$ - $5/2^-$ energy level separation is changing very rapidly in this series of nuclei, the $9/2^+$ state actually being the lower state in ^{81}Rb. This trend may suggest that the 2970 keV state in ^{87}Rb is $9/2^+$, an assignment which is consistent with the log ft value of the β transition to the level[1]. Very little is known about the level schemes of these other odd mass rubidium isotopes, suggesting the need for further investigation in this region before established systematic trends of the single particle levels are available.

The higher energy states in ^{83}Rb probably arise from more complicated shell model configurations, as well as particle motion coupled to collective excitations of the core. It is interesting to attribute the strongly excited 423.5 and 804.6 keV states to the latter phenomenon. This can be done from two slightly different points of view, although there are objectionable features to both interpretations. First, it is noted that the 804.6, 423.5 and 42.3 keV states are connected by relatively pure E2 transitions of comparable energy, which suggests a vibrational structure built on the $9/2^+$ single particle state. However, when compared to the neighboring ^{82}Kr even-even nucleus[6], the cross-over to cascade ratio appears to be a factor of 7 too strong and the phonon energy (expected to be approximately 780 keV)

would have to be reduced by a factor of two, to 381 keV. The other point of view, based on the core coupling model of de Shalit[32], assumes the 804.6 ($7/2^+$) and 423.5 ($5/2^+$) keV states are part of a multiplet of states produced by coupling of the 2^+ core excitation with the $9/2^+$ particle state. If this is the case, the crossover to cascade ratio, as well as the phonon energy are more nearly what one would expect them to be. However, transitions between members of the multiplet should be predominantly M1, whereas an upper limit of 40% has been placed on the M1 contribution of the observed transition. In either event, if the 804.6 keV state is truly of collective nature, the E2 transition probability of the 762.5 keV gamma ray should be greatly enhanced over the Weisskopf single particle estimate[8]. A measurement of the lifetime of the state might serve to test the hypothesis.

Finally, one would expect similar collective states built on the ground and 5.0 keV state in much the same manner as they seem to be built on the $9/2^+$ state. The 389 keV level may indeed have such a composition. However, most of the states so formed may be inaccessible to the β decay process, since it requires a $g_{9/2}$ neutron to be transformed into an $f_{5/2}$ or $p_{3/2}$ proton, a process which is both j and ℓ forbidden. On the other hand, one might expect the $g_{9/2}$ extra core neutron in ^{83}Sr to very effectively populate levels built on the $g_{9/2}$ proton states in the ^{83}Rb daughter.

CHAPTER 5

AN ANALYSIS OF THE EXPERIMENTAL RESULTS

5.A. The Necessity for Electron Measurements and Magnetic Spectrometers

It was mentioned in sect. C of the Introduction that there are instances, such as have been encountered in the studies of the two nuclei reported here, where spin-parity assignments to the nuclear levels are extremely difficult to make on the basis of gamma-ray studies only. In order to obtain more information on the states of interest, a magnetic spectrometer has been constructed for the purpose of measuring conversion coefficients and analyzing continuous beta spectra. In addition, it was known that energy level determinations would indeed be very difficult on the basis of gamma ray measurements alone if the spectrum contained low energy, highly converted transitions. That such situations exist has been very well exemplified by the study of the decay scheme of ^{83}Sr where the proposed level structure depends very sensitively on the multipolarity of the 42.3 keV transition. The multipolarity, in turn, was accurately determined by internal conversion electron measurements. Of course, a very considerable amount of additional information on the other levels of ^{83}Rb and ^{131}I has also been obtained, which would not have been possible without the ability to measure internal conversion coefficients.

Subsequent to the time the orange spectrometer construction was begun, the quality and availability of solid state gamma-ray and electron detectors have been greatly enhanced. The solid state electron counters have proven to be such versatile instruments that one is tempted to ask if there is still a need for an intermediate resolution magnetic spectrometer, such as the orange spectrometer. The experience gained in the study of the ^{83}Sr decay scheme has vividly demonstrated that there is a strong need. The first objection to the solid state detectors is that they have an appreciable Compton scattering cross section, giving rise to a large background if high energy gamma rays are present. Thus, internal conversion lines from transitions in low Z nuclei (conversion coefficients are small for low Z nuclei) or from weak transitions may be masked by underlying Compton distribution in the recorded spectrum. Even more serious is the presence of an intense β^+ continuum, where it occurs. For example, the strong high energy positron groups in ^{83}Sr completely masked the conversion lines of transitions in ^{83}Rb in a spectrum recorded with a solid state detector. Both problems are eliminated in a transverse field magnetic spectrometer. The former problem is eliminated because the detector is shielded from gamma radiation, and the latter because positrons are bent in a direction opposite to that of the electrons—thus, only electrons of one sign reach the detector. (The lens type spectrometer has to be modified to discriminate between positrons and electrons.) It can be concluded that solid

state detectors are capable of removing much of the burden from the slower magnetic spectrometers, but that the latter remain an indispensable tool of nuclear spectroscopy.

5.B. Comparison of the Experimental Results with Predictions Based on Nuclear Models

It has been pointed out in chapters 3 and 4 that the data available for the nuclei studied are insufficient to allow detailed comparisons with theoretical model predictions. However, with the much improved energy level structures that are now available from these studies, it has been possible to present some qualitative arguments correlating the data with some of the predictions.

There are no specific calculations existing for the ^{83}Rb nucleus, but the spins and parities of the low energy states correspond well with what is expected on the basis of the shell model. Without any basis for detailed comparisons, only speculations can be made concerning the origins of the higher energy states of ^{83}Rb.

The ground state assignment of $7/2^+$ for ^{83}Sr does not correspond with the predictions of Talmi and Unna[5]. However, their calculations do indicate the presence of a low-lying $7/2^+$ state at 320 keV. It has been pointed out by Kisslinger and Sorensen[3] that the Talmi-Unna calculation is the only one that has been performed which can depress the $7/2^+$ states enough to qualitatively agree with experi-

mental results in this region of the periodic table.

The low energy states of ^{131}I, as well as the systematic behavior of these states with respect to the addition of neutron pairs, can be said to be in qualitative agreement with the pairing plus quadrupole force calculations of Kisslinger and Sorensen[3]. However, neither this set of calculations nor the core coupling calculations of O'Dwyer and Choudhury[4] are able to explain the higher energy negative parity states that were observed in these studies. Some evidence has been presented which indicates that the positive parity states are due to quasi-particle-phonon coupling.

In any event, the above results indicate the need for additional experimental and theoretical investigations in both of the regions of the periodic table studied here. The results that have been presented can form a good foundation for both types of examination. With respect to calculations for the iodine isotopes, any future theoretical investigations should, as one of the objectives, explain the quadratic behavior of the single particle energy separations as a function of neutron number.

BIBLIOGRAPHY

1) Nuclear Data Sheets (The National Academy of Sciences - National Research Council, Washington, D.C.)

2) Nuclear Science Abstracts (U.S.A.E.C., Division of Technical Information)

Physics Abstracts (The Institution of Electrical Engineers, London)

3) L. S. Kisslinger and R. A. Sorensen, Rev. Mod. Phys. 35 (1963) 853

L. S. Kisslinger and R. A. Sorensen, Matt. Fys. Medd. Dan. Vid. Selsk. 32, No. 9 (1960)

4) T. F. O'Dwyer and D. C. Choudhury, Bull. Am. Phys. Soc. 11 (1966) 321.

5) I. Talmi and I. Unna, Nucl. Phys. 19 (1960) 225

6) R. C. Etherton and W. H. Kelly, Nucl. Phys. 84 (1966) 129

7) H. Fraunfelder and R. M. Steffan, Angular Distribution of Nuclear Radiation, in α - β - γ Ray Spectroscopy, edited by Kai Siegbahn (North-Holland Publishing Co., Amsterdam, 1965) Chap. 19

8) A. H. Wapstra, G. J. Nijgh and R. Van Lieshout, Nuclear Spectroscopy Tables (North-Holland Publishing Co., Amsterdam, 1959) 58

9) Nuclear Data 1, No. 1B (Academic Press, New York) Edited by K. Way

10) M. E. Rose, Internal Conversion Coefficients (Interscience Publishers, Inc., New York, 1958)

11) K. M. Bisgård, Nucl. Inst. and Meth. 22 (1963) 221

12) M. A. Preston, Physics of the Nucleus (Addison-Wesley Publishing Co., Inc., Reading, Mass., 1962)

13) M. Goeppert Mayer, Phys. Rev. 75 (1949) 1966; Phys. Rev. 78 (1950) 16, 22

14) O. Haxel, J. H. D. Jensen and H. E. Suess, Phys. Rev. 75 (1949) 1766; Z. Physik, 128 (1950) 295

15) E. Wigner, Phys. Rev. 51 (1937) 947

16) M. Goeppert Mayer and J. H. D. Jensen, Elementery Theory of Nuclear Shell Structure (Wiley, New York, 1955)

17) D. Kurath, Intermediate Coupling, in α - β - γ Ray Spectroscopy, loc. cit. Chap. 9B

18) J. D. Elliot and B. H. Flowers, Proc. Roy. Soc. (London) A 229 (1955) 536

19) S. T. Belyaev, Matt. Fys. Medd. Dan. Vid. Selsk. 31, No. 11 (1959)

20) R. A. Sorensen, Phys. Rev. 133 (1964) B 281

21) B. R. Mottleson, in Proc. Int. Conf. on Nuclear Structure, Kingston, 1960 (University of Toronto Press, Toronto, 1960) 525

22) M. Baranger and K. Kumar, Nucl. Phys. 62 (1965) 113
E. R. Marshalek, U.C.R.L. - 10046 and numerous references cited therein. (Ph.D. thesis)

23) K. Kumar, lecture at M.S.U., 1966

24) S. G. Nilsson, Matt. Fys. Medd. Dan. Vid. Selsk 29, No. 16 (1955)

25) E. Marshalek, L. W. Person and R. K. Sheline, Rev. Mod. Phys. 35 (1963) 108 and references cited therein

26) B. R. Mottleson and S. G. Nilsson, Matt. Fys. Skr. Dan. Vid. Selsk. 1, No. 8 (1959)

27) E. B. Paul, Phil. Mag. 2 (1957) 311

28) A. Bohr, Matt. Fys. Medd. Dan. Vid. Selsk. 26, No. 14 (1952)

29) A. Bohr and B. R. Mottleson, Matt. Fys. Medd. Dan. Vid. Selsk. 27, No. 16 (1953)

30) A. S. Davydov and G. F. Filippov, Nucl. Phys. 8 (1958) 237;
A. S. Davydov and V. S. Rostovsky, Nucl. Phys. 12 (1959) 58;
A. S. Davydov, Nucl. Phys. 16 (1960) 597
A. S. Davydov and R. A. Sardaryan, JETP 40 (1961) 1429;
A. S. Davydov, Nucl. Phys. 24 (1961) 682;
A. S. Davydov and A. A. Chaban, Nucl. Phys. 20 (1960) 449

31) V. V. Pashkevich and R. A. Sardaryan, Nucl. Phys. 65 (1965) 401

32) A. de Shalit, Phys. Rev. 122 (1961) 1530

33) D. C. Choudhury, Matt. Fys. Medd. Dan. Vid. Selsk. 28, No. 4 (1954)

34) N. K. Glendenning, Phys. Rev. 119 (1960) 213

35) B. Bannerjee and K. K. Gupta, Nucl. Phys. 30 (1962) 227

36) A. K. Kerman, Matt. Fys. Medd. Dan. Vid. Selsk. 30, No. 15 (1956)

37) G. Berzins and W. H. Kelly, Nucl. Phys. A92 (1967) 65

38) J. Danysz, Le Radium 9 (1912) 1

J. Danysz, Ann. de Chem. et de Phys. 8 (1913) 240

39) K. Siegbahn, in α - β - γ Ray Spectroscopy, loc. cit., Chap. 3

40) O. Kofoed - Hansen, J. Lindhard and O. B. Nielsen, Matt. Fys. Medd. Dan. Selsk. 25, No. 16 (1950)

41) O. B. Nielsen and O. Kofoed - Hansen, Matt. Fys. Medd. Dan. Selsk. 29, No. 6 (1955)

42) J. S. Geiger, AECL - 2237 (1965)

43) A. H. Jaffey, C. A. Mallman, J. Saurez - Etchepare, and T. Suter, Argonne National Laboratory Report ANL-6222 (1960)

44) K. M. Bisgard, private communication (1963)

45) A. M. Patlach, Electronics (Nov. 1960) 66

R. L. Garwin, Rev. Sci. Inst., 29 (1958) 223

R. L. Garwin, Rev. Sci. Inst., 20 (1958) 900

R. L. Garwin, D. Hutchinson, S. Penman, and G. Shapiro, Rev. Sci. Inst., 30 (1959) 105

46) P. G. Hansen, H. L. Nielsen, and K. Wilsky, Risø Report No. 68 (1963)

47) M. S. Freedman et al. Nucl. Instr. and Meth. 8 (1960) 255

N. A. Burgov et al. Nucl. Instr. and Meth. 12 (1961) 316

48) R. L. Auble and W. H. Kelly, Nucl. Phys. 73 (1965) 25

49) G. Berzins, L. M. Beyer, and W. H. Kelly, Bull. Am. Phys. Soc. 11 (1966) 395

50) G. Berzins, L. M. Beyer, W. H. Kelly, W. B. Walters, and G. E. Gordon, Nucl. Phys. A93 (1967) 456

51) W. B. Walters, (M.I.T.) private communication

52) E. Hebb, Phys. Rev. 97 (1955) 987

53) J. M. Ferguson and F. M. Tomnovec, Nucl. Phys. 26 (1961) 457

54) A. Bedescu et al., Iz v. Nauk SSSR, Ser. Fiz. 23 (1959) 1434;
Columbia Tech. Trans., p. 1424

55) A. Bedescu et al. JETP 13 (1961) 65

56) A. Bedescu et al., Rev. Phys., Acad. Rep. Populaire Roumaine 7 (1962) 173

57) S. H. Devare, R. M. Singru, and H. G. Devare, Phys. Rev. 140 (1965) B536

58) H. H. Bolotin, private communication (1963)

59) G. T. Ewan and A. J. Tavendale, AECL No. 2079 (1964) and references cited therein

60) R. L. Auble, W. H. Kelly, and H. H. Bolotin, Nucl. Phys. 58 (1964) 337

61) W. B. Walters, C. E. Bemis, and G. E. Gordon, Phys. Rev. 140 (1965) B268

62) S. H. Devare, P. N. Tandon, and H. G. Devare, Phys. Rev. 131 (1963) 1750

63) L. J. Velinsky, Ph.D. thesis, Michigan State University (1964)

64) R. M. Singru and H. G. Devare, to be published

65) L. M. Beyer, G. Berzins, and W. H. Kelly, Nucl. Phys. A93 (1967) 436

66) W. B. Walters, private communication (1966)

67) G. Berzins, private communication (1966)

68) R. L. Robinson et al., Nucl. Phys. 74 (1965) 281

69) R. C. Etherton, L. M. Beyer, W. H. Kelly, and D. J. Horen, to be published

70) I. Dosbrovsky, S. Katcoff, and R. W. Stonner, J. Inorg. Nucl. Chem. 26 (1964) 209

71) S. V. Castner and D. H. Templeton, Phys. Rev. 88 (1952) 1126

72) T. Kuroyanagi, J. Phys. Soc. Japan 16 (1961) 2363

73) V. Maxia, W. H. Kelly and D.J. Horen, J. Inorg. Nucl. Chem. 24 (1962) 1175

74) K. R. Reddy, A. S. Johnston, and S. Jha, Bull. Am. Phys. Soc. 9, No. 1 (1964) 17

75) D. N. Sunderman and C. W. Townley, The Radiochemistry of Barium, Calcium and Strontium (The National Academy of Sciences, Washington, D.C., 1960) NAS-NS 3010

76) Ioshiyasu Kiba and Shigeru Mizukami, Bull. Chem. Soc. of Japan 31 (1958) 1007

77) Ioshiyasu Kiba and Shigeru Mizukami, Bull. Chem. Soc. of Japan 31 (1958) 1013

78) J. P. Hobson et al., Phys. Rev. 104 (1956) 101

79) J. C. Hubbs et al., Phys. Rev. 107 (1957) 723

80) J. S. Merritt and J. G. V. Taylor, Anal. Chem. 37 (1965) 351

81) R. L. Auble, unpublished results (1963)

82) Y. Y. Chu and M. L. Perlman, Phys. Rev. 135 (1964) B319

83) M. E. Rose, private communication (1966)

84) M. L. Perlman and M. Wolfsberg, BNL 485 (T-110) (1958)

85) Nuclear Data Group, Nuclear Data 1, No. 4 (1966), compiled by A. Artna

86) J. M. Hollander, in Internal Conversion Processes, edited by J. H. Hamilton (Academic Press, New York, 1966) Chap. 5